ESTI European Society of Thoracic Imaging

ESTI 2022

28th ANNUAL SCIENTIFIC MEETING OF THE EUROPEAN SOCIETY OF THORACIC IMAGING

JUNE 09-11, 2022

OXFORD, UNITED KINGDOM

www.myESTI.org

ONLINE ABSTRACT SYLLABUS

INVITED ABSTRACTS

Abstracts appear as submitted to the system and have not been checked for correctness and completeness.

Staging the mediastinum for lung cancer – Arcane and novel methods

H. Prosch, Vienna/AT

Body: Hilar and mediastinal lymph node involvement is one of the most important predictors of prognosis in patients with resectable lung cancer. Consequently, a thorough evaluation of potential lymph node involvement is of paramount importance in all patients who are candidates for curative therapy. The diagnostic criterion for positive lymph nodes on CT, a short axis diameter of 1cm or more, has a very low positive (60 %) and negative predictive value (80 %). Because PET/CT also suffers from a rather low positive predictive value (63 %), the role of imaging lies primarily in the detection of suspicious lymph nodes, which then need to be further investigated by endobronchial ultrasound-guided biopsies or mediastinoscopy. Modern imaging modalities, such as diffusion-weighted imaging or spectral imaging, have shown some promise; however, the available data is still too limited to suggest the routine use of these techniques in lung cancer patients

Take Home Points:
- Lymph node involvement is an important predictors of prognosis lung cancer patients
- Imaging is essential to guide invasive staging of hilar or mediastinal lymph nodes

The Lung Cancer Diagnostic Pathway – Are delays significant

D. Baldwin, Nottingham/UK

Body: Lung cancer is not only the leading cause of cancer deaths in both sexes, but also an aggressive cancer with a short survival for most of those who are diagnosed. Early diagnosis is a major priority in lung cancer and this is supported by the developing screening programmes and awareness initiatives. However, fast diagnosis is also important for a cancer that can be so quickly fatal. People with lung cancer often lose their pre-disease levels of fitness and are less likley to receive treatment as well as being less likely to benefit from treatment. This can happen within weeks of presentation and so diagnostic pathways need to move quickly to ensure maximum benefit. In England, the National Optimal Lung Cancer Pathway was one of the first of a series of faster diagnosis pathways. The pathway is challenging to deliver and features rapid progress to CT with clinical triage and subsequently bundles of diagnostic and staging tests followed by challenging pathology turnaround times and times to treatment. The evidence for faster diagnosis improving outcomes is difficult to interpret becuase of the sicker-quicker effect where very ill people take priority to diagnosis but unfortunately are in the worst prognostic group. Where this is at least partly accounted for, there is evidence that faster treatment improves survival, even fro early stage disease. The recent covid pandemic, where patients were encouraged to stay at home (necessary to control the R value), resulted not only in more people with later stage disease, but also fewer treatments and a quarter to a third fewer diagnoses. The latter explained by deaths from lung cancer without it being diagnosed, a reflection of the rapid progression of the disease.
Patients, of course, expect fast progress to treatment at what is an incredibly distressing time for them. Faster diagnosis pathways, by virtue of the rapid progress to CT, also help early diagnosis where red flag symptoms are due to comorbidity rather than more advanced lung cancer.
The challenge is how the improved logistics of the faster pathways are implemented in systems where capacity is limited. An understanding of the potential benefit to lung cancer patients by all those clinicians and administrators involved in delivering the pathway is vital.

Take Home Points:
- Faster diagnosis pathways aim to treat patients before there performance status deteriorates so they benefit more
- The pathways use improved logistics to minimise time to treatment and maximise efficiency
- Used correctly this means fewer MDT discussions and clinic visits
- The covid pandemic has shown how important early presentation and faster diagnosis is in lung cancer

State of the art lung biopsy

S. Padley, Royal Brompton Hospital, Radiology, London/UK

Body: Percutaneous needle biopsy should not be undertaken in situations where the result will not affect patient management or prognosis.
Nevertheless there are multiple circumstances under which lung needle biopsy will be required, including as part of presurgical workup and also to guide other treatment options including thermal ablation and radiotherapy.
When the patient is known to be inoperable, tissue sampling will still be required for molecular analysis to allow tailored systemic anti cancer treatment to be optimised.
Arriving at a specific benign diagnosis may also be the goal in certain circumstances, particularly through the use of cutting needle biopsies.
This presentation will discuss the indications and contraindications for lung needle biopsy, describing current techniques.

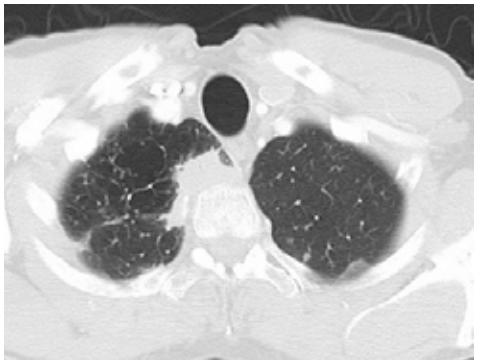

It will also discuss tips and tricks for accessing aqnatomically challenging lesions and undertaking biopsy in high risk patients with coexisting pathologies.

Take Home Points:
- When to biopsy, when not to biopsy.
- Pre-biopsy planning steps.
- Biopsy technique.
- Anticipating and dealing with complications.

Novel treatments for COPD and role of imaging

J. Babar, Cambridge/UK

Body: CT has an important role in phenotyping patients with COPD and providing formal quantification of emphysema, gas trapping and large airway wall thickness which can serve as biomarkers.
Emphysema predominant phenotype COPD contributes to lung hyperinflation, airflow limitation, and poor exercise capacity. Whilst medical therapies act primarily to relax airway smooth muscle and improve airflow limitation, these do not address the problem of mechanical disruption and tissue damage. Surgical interventions aim to reduce the hyperinflation that result from lung damage in advanced COPD. Current interventional therapies include bullectomy, lung volume reduction procedures (surgical and bronchoscopic) and lung transplantation. This talk will review bronchoscopic interventions and the central role imaging has in careful patient selection and helping to guide novel treatments, with target lobe identification and in the post-procedural management of adverse events.

Take Home Points:
Treatment success is highly dependent on patient selection, for which imaging plays a vital role.

Imaging of post surgical appearances

P. Beddy, Dublin/IE

Body: The first section of this talk will review the common operations for lung cancer surgery and the normal post operative appearance. It will also review common complications encountered in the early and late phases post surgery.
The second section of my talk will review the common sites of disease recurrence post thoracic cancer surgery and the latest literature on surveillance for lung cancer patients.

Take Home Points:
1. Understanding the different operations used for lung cancer surgery is key to identifying complications and disease recurrence.
2. Local recurrence can be very subtle and review of sequential imaging is of crucial importance.
3. Early identification of lung cancer recurrence can enable salvage curative treatment.

Ablation of lung tumours – Complications and outcomes

A.R. Larici[1], G. Cicchetti[2], A. Tanzilli[1], A. Posa[2], A. Contegiacomo[2], R. Iezzi[1]; [1]Catholic University of the Sacred Heart, Department of Radiological and Hematological Sciences, Rome/IT; [2]Fondazione Policlinico A. Gemelli IRCCS, Department of Diagnostic Imaging, Oncological Radiotherapy and Hematology, Rome/IT

Body: Image-guided percutaneous ablation is emerging as a safe and effective loco-regional alternative to surgery and stereotactic body radiation therapy for the treatment of either primary early-stage or metastatic pulmonary tumours. Ablation technology has rapidly evolved with substantial technical and procedural improvements, allowing significant expansion of its clinical indications and improving outcomes and safety profiles, with both curative and palliative indications.
Among tumour ablation techniques, the most commonly used for pulmonary tumours are represented by radiofrequency (RFA), microwave (MWA), and cryoablation. In detail, thermal energy is used to directly heat (RFA, MWA) or cool (cryoablation) the target tissue, causing acute cellular necrosis. Although similar purposes, each technique has specific and optimal indications, with different advantages and disadvantages. RFA is a robust technique with favourable results for tumours up to 2 cm in size. The theoretical superiority of MWA is highlighted for larger tumours (> 2 cm) located in proximity to large vessels. Cryoablation, which usually takes longer procedural time, is feasible to treat complex lesions located close to the hilum, or chest wall/pleura and diaphragm, owing to the better preservation of tissue architecture. Local efficacy of RFA, MWA or cryoablation applied to lung tumours, appears comparable even though no randomized studies have been conducted to this aim. Furthermore, although no randomized studies comparing image-guided percutaneous lung ablation with surgery or stereotactic radiation therapy are available, the current literature demonstrates equivalent survival rates.
Generally, following RFA and MWA, the appearance of the ablation zone on computed tomography (CT) is quite similar due to the use of heat energy in both procedures, while findings after cryoablation can be slightly different. Immediately after RFA or MWA (early phase), CT showed the physiological enlargement of the tumour with perilesional ground glass (GG), and 48 hours later the tumour is surrounded by two layers of GG and thick consolidation („cockade phenomenon"). CT performed 30 days later (intermediate phase), usually depicts a reduction in size of the ablation zone, with resolution of GG. A cavitary evolution of the lesion, with thick margins and peripheral contrast enhancement, might occurr. CT performed three to six months later (late phase), shows a progressive reduction of the ablated area and resolution of eventual cavitations, with a consolidative appearance initially and a scar later. During cryoablation, after the first thaw, a GG area can be visualized on CT images around the cryoprobe, representing the "ice ball", which consists of a thin denser rim that should be located 4-5 mm beyond the tumour margins to assure an effective coagulation necrosis. At the end of the cryoablation cycles, in some cases the ablated zone appears relatively well defined and surrounded by a thin mixed GG/consolidative rim determined by parenchymal haemorrhage.
Complications of percutaneous ablation therapies are most often detected during the early phase. The most common reported complication is pneumothorax (28.3%), followed by pleural effusions (14.8%). However, only < 25% of the reported pneumothoraces required chest tube placement. In the persistence of pneumothorax, a bronchopleural fistula, which can appear when necrotic tissue of a subpleural ablation is evacuated with development of air leak, should be suspected. These cases are mostly managed with prolonged chest tube drainage and may require pleurodesis or surgery. After cryoablation the rate of pulmonary haemorrhage and haemoptysis is usually higher, due to fracture of small blood vessels as well as the lack of cautery effect determined by RFA and MWA. Pleural effusion or haemorrhage especially occurs in case of ablated lesion adjacent to the pleura. In the immediate periprocedural period the effusion usually has a haemorrhagic component, with increased attenuation on CT images, while effusions presenting several days after the procedure are more likely to be reactive. Postprocedural pneumonia and abscess formation, even though relatively uncommon, are potentially serious complications that can result in procedure-related death. Also other extremely rare complications have been reported, such as systemic air embolisms and pulmonary artery aneurysm formation.
In this presentation, expected imaging findings on CT as well as complications after lung tumour ablation, occurring in the early phase, will be highlighted. Efficacy and outcomes of these procedures will be discussed according to the updated literature.

Take Home Points:
1. Image-guided percutaneous ablation is emerging as a safe and effective loco-regional alternative to surgery and stereotactic body radiation therapy for the treatment of either primary early-stage or metastatic pulmonary tumours.
2. Ablation technology has rapidly evolved with substantial technical and procedural improvements, allowing significant expansion of its clinical indications and improving outcomes and safety profiles, with both curative and palliative indications.
3. Among tumour ablation techniques, the most commonly used for pulmonary tumours are represented by radiofrequency (RFA), microwave (MWA), and cryoablation. Although similar purposes, each technique has specific and optimal indications, with different advantages and disadvantages.
4. Complications of percutaneous ablation therapies are often detected during the early phase, and the most common are pneumothorax and pleural effusions, which usually resolve spontaneously. Persistent pneumothorax should rise the suspicion of a bronchopleural fistula. Hemorrhage and haemoptysis have higher rate after cryoablation. Postprocedural pneumonia and abscess formation, even though relatively uncommon, are potentially serious complications. Extremely rare complications are systemic air embolisms and pulmonary artery aneurysm formation.
5. Local efficacy of RFA, MWA or cryoablation applied to lung tumours, appears comparable and, although no randomized studies comparing percutaneous lung ablation with surgery or stereotactic radiation therapy are available, the current literature demonstrates equivalent survival.

CT and genetic mutations in lung cancer

J. Dinkel, Munich/DE

Body: Lung cancer is a very heterogeneous disease, at a genetical and histological level which translates into an equally varied CT phenotyping. Noninvasively determination of mutation status in lung cancer before targeted therapy remains challenging. This presentation will show the state of the art in the CT analysis of lung cancer especially using CT image-based radiomic features to predict the existence of a mutation.
With advances in the treatment of lung cancer using the molecular testing, the prediction of oncogenes and even drug resistance gene mutations have become key to individualized treatment. The development of CT radiomics is a promising quantitative method for predicting different gene mutations.

Take Home Points:
- Noninvasively determination of mutation status in lung cancer
- CT analysis of lung cancer using CT image-based radiomic features

Dual energy in pulmonary vascular disease

M. Remy-Jardin[1], I. Oufriche[2], L. Guiffault[3], J. Remy[3]; [1]Lille/FR; [2]Cardio-Thoracic Hospital, Thoracic Imaging, Lille/FR; [3]Cardio-Thoracic Hospital, Lille/FR

Body: Dual-energy CT (DECT), also known as spectral or multi-energy CT, has gained wide acceptance in clinical practice owing to its unique post-processing capabilities enabling optimization of morphologic imaging and introduction of functional imaging. This is accomplished by an almost simultaneous acquisition of datasets with two x-ray beams of different energy, or by using spectral detectors, and then processing the data. Among the most important DECT reconstructions are virtual monoenergetic images, virtual unenhanced images, virtual noncalcium images and iodine maps for perfusion imaging.
In the context of chest imaging, the most frequent clinical objective of DECT angiographic examinations is to provide simultaneous assessment of the pulmonary vasculature and analysis of the parenchymal iodine distribution, both generated from the same data set at a radiation dose similar or moderately higher than single-energy CT pulmonary angiography. The pattern of iodine enhancement has been shown to correspond to lung blood volume at planar scintigraphy and single photon-emission CT and is considered a surrogate marker of lung perfusion.
In the field of pulmonary vascular diseases, detection of perfusion alterations can help in the diagnostic approach of acute and chronic pulmonary embolism but also in the diagnostic work-up of pulmonary hypertension. Numerous additional applications have also been reported in smoking-related diseases, interstitial lung diseases and to predict post-operative lung function while detection of lung microvascular disease in the context of COVID-19 has been shown to be accessible to DECT lung perfusion imaging.
The technique for assessing pulmonary perfusion on DECT angiographic examinations is based on material decomposition of iodine from other materials to visualize the regional pulmonary distribution of intravenous contrast in distal pulmonary vessels including the capillaries. Whereas the iodine distribution is interpretable in the majority of cases, there is a well-known influence of patient morphotype on the overall image quality, with a level of image noise increasing with the patient BMI. If image graininess is not a limiting factor for detection of PE-type defects, it may preclude confident depiction of patchy perfusion defects. As an alternative to the established Lung BPV algorithm, dual-energy images of the lungs can also be processed by subtracting virtual monoenergetic images of different energy levels. This approach takes advantage of the improved iodine, contrast-to-noise ratio

(CNR) of virtual monoenergetic images, in particular at low energy levels, while maintaining spatial resolution. To avoid noise increase at lower calculated energies, which is a known drawback of virtual monoenergetic images at low kilo-electron volt, a regional spatial frequency-based recombination of the high signal at lower energies and the superior noise properties at medium energies can be performed to optimize CNR.
The purpose of this presentation is to highlight the practical applications of dual-energy CT in daily routine and to discuss lung perfusion changes in the era of photon-counting CT.

Take Home Points:
- Dual-energy CT offers simultaneous depiction of morphologic and functional changes
- Dual-energy CT can help depiction of abnormalities within pulmonary circulation that are not accessible to standard cross-sectional imaging
- Photon-counting CT technology enables considerable improvement of lung perfusion imaging at considerably lower radiation doses.

Imaging pulmonary haemorrhage

E. Castañer González, Sabadell/ES

Body: Diffuse pulmonary hemorrhage (DPH) is an uncommon syndrome that results in intraalveolar hemorrhage. The histopathologic differential diagnosis of DPH includes diseases associated with pulmonary capillaritis and those associated with normal vessels or bland hemorrhage. DPH is a life-threatening condition associated with a wide variety of underlying causes. Most cases of DAH are caused by capillaritis associated with systemic autoimmune diseases such as ANCA-associated small-vessel vasculitis, Goodpasture syndrome, and systemic lupus erythematosus.
Whatever the underlying cause, the appearance depends on the amount of blood filling the alveoli, ranging from small opacities to consolidations. Therefore, the radiological appearance is totally non-specific and the main differential diagnoses will be with heart failure and infection. Cough, hemoptysis, fever, and dyspnea are common initial symptoms, although hemoptysis may be absent in up to 33 % of patients. New radiographic opacities, a falling hemoglobin level, and the finding of increasing hemorrhagic fluid on sequential bronchoalveolar lavage (BAL) favor the diagnosis. Once the diagnosis is made, the underlying cause is sought through careful history review (including medication use, toxic or infectious exposures, extrapulmonary symptoms) and laboratory tests.

Take Home Points:
- DPH is uncommon. Radiologic signs of DPH are nonspecific and variable but must be considered in patients with otherwise unexplained alveolar opacities, particularly when seen with new-onset renal insufficiency or a connective tissue disease.
- As the radiological findings of DPH are non-specific, I would emphasize the importance of combine radiological signs with the clinical features and laboratory results.

The Tree in Bud pattern – State of the art interpretation and diagnosis

J. Verschakelen, W. De Wever, A. Dubbeldam, J. Coolen; UZ Leuven, Department of Radiology, Leuven/BE

Body: The tree-in-bud pattern is a CT pattern that represents branching centrilobular linear opacities that are connected to micronodules resembling a tree in bud. This lecture will start with a short review of the anatomy of the secondary pulmonary lobule to understand why and how this pattern may develop. An overview will then be given of the most frequent causes. Finally, features will be discussed that can be helpful to differentiate between the causes and relation with other centrilobular changes that may occur will be explained.

Take Home Points:
1. Review the anatomy of pulmonary lobule to understand the tree-in-bud pattern.
2. Review the abnormalities that may be associated with this pattern.
3. Show features that may be helpful to differentiate between the different causes.

Pulmonary Hypertension and the right ventricle on CT

L.J. Meijboom, Amsterdam UMC, Radiology and Nuclear medicine, Amsterdam/NL

Body: Pulmonary hypertension is defined by a mean pulmonary artery pressure greater than 20 mmHg and a pulmonary vascular resistance⩾3 Wood Units. Radiographic recognition of early signs of pulmonary hypertension on CT is very important to reduce the diagnostic delay. This talk will focus on the CT appearance of pulmonary hypertension as well as provide a diagnostic approach to its subgroups.

Take Home Points:
- Learn to recognize pulmonary hypertension on CT and the role of the right ventricle.
- How to differentiate the different subgroups of pulmonary hypertension on CT
- What is the role of the different thromboembolic lesions in the pulmonary arterial system for early detection of chronic thromboembolic pulmonary hypertension.

Mesothelioma and pleural surgery

T. Frauenfelder, Zurich/CH

Body: Imaging plays an important role in the detection, diagnosis, staging, response assessment, and surveillance of malignant pleural mesothelioma. The etiology, biology, and growth pattern of mesothelioma present unique challenges for each modality used to capture various aspects of this disease. Clinical implementation of imaging techniques and information derived from images continue to evolve based on active research in this field worldwide.
Pleural mesothelioma is notoriously a tumour with high mortality rate and has a mean survival of 10 months, so that cause-specific mortality well reflects the incidence of disease. Clinical manifestations of mesothelioma are not specific, so the diagnosis of malignant mesothelioma can be difficult with symptoms and clinical findings that can mimic and be mimicked by other diseases. Chest X-ray is the first-line approach and it is generally abnormal in advanced stages of disease, showing in most cases the presence of unilateral pleural effusion or pleural thickening. Diagnostic accuracy of chest X-ray is obviously low, but can be adequate in early stages to suspect the disease. Suspicion is based on the presence of some radiographic signs easily observed: drug-resistant unilateral pleural effusion, unilateral lobulated pleural thickening with or without thickening pleural fissures, multiple masses with peripheral distribution, and loss of volume in the hemithorax involved.
Contrast-enhanced volumetric computed tomography (CT) scan of the chest represents the gold standard to the imaging diagnosis. The features of malignant pleuropathy can be summarized as: circumferential pleural thickening (pleural rind); thickened mediastinal pleura; nodular or lobular borders within the internal profile; irregular borders of the external profile (infiltration of the wall); mediastinal and pericardial infiltration, lymph nodes in extra pleural fat tissues. Pleural effusion is an unspecific sign and pleural calcific or not calcific plaques are indicative of asbestos exposure but not of neoplastic pathology.
Main differential diagnosis is metastatic pleuropathy, which have a more "discrete" and discontinuous distribution, while mesothelioma tends to manifest with a continuous distribution, like a rind. However, there are not specific diagnostic criteria to perform differential diagnosis between metastatic pleuropathy and MPM; considering that pleural metastasis is more frequent than MPM with a ratio of above 95:5.
MPM's CT staging is similarly based on some characteristic features: thickening of the visceral pleura, which is discernible only when effusion is present, and infiltration of contiguous structures such as lung parenchyma, mediastinal organs, chest wall, diaphragm and peritoneum, more visible with multiplanar reconstruction. CT underestimates some features of T staging such as chest wall and peritoneum invasion; furthermore, it has low diagnostic accuracy for N staging (about 50 %). Nevertheless, CT is considered mandatory for patients' staging and follow-up.
Magnetic resonance imaging (MRI) is not routinely performed in the clinical practice for patients with MPM; there is some evidence in literature that MRI signal could be useful to differentiate MPM from benign pleural fibrous plaque. MRI is better than CT for detecting invasion of chest wall, mediastinal and nervous structures as brachial plexus, and peritoneum and is generally reserved for those patients eligible for surgical treatment. Moreover current data shows, DWI could be a useful tool for personalized care in mesothelioma patients.
^{18}F-FDG-PET/CT can show metabolic activity at the level of pleural thickening in case of mesothelioma, allowing differential diagnosis with fibrous pathology in most cases. It can demonstrate lymphadenopathy and distant metastasis with sensibility of 90 % and specificity close to 80 %. PET/CT is better than CT and MRI for N and M staging, improving inter-observer agreement and preoperative staging accuracy.
When MPM is suspected by clinical or radiological data the diagnostic accuracy of thoracoscopy is very high, exceeding 90 %, and complications occur in less than 10 % of cases. Throughout the years different surgical approaches have been proposed, but a great debate around the role of surgery is currently ongoing. Initially P/D was considered only palliative, but during the decades its role was redefined and this type of surgery gained an important position as a radical surgery. Recent studies have shown that survival time after EPP and P/D is similar, while mortality and morbidity are higher post EPP. Moreover, patients treated with P/D appear to have more chances for additional therapies after surgery, also in case of recurrence. Therefore, survival after recurrence seems to be better in patients initially treated with P/D.

Take Home Points:
- Dynamic contrast-enhanced CT is currently the imaging modality of choice for imaging diagnosis, staging and follow-up, but
- MR may be the future one-stop-shop image modality
- Contrast-enhancement in MRI may provide additional information concerning invasion of chest wall, mediastinal and nervous structures
- PET/CT is better than CT and MRI for N and M staging
- Pleurectomy/decortication (P/D) seems to be favourable for patients with resectable tumor.

The work needed to implement the use of AI in CXR interpretation

A.P. Parkar, Bergen/NO

Body: After you have decided to acquire an AI system for your department you need to clarify quite a few important issues before the system is fully operational.
If you are yet to decide what to buy, you should consider Technicathe following:
Is the system approved for use in your country? Are there any GDPR issues?
Is it fully compatible with your IT system?
What is the goal of the system? Detection, workflow prioritisation or diagnosing? Which diagnosis are not identified by the system?
How was the system validated?
Has the vendor disclosed the systems shortcomings and failures?
How are you going to teach the radiologists how to use it? Will there be potential negative changes in workflow?
Do you know if the AI will evolve with your use or is it fixed? If evolving- how can deterioration be picked up; if fixed -how can new targets be added? Who can aid in cases of technical failure, your in-house IT or vendor? If vendor, what is their availability?
What is the liability in cases of failure which causes harm to patients? Have you considered how the use will affect training of new radiologists? How long is the contract and are you prepared for future pricing changes?

Take Home Points:
When implementing an AI system for use in your radiology department you have to consider all aspects from legal, technical, diagnostic, radiology training, patient safety to financial issues.

AI in nodule classification

C. Jacobs, Nijmegen/NL

Body: The success of deep learning, the implementation of lung cancer screening, and recent public challenges have led to numerous publications and commercial products for AI in nodule classification. In this talk, I will give an overview of deep learning algorithms for nodule classification. I will focus on AI for differentiation of different nodule types and AI for nodule malignancy risk estimation. Public challenges, such as the LUNA16 challenge and the Kaggle Data Science Bowl 2017 challenge, and publicly available databases have been drivers for development of novel deep learning algorithms and the performance of these novel algorithms is promising. However, there are remaining challenges that need to be solved. Multiple rounds of external validation and more real-world evidence on the effectiveness of these algorithms is needed. Next to this, integration of these algorithms into clinical practice is still not easy, and combined with an unclear business case, this is currently hindering adoption of this technology in clinical practice.

Take Home Points:
- Publicly available datasets and public benchmarks are important for training and benchmarking of different AI approaches and products
- More modern public databases and more external validation will increase trust in the available AI algorithms
- Adoption of these algorithms in clinical practice is complicated by difficulties with integration and an unclear business case.

AI in Interstitial Lung Disease

J. Jacob, University College London, CMIC, UCL, UCL Respiratory, London/UK

Body: Visual scoring of CT scans to understand disease severity in fibrosing lung disease has been performed for over 20 years. Yet quantifying change in CT patterns over time remains challenging and often does not strongly predict functional measures of disease progression or survival well.
This talk will discuss challenges with visual CT interpretation and the utility of computer analysis of CT imaging. I will discuss ways in which computers have been used to quantify fibrosing lung diseases and touch on some novel patterns of disease that computers have helped identify.

Take Home Points:
- Understand the processes by which computers learn lung CT patterns
- Understand advantages of computer analysis of CTs over visual CT analysis
- Understand the importance of pleuroparenchymal fibroselastosis as an imaging feature in patients with lung fibrosis

Imaging Blunt Thoracic Trauma

B. Hussain, Rotterdam/NL

Body: Our body structures are needed for function.
Trauma is the impact of an external force causing damage to the structures, causing loss of function.
Penetrating injury disrupts the structure of organs and is very visible and clear in its mechanism.
Blunt injury is less visible.
Imaging, especially CT, is amazing in its detection of all kinds injuries and is essential for determining the treatment and prognosis.
The big injuries are obvious for every doctor. Our task as radiologists is to detect the more difficult injuries and to understand what the relevance of each abnormality is.

Take Home Points:
1. Checklist of every structure/organ in the chest and its associated injuries.
2. The underlying mechanism causing the damage.
3. Which function is lost due to the damage.
4. Prognosis.

Incidental findings in thoracic trauma scans

E. Dick, Imperial College NHS Trust, Radiology, London/UK and Imperial College London, Faculty of Medicine, London/UK

Learning Objectives:
1. Relate mechanism of injury in blunt and penetrating trauma to imaging findings
2. Interpret findings in light of patient physiology, and mechanism of injury
3. Distinguish between findings that are trauma related and those that are not
4. Implement a check list to avoid missing incidental injuries

Pulmonary embolism in pregnancy

A. Beale, Great Western Hospital, Radiology, Swindon/UK

Body: Pulmonary embolism remains the leading cause of mortality in pregnancy. There are specific differences in pregnancy when investigating the possibility of PE, primarily related to the need to protect the foetus. However, context is required, as the incidence of PE in pregnancy remains very low, and death extremely unlikely. Although there are specific physiological features in pregnancy that do increase the risk, including pelvic vein compression and hypercoagulable states, the difficulty arises in that breathlessness and chest pains are part of normal pregnancy. Realistically there are only 2 modes of investigation available, CTPA and Perfusion (Q) scans as conventional pulmonary angiography is almost never performed. Wells criteria have not been validated in pregnancy and the role of DVT leg duplex imaging is limited, as invariably negative, and therefore neither cost effective or timely. There are techniques available to minimise dose in CTPA both to the foetus and the mother. The role of measuring D-Dimer is still debated and probably under-utilised in practice. Management of small subsegmental emboli will be discussed as treatment may be more dangerous than ignoring.

Take Home Points:
- CTPA is the most appropriate investigation of PE in pregnancy.
- D-Dimer may have a role to play.
- The positivity of CTPA is extremely low in practice.

Haemothorax and cardiac trauma imaging

M. Brink, Radboud University Nijmegen Medical Center, Department of Imaging, Nijmegen/NL

Body: Initial diagnosis of chest injury should focus on diagnosing potential life-threatening injuries first. In patients with haemothorax and cardiac injury, imaging can help in deciding whether control of bleeding, decompression, resuscitation, or treatment of coronary injury should be started as soon as possible.
This session discusses the role of imaging in the diagnosis and management of haemothorax and cardiac injury, and associated injury patterns and signs at chest imaging. Finally, diagnostic pitfalls and radiological relevant complications of these injuries will be discussed.

Take Home Points:
1. Don't be afraid of chest ultrasonography
2. The heart is not a black box
   - Take direct and indirect signs of cardiac injuries into consideration, including mechanism of trauma
   - Be aware of potential complications, pitfalls and differential diagnoses of cardiac trauma and heamothorax

PET-CT in Lung Cancer

A. Scarsbrook, York/UK

Body: FDG PET-CT is widely utilized in the initial work-up of patients with potentially radically treatable lung cancer due to established superior accuracy for staging of disease compared to other imaging modalities. Tracer uptake is not specific to malignancy and an appreciation of the range of causes of false positive and false negative FDG uptake is critical to ensure accurate interpretation. FDG PET-CT has additional potentially valuable roles in radiotherapy planning and multi-modal treatment response assessment in lung cancer patients. Emerging applications which are the focus of many recent publications include the potential utility of imaging features extracted using advanced analysis (radiomics) to non-invasively characterise tumour phenotype and predict treatment outcome. In addition, the use of artificial intelligence techniques to augment diagnostic utility and improve the efficiency of image evaluation are under evaluation. Finally, a range of non-FDG tracers are under development which may help guide optimal therapeutic strategies for individual patients and reduce the toxicity associated with lung cancer treatments.

Take Home Points:
- FDG PET-CT is highly accurate and cost-effective for confirmation of disease extent in patients with potentially radically treatable lung cancer.
- FDG uptake occurs in a variety of inflammatory processes which can cause false positives. Small primary tumours or metastatic deposits and some well differentiated lung neoplasms may not take up FDG causing false negative results.
- Recent multidisciplinary guidance provides practical recommendations for incorporating FDG PET-CT into radiation treatment planning. Evidence is also growing for the use of FDG PET-CT to assess multi-modal therapeutic response in selected patients.
- Emerging applications include the potential use of radiomics and AI techniques and the advent of novel tracers which show future promise.

Lung cancer pre- and post radiotherapy

H. Prosch, Medical University of Vienna, Department for Biomedical Imaging and Image-Guided Therapy, Computational Imaging Research Lab, Vienna/AT

Body: Radiation therapy is, in addition to surgery and systemic therapy, one of the most important treatment options in patients with lung cancer. In patients with non-small-cell lung cancer, radiotherapy is primarily indicated in peripheral small tumors in patients who are medically inoperable or refuse surgery, in patients with stage III tumors concurrent with chemotherapy, and in patients with stage IV oligometastatic disease and symptomatic primary tumors or distant metastases. Furthermore, radiation therapy is also a mainstay in the treatment of patients with stage I-III (limited stage) small-cell lung cancer.
Imaging plays a central role not only in the planning of radiation therapy, but also in the evaluation of treatment response, complications, and follow-up. Importantly, the response pattern depends, among other factors, on the applied radiation technique. In particular, in stereotactic body radiation therapy, the observed tissue reactions differ from those observed after conventional radiotherapy. Radiologists need to be aware of the typical findings after radiotherapy and their temporal course, and must be familiar with complications and be able to recognize the signs of recurrence.

Take Home Points:
- Radiation therapy is one of the most important treatment options in patients with lung cancer.
- Response pattern depends on the applied radiation technique

Lung Cancer Survivorship: Follow-up of the Lung Cancer Patient after Curative Intent Therapy

J. Taylor, Montreal, Quebec/CA

Body: The objectives of this talk will be to define lung cancer survivorship and how this population will potentially be impacted by lung cancer screening, to recognize the timing and incidence of local recurrence and second primary malignancies in this population, and to be aware of the current follow up recommendations for lung cancer survivors and the existing knowledge gaps for this population.

Take Home Points:
With lung cancer screening, there is an increasing incidence of detection of early stage lung cancers and lung cancer survivors. In this patient population, the risk of local recurrence is highest at 2-4 years and then declines. This population also remains at risk for development of second lung primary lung cancers. CT surveillance can detect >60% of local recurrences and >90% of second primary lung cancers.
Current guidelines for long term follow up of lung cancer survivors vary slightly but in general recommend diagnostic CT every six months in the first two years after initial diagnosis followed by long term surveillance with annual low dose CT. These guidelines are informed by expert opinion with limited empirical data and no clear evidence for improved survival in asymptomatic patients. In the future, a patient-specific approach based on multiple factors may help to guide follow up recommendations.
As the number of early stage cancers detected increases with lung cancer screening, and as treatment options continue to improve for this population, this may increase the importance of surveillance and early detection of recurrence or second primary cancers.

Thoracic Ultrasound

T. Frauenfelder, Zurich/CH

Body: In the last years, a new imaging application of sonography has emerged in the clinical arena: lung ultrasound (LUS). From its traditional assessment of pleural effusions and masses, LUS has moved towards the approach of imaging the pulmonary parenchyma, mainly as a point-of-care technique. Although limited by the presence of air, LUS has proved to be useful in the evaluation of many different acute and chronic conditions, from cardiogenic pulmonary edema to acute lung injury, from pneumothorax to pneumonia, from interstitial lung disease to pulmonary infarctions and contusions. It is especially valuable since it is a relatively easy-to-learn application of ultrasound, less technically demanding than other sonographic examinations. It is quick to perform, portable, repeatable, non-ionizing, independent from specific acoustic windows, and therefore suitable for a meaningful evaluation in many different settings, both inpatient and outpatient, in both acute and chronic conditions.

Take Home Points:
- To describe and interpret the different Lung US pattern.
- To become familiar with the strengths and limitations of the technique.
- To learn when and how to perform a US study in the intensive care patient.
- To be familiar with POCUS.

Why chest radiologists should be involved in coronary CTA

J. Bremerich, University Hospital, Department of Radiology, Basel/CH

Purpose: Coronary calcium scoring combined with CT Angiography (CTA) of coronary arteries are powerful tools for management of patients with suspected / known stable coronary artery disease. This has been highlighted in the 2019 guidelines from the European Society of Cardiology for diagnosis and management of chronic coronary syndrome. The European Society of Cardiovascular Radiology (ESCR) expects a sustainable substantial increase of coronary CTA and would like to encourage all radiologists to be involved in cardiac imaging.

Background and Methods: Coronary calcium scoring from native cardiac CT is currently used to compare individual results with a reference population to obtain "coronary age" and "percentile of coronary calcifications". This information is very helpful to guide preventive care such as life-style modification or specific medication (e.g. statins). Coronary CTA is an attractive complement, since it discloses soft and calcified plaques in coronary arteries as well as the degree of stenosis (Figure). Unlike catheter angiography, CTA enables visualization of wall based plaque without visible stenosis, but with elevated risk for plaque rupture and subsequent coronary embolisation.

Conclusion: Given the high impact of coronary calcium scoring combined with CTA as highlighted by current guidelines and the continously growing demand, ESCR encourages all radiologists to get involved in coronary imaging.

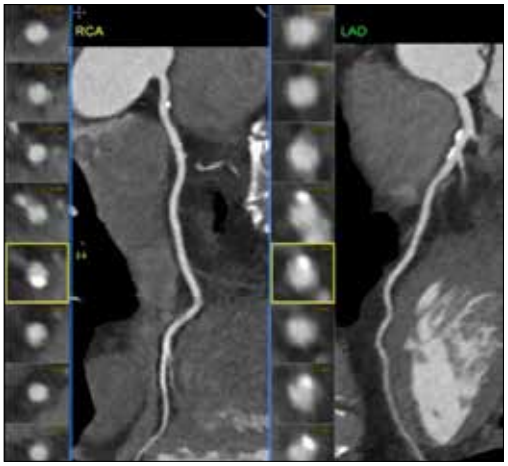

Curved reformats of coronary CT Angiography show left anterior descending (LAD) and right coronary artery (RCA). Reconstructions perpendicular to the vessel centerline (small images on the left) are used to quantify stenoses, in this case < 50% and thus not hemodynamically relevant.

Take Home Points:
ESCR encourages all radiologists to get involved in coronary calcium scoring and CTA.

How to do coronary CTA in 20 minutes

R. Vliegenthart, University Medical Center Groningen, Radiology, Groningen/NL

Body: In this presentation, an introduction is given to the indications, preparation, scanning and reconstruction techniques, and evaluation of coronary arteries in coronary CTA. This presentation is aimed as an introduction into coronary CTA for radiologists without prior experience. The importance of coronary CTA in the work-up of patients with chest pain will be highlighted.

Take Home Points:
- Coronary CTA has gained an important role as a first-line test in the work-up of patients with chest pain and low-intermediate pre-test probability of coronary artery disease.
- In the coming years, numbers of coronary CTA are expected to show an important increase.
- Nowadays, diagnostic images of the coronary arteries can be obtained in most patients and at acceptable radiation dose, including patients with higher body mass or irregular/high heart rate.
- Even in non-cardiac chest CT scans, especially those obtained with higher temporal resolution, the coronary arteries may be assessable.

NSIP revisited

A. Devaraj, London/UK

Body: Importance has been placed in recent guidelines on the distinction between a UIP pattern of lung fibrosis and other conditions, including NSIP. This presentation will re-cap the clinical and radiological features of NSIP. Emphasis will be placed on a practical approach to evaluating NSIP on CT. Recent literature including novel CT signs will be reviewed, including in the setting of connective tissue diseases and IPAF.

Take Home Points:
- A diagnosis of connective tissue disease related NSIP may sometimes be suspected based on CT signs.
- Understanding how clinical +/- pathological features integrate with CT is important for establishing final MDT diagnosis in many instances

Smoking related ILD

A. Oikonomou, Toronto/CA

Body: Apart from lung cancer and chronic bronchitis smokers' lungs may develop a large spectrum of pathologic abnormalities involving the interstitium, extending from inflammation, to fibrosis and emphysema. Although in early stage most of these entities are asymptomatic they may ultimately progress to pulmonary fibrosis and are associated with a high-risk of all-cause mortality. In addition to that approximately 8 % of smokers have interstitial lung abnormalities (ILA) which have been associated with reduced survival.
Acute eosinophilic pneumonia (AEP) is associated with significant changes in smoking habits and in two thirds of cases patients are smokers. It is the only entity that is associated with acute symptoms and mechanical ventilation is often required. Imaging findings simulate pulmonary edema, infection, drug toxicity and ARDS.
Pulmonary langerhans histiocytosis (PLCH) is associated with smoking history in 95 % of cases and 20 % of patients may be asymptomatic at diagnosis. CT findings include upper lobe predominant bizarre-shaped cysts, cavitary nodules and ground glass opacities. Sparing of the lung bases and anteromedial aspects of middle lobe and ligula is characteristic.
Respiratory bronchiolitis (RB) and desquamative interstitial pneumonia (DIP) are uncommon entities of the same spectrum related to smoking with more insidious symptoms of dyspnea and cough with DIP having worse prognosis. CT findings in RB include upper lobe predominant hazy centrilobular micronodules with emphysema, bronchial wall thickening and air-trapping, while in DIP there is lower lobe predominant ground glass opacities with subtle reticulation.
Airspace enlargement fibrosis or smoking related interstitial fibrosis is characterized by subpleural and peribronchiolar fibrosis with preservation of the lung architecture. RB and emphysema are seen. On CT there are subpleural sparing thin-walled lung cysts in the deeper lung parenchyma associated with reticular and ground glass opacities. Differentiation from UIP on CT may be challenging. The prognosis is favorable than UIP.
Smoking may cause NSIP (non-specific interstitial pneumonia)-pattern fibrosis. Differentiating DIP and NSIP on imaging in smokers can be challenging and they may also overlap. However NSIP is more likely to progress to severe fibrosis in smokers compared to DIP.
Smoking is strongly associated with UIP and commonly coexists with emphysema. Typical CT findings include subpleural basal predominant traction bronchiectasis and honeycombing and the prognosis is worse.
Due to significant overlapping of imaging and pathologic findings in smokers interstitial lung disease in smokers may be classified as "unclassifiable IIP" with airway centered cystic lesions with fibrosis.
Management decisions should be based on integration of pathologic, radiologic and clinical findings and consideration of the expected disease behavior in multidisciplinary discussions (MDD).

Take Home Points:
1. Smoking related interstitial lung diseases encompass a large variety of different entities affecting the interstitium.
2. Although asymptomatic or mildly symptomatic at early stages, they may lead to pulmonary fibrosis and may be related with reduced survival.
3. Significant overlapping occurs in SRILDs and often management decisions need to be based on multidisciplinary discussion meetings.

Photon-counting CT – Technical and clinical applications in the imaging of coronary artery disease

C. Xie, Acute Vascular Imaging Centre, John Radcliffe Hospital and University of Oxford, Oxford/UK

Body: Cardiovascular CT is the most used non-invasive imaging modality for the assessment of coronary artery disease. However, there are image resolution limitations due to the functionality of the conventional energy-integrating detectors of the current CT scanners. Photon-counting detectors, on the other hand, is capable of direct discrimination of each single incoming x-ray photon according to its energy. This technologic advancement offers the potential to significantly improve spatial resolution, reduce blooming artefact, and provide multi-energy acquisition for better tissue discrimination. The objective is to present these technologic developments of photon-counting CT and demonstrate the use of the novel scanner in the imaging of coronary artery disease.

Take Home Points:
- The image resolution of current CT scanners is limited by the use of energy-integrating detectors
- Photon-counting detectors directly convert individual x-ray photons according to their energy
- The technology offers improvements in image resolution and better tissue discrimination in the imaging coronary artery disease

MRI of the Airways

J. Biederer, University Hospital Heidelberg, Diagnostic and interventional Radiology, Heidelberg/DE

Body: The diagnostic scope of common clinical tests like pulmonary function tests (PFT, i.e., spirometry), lung diffusion (DLCO) and blood gas analysis is limited since they do not account for regional changes of lung function. Furthermore, they are insensitive to early changes of peripheral airways, while these contribute little to total airway resistance and thus can hide a significant amount of disease.
Typically, computed tomography (CT) has become the technique of choice to complement the standard tests. Alternatively, magnetic resonance imaging (MRI) offers radiation free imaging, but at lower spatial resolutions. Native MRI shows healthy airways down to the first sub-segmental level/4th order (CT: 8th). Bronchiectasis can be identified by wall thickening and accumulation of fluid. Smaller airways become visible, when altered by peribronchiolar inflammation or mucus retention (tree-in-bud).
However, the particular strength of MRI is functional imaging. Expiratory airway collapse can be directly visualized down to the segmental level with dynamic MRI (CT: lobar level). Air trapping on expiratory scans indicates small airways disease. Indirectly, airway obstruction is represented by perfusion deficits from hypoxic vasoconstriction on dynamic contrast enhanced MRI (DCE-MRI). Direct visualization of the large airways and peripheral ventilation deficits can be achieved with hyperpolarized noble gases (^{3}He, ^{129}Xe). Non-contrast enhanced ventilation-/perfusion-weighted MR imaging with Fourier decomposition may serve as an alternative to these elaborate techniques.
Altogether, for research (e.g., in chronic obstructive lung disease), but also increasingly in clinical work (e.g., in cystic fibrosis) MRI of the lungs excels with its unique combination of morphologic and functional aspects.

Take Home Points:
- Airways are directly visualized down to the 4th order (MRI).
- Bronchiectasis and mucous plugging increase the visibility of small airways.
- Mosaic perfusion and air trapping are indirect signs of small airways disease.
- Perfusion deficits after i.v.-contrast reflect hypoxic vasoconstriction in ventilation disorders.
- MRI with hyperpolarized noble gases directly visualizes large airways and ventilation deficits.

Imaging in fungal infection

T. Franquet, Hospital de Sant Pau, Radiology, Barcelona/ES

Body: Imaging plays a crucial role in the detection and management of patients with a suspected acute or chronic respiratory fungal infection. Although some chest radiographic findings are pathognomonic for specific conditions, in most cases, the diagnostic process depends upon correlating the chest radiographic findings with the clinical scenario.
Although fungal lung infections can occur both in immune-competent and immune-compromised individuals, the increasing incidence is likely multifactorial and related to an ever-growing population of susceptible patients, including immunocompromised individuals and transplantation patients, as well as massive implementation of combination antiretroviral therapy (cART).
Despite the declining incidence of Pneumocystis jiroveci pneumonia (PJP) among HIV patients, people living with human immunodeficiency virus (PLWH) are at risk of developing fungal infections, which require intact T-cell function for containment.
In PLWH, major risk factors for invasive pulmonary aspergillosis include CD4 cell counts <50 cells/mm^3 and neutropenia. Chronic pulmonary aspergillosis can occur in COPD patients and in those having pre-existing fibrotic diseases.
The Mucor species are ubiquitous, saprophytic molds, usually found in soil and in decaying food. Radiographic manifestations are non-specific and include consolidation, cavitation or abscess formation, nodules, and masses.
Candida sp. have been increasingly recognized as an important source of fungal pneumonia in patients with hematologic malignancies (acute leukemia and lymphoma) and allogeneic bone marrow transplant recipients.
The aim of this lecture is to review the imaging findings related to fungal infections diseases emphasizing some uncommon manifestations.

Take Home Points:
- Combining clinical factors with characteristic imaging features yields the most specific and accurate differential diagnosis for radiologic findings in fungal infections
- The chronic form of Aspergillus infection can occur in patients with COPD and coexiist with non-tuberculous mycobacteria

TB: What's new and what's old?

I. Tyurin, Moscow/RU

Body: Approximately 1.7 billion people worldwide are infected with Mycobacterium tuberculosis, of which more than 20 million are active cases. The reasons for resurgence of infection include a rise in reactivation disease in the elderly, a growing migrant population and spread of drug resistant strains as well as persistent HIV epidemic. The incidence of pulmonary nontuberculous mycobacterial infection is also on the rise, and imaging signs of lung disease often may be indistinguishable with usual MBT. The pathology of the pulmonary infection depends on the sensitivity of the infected host and is classified as primary or postprimary. Primary pattern represents infection from recent contact with the pathogen. Post primary pattern results from reactivation of a dormant focus within the lungs or repeat exogenous contamination. Thoracic tuberculosis produces a broad spectrum of radiological abnormalities. The main patterns include parenchymal, airway, vascular, mediastinal, pleural, and chest wall lesions. Common causes of a missed diagnosis of thoracic tuberculosis are failure to recognize hilar and mediastinal lymphadenopathy as a manifestation of primary disease in adults, overlooking of minimal productive lesions or reporting them as inactive. In HIV infected patients the imaging features depend on the degree of immune suppression. A pattern of post primary disease is also usually seen among patients with decreased immunity due to alcoholism, renal failure, diabetes mellitus, ageing, malignancy, renal and cardiac transplantation. New imaging modalities are commonly used now for evaluation of mycobacterial disease, including PET/CT as a marker of disease activity and EBUS for morphological confirmation of mediastinal lymphadenopathy. Digital tomosynthesis with or without a low-dose technique is superior to radiography for the detection of lung lesions in patients with pulmonary mycobacterial disease. Chest X-Ray remains an important tool for screening of tuberculosis in high-risk population. CAD plays an increasing role in detecting, characterization, and even differential diagnosis of pulmonary tuberculosis with pneumonia and lung cancer. CAD also can be used to identify a large proportion of normal CXRs in a TB screening setting at high sensitivity and could therefore be an instrument of triage.Future work should focus on further increasing CAD specificity and prospective evaluation in screening programmes. It's even more important in high-burden, low-resource countries, where the availability of skilled radiologist is limited, CAD could be used as the sole reader for screening

Take Home Points:
- *Mycobacterium tuberculosis* remains an important and even more complex option for differential diagnosis in thoracic imaging
- Common imaging patterns includes hilar and mediastinal lymphadenopathy, cavities, and signs of bronchogenic spread
- The imaging features of tuberculosis are strongly depended on the degree of immune suppression
- Imaging signs of nontuberculous mycobacterial infection often identical to those of usual mycobacterial tuberculosis
- New imaging modalities include PET/CT as a marker of disease activity and EBUS for morphological confirmation of mediastinal lymphadenopathy.
- CAD plays an increasing role in detecting, characterization, and even differential diagnosis of pulmonary tuberculosis

Acute and long term Covid imaging

W. de Wever, Leuven/BE

Body: The most important lung-findings in the acute stage of Covid-19 infection are peripheral and bilateral ground glass opacities (GGO) and consolidation when the disease progresses. Other signs are crazy-paving pattern, reticulation and cystic changes. Disease severity, age, longer hospital stay and a high CT severity score at baseline are predictors of long-term sequelae of Covid infection. At discharge, residual disease has been reported in up to 94 % of patients. The rate of full resolution at patient discharge varies between studies, according to the initial severity of the infection. Chest CTs improve gradually over time as reflected in a significant reduction in CT severity scores. About half of the patients have a normal chest CT at 3 months. Commonest abnormalities at 3 months are multifocal ground glass opacities and reticulations. Residual CT changes at 1 year are mostly mild. CT findings consistent with fibrosis are present in about 10 % at 1 year.
At 3 months follow-up, GGO are the most frequently founded CT findings, observed in up to two-third or more of patients. Other CT findings include band-like and perilobular opacities, reticulation and interstitial thickening. Fibrotic-like lung changes on CT are reported in up to 26 % of patients. There is a risk of overestimating definite fibrotic changes like traction bronchiectasis. A mosaic attenuation pattern is reported in 66 % of patients with previous severe/critical disease. Mosaic attenuation might be due to either microvascular obstruction or residual small airway disease.
At 6 months follow-up, fibrotic-like changes are reported in 35% of covid-19 patients who had severe disease. These fibrotic-like changes included bronchodilatation and honeycombing, as well as interlobular thickening and thickening of the pleura.
At 12 months after discharge, persisting of lung changes is reported in up to 24% of patients. Together with the reduction of CT abnormality prevalence, the spectrum of findings changed. The predominant residual finding is ground glass opacities.
Imaging follow-up should be performed after a delay to allow resolution of the reversible inflammatory process. There are recommendations to perform CT follow-up at 12 weeks post discharge in patients with persistent respiratory symptoms.

Take Home Points:
- Disease severity, age, longer hospital stay and a high CT severity score at baseline are predictors of long-term sequelae of Covid infection.
- Chest CTs improve gradually over time as reflected in a significant reduction in CT severity scores.
- At 3 months follow-up, GGO are the most frequently founded CT findings, observed in up to two-third or more of patients.
- At 6 months follow-up, fibrotic-like changes are reported in 35% of covid-19 patients who had severe disease.
- At 12 months after discharge, the predominant residual finding is ground glass opacities.
- Imaging follow-up should be performed after a delay to allow resolution of the reversible inflammatory process.

Measuring nodule size – Methods and outcomes

A. Nair, London/UK

Body: Pulmonary nodule size and growth remain the primary determinants of management strategies for solid nodules that do not demonstrate unequivocal benign or malignant features. Diameter measurement is convenient and easy to perform, and is the preferred method of assessment in most pulmonary nodule guidelines. However, its susceptibility to inter- and interobserver variation, and tendency to both over- and underestimate nodule size, can limit its utility in accurately detecting growing nodules, or leading to overzealous investigation of benign nodules. Volumetric assessment is now the main method of recommended assessment in European lung screening and British nodule management guidelines, but is also susceptible to variation in software and technical factors. Volume doubling time (VDT) is used in both the latter guidelines to determine surveillance intervals or the need for immediate investigation. For solid nodules, a greater size at baseline does predict the likelihood of malignancy, and has been incorporated into risk prediction models.
Conversely, measurement for sub-solid nodules (SSNs) – nodules that are more likely to represent lesions in the pulmonary adenocarcinoma spectrum – still relies on diameter assessment, and this requires measuring both the solid component and whole nodule. Variation in designating a nodule as part- or non-(ie ground-glass) solid invetiably leads to variations in measuring these components too. An increased solid component at baseline, as well as a growing solid component, are associated with an evolving invasive element. In other words, the size of SSNs is used not so much for predicting the likelihood of malignancy, but more for assessing aggressiveness. However, accurate measurement needs to be accompanied by assessment of changes in density and adverse morphological features that also herald invasion.

Take Home Points:

1. Measurement methods for solid nodules differ between guidelines: Fleischner Society and ACR Lung-RADS recommend average diameter measurement, while British and European screening guidelines recommend volumetric assessment when reliable and available, or maximum diameter when not.
2. Baseline size and nodule growth, as assessed by Volume Doubling Time (VDT), are used to determine nodule management in European screening and British guidelines.
3. Both diameter and volumetric assessment are susceptible to certain factors that influence variation, but the magnitude of variation is in general greater for diameter.
4. The reliability of volumetric segmentation of solid pulmonary nodules is still assessed subjectively – there is no objective measure.
5. Maximum Diameter assessment – of primarily the solid component but also whole nodule – is the main method of measurement for subsolid nodules, but has to be accompanied by assessment of other morphologic features and density.

Importance of morphological assessment

A. Farchione, Fondazione Policlinico Universitario Agostino Gemelli IRCCS, Department of Diagnostic imaging, oncologic radiotherapy and hematology, Rome/IT

Body: The definition of malignancy of lung nodules is a challenging task, especially for smaller ones: the early diagnosis of cancer is important to ensure the possibility of treatment, however it is essential to minimize false positive results in order to avoid unnecessary and expensive exams. According to international guidelines, the work-up includes the definition of the pre-test probability of malignancy, based on clinical data, and then the evaluation of imaging results.

The most important imaging parameters, in both screening and non-screening contexts, are dimension/growth rate and the morphological characteristics of the nodule. Morphological parameters are determined by the histopathology of the nodule and, on imaging, they describe the density (solid or sub-solid), internal characteristics (e.g. content of fat, calcification, air elements), shape (e.g. round, oval), margins (e.g. smooth, lobulated, spiculated) and the effect on the surrounding structures (e.g. pleural retraction, vascular convergence) of the nodule itself. The most reliable morphological imaging features are those that are indicative of benignity, like triangular morphology, fat attenuation and internal calcifications. Multiple features are associated with malignancy for example spiculations, air bronchogram/bubble-like lucencies and pleural retraction. Among them, morphological parameters are fundamental in identifying the presence of a tumour characterized by slow-growth, such as how an adenocarcinoma may behave. Finally the dynamic behaviour after contrast medium administration is an additional instrument for selected cases.

To support the estimation of the probability of malignancy, predictive models that combine a patient's clinical characteristics with nodule imaging features have been implemented. Several risk calculators that use nodule dimensions and morphological characteristics have been described and, recently, machine learning/deep learning models have been developed to automatically extract mathematical descriptors of nodule structure.

Take Home Points:

- The most important imaging parameters useful in defining the nodule probability of malignancy are dimension/growth rate and morphological characteristics.
- Morphological parameters describe density, internal characteristics, shape and margins of a nodule, and the effect on the surrounding structures.
- The most reliable morphological features are those that are indicative of benignity, moreover morphological parameters are fundamental in identifying the presence of slow-growth tumours.
- Multiple predictive models of nodule malignancy have been implemented, combining the patient's clinical characteristics with nodule imaging features, both „traditional" and obtained by Artificial Intelligence.

Benign lung tumours

A. Snoeckx, Edegem/BE

Body: Although the majority of lung masses are histologically classified as malignant, a variety of rare benign lung tumors can be seen. Benign lung tumors can manifest as a solitary nodule, mass or endobronchial lesion. Histopathologically this group of tumors comprises of papillomas, adenomas, cystadenoma, carcinoids, hamartoma, chondroma, inflammatory myofibroblastic tumors. Computed Tomography is the imaging modality of choice, but diagnosis can be challenging. Although some lesions show characteristic features, findings are often non-characteristic. Besides characterization, imaging plays an important role in defining the precise anatomic location, relationship to surrounding structures, extent, and surgical or therapeutic guidance. Benign lung tumors should be differentiated from non-tumoral lesions that present with a mass-like appearance.

Take Home Points:
- Some benign lung tumors show specific imaging characteristics
- A number of benign lung tumors may show high uptake on PET
- Imaging diagnosis of benign lung tumors can be challenging

ORAL + KSTR ABSTRACTS

Abstracts appear as submitted to the system and have not been checked for correctness and completeness.

Automatic evaluation of Bronchial Parameters using a combined Open-Source Artificial Intelligence and Optimal-Surface Graph-Cut Method

I. Dudurych[1], A. Garcia-Uceda[2], J. Petersen[3], R. Vliegenthart[1], M. de Bruijne[2]; [1]University Medical Centre Groningen, Radiology, Groningen, Netherlands; [2]Erasmus MC, Rotterdam, Netherlands; [3]University of Copenhagen, Copenhagen, Denmark

Purpose/Objectives: Diverse CT-based bronchial parameters correlate with disease status. However, accurate segmentation and measuring of the bronchial lumen and walls remain a challenge, often requiring much time and manpower.
We propose a joint methodology to obtain automatically bronchial parameters from CT scans, by combining a deep learning method to extract the airway lumen with an optimal surface graph-cut method to segment the airway wall.

Methods and Materials: Manually corrected bronchial segmentations of 24 ImaLife (Imaging in Lifelines) low-dose chest CT scans were used to train a 3D-U-Net (Bronchinet) for lumen segmentation. The method performance was assessed by the Dice similarity coefficient and percentage centreline completeness. The settings of the optimal surface graph-cut method (Opfront) were optimised using the COPDGene phantom scanned with the ImaLife protocol. Bronchinet lumen segmentation were used as initial seed for Opfront to automatically segment the airway walls. The tool-chain was used to segment and quantitatively measure the airways for 191 ImaLife participants who underwent a repeat scan an average of 3 months from their initial scans. Limits of Agreement (LoA) and coefficient of determination (R^2) were calculated for the initial and repeat scan bronchial parameters of wall area percentage (WA %), luminal area (LA) and square root of the wall area of a hypothetical airway with an internal perimeter of 10 mm (Pi10), to assess reproducibility of the automated method.

Results: The Bronchinet Dice coefficient was 0.876±0.076, and segmentation completeness was 83.8%±7.9 %, both compared to the ground truth segmentations. Graph-cut segmentation of the COPDGene phantom resulted in sub-voxel accuracy; it estimated the inner diameter within an average unsigned error of 3.1 % (0.13±0.07 mm), and the outer diameter with an average unsigned error of 5.8 % (0.35±0.20 mm). 376 (98 %) Scans were successfully segmented and measured automatically. The time to process a scan was 28±4 min. R^2 ranged from 0.93 at the trachea to 0.47 at the 6th generation for LA, and from 0.84 to 0.50 for WA %. LoA was ±0.1 mm for Pi10 with a mean difference of 0.00 mm. For LA, LoA and mean difference ranged from ±34 mm^2 and -1.3 mm^2 at the trachea to ±4.6 mm^2 and 0.1 mm^2 at the 6th generation. For WA %, LoA ranged from ±1.5 % and 0 % at the trachea to ±4.9 % and 0 % at the 6th generation.

Conclusion: The proposed fully automatic bronchial parameter measurement approach has a high success rate and is a reliable way to automatically and quantitively assess the airway tree of participants up to the 6th generation with a low-dose chest CT scan.

Deep learning-based air trapping quantification analysing structure-function relationships in children with cystic fibrosis using paired inspiratory-expiratory ultra-low dose CT

S.M. Muller[1, 2, 3], S. Ram[4, 5], K.J. Bayfield[6], J.H. Reuter[1, 2, 3], S. Gestewitz[1, 2, 3], L. Yu[7], M.O. Wielpütz[1, 2, 3], H.-U. Kauczor[1, 2, 3], C.P. Heussel[2, 3], T.E. Robinson[8], B.J. Bartholmai[7], C.R. Hatt[5, 9], P.D. Robinson[6], C.J. Galban[4, 5], O. Weinheimer[1, 2, 3]; [1]University Hospital Heidelberg, Diagnostic and Interventional Radiology, Heidelberg, Germany; [2]German Center for Lung Research (DZL), Translational Lung Research Center Heidelberg (TLRC), Heidelberg, Germany; [3]Thoraxklinik at University of Heidelberg, Department of Diagnostic and Interventional Radiology with Nuclear Medicine, Heidelberg, Germany; [4]University of Michigan, Department of Biomedical Engineering, Ann Arbor, MI, United States; [5]University of Michigan, Department of Radiology, Ann Arbor, MI, United States; [6]The Children's Hospital at Westmead, Department of Respiratory Medicine, Westmead, New South Wales, Australia; [7]Mayo Clinic, Department of Radiology, Rochester, MN, United States; [8]Center for Excellence in Pulmonary Biology, Stanford University Medical Center, Department of Pediatrics, Palo Alto, CA, United States; [9]Imbio LLC, Minneapolis, MN, United States

Purpose/Objectives: Cystic fibrosis (CF) lung disease is a progressive, genetic disease and air trapping (AT) is considered to be one of its important early markers. The correct radiographic assessment of AT requires the examination of paired inspiratory-expiratory computed tomography (CT) scans and is subject to inter-reader variability [1]. Conventional threshold-based solutions are primarily designed for adults and, due to higher lung densities in children, less suitable for the quantitative CT analysis in pediatrics. Because of the ongoing trend towards lower radiation doses in lung CT imaging, a continuous revision of quantitative post-processing methods is needed. We examined a deep learning approach for AT quantification, adopted from Ram et al. [2], and addressed the extractability of functional information by focusing on maintaining structure-function relationships for ultra-low dose (ULD) compared to low dose (LD) CT.

Methods and Materials: 52 CF subjects (11.3±3.6 years) underwent paired spirometry-guided inspiratory-expiratory CT scans preformed at LD (CTDI 1.22±0.56mGy) and ULD (CTDI 0.22±0.05mGy) in the same session. Multiple breath washout was conducted to evaluate the lung ventilation functionality in form of the lung clearance index (LCI). The inspiratory CT scan was registered to the expiratory CT scan. A densely connected convolutional neural network (DenseNet) was trained to segment AT using 2D axial slices of the expiratory and the corresponding registered inspiratory CT scan as two-channel input and the radiographic assessment, performed by a trained radiologist, as ground truth. To define the ground truth segmentation, each expiration and corresponding inspiration CT scan were viewed next to each other in the in-house software YACTA [3]. An appropriate threshold to highlight severe AT regions was chosen using an integrated slider functionality.

Results: For each patient in the test set, the normalized sum of the DenseNet output probabilities was computed over the entire lung. Analysing the correlation with the LCI, a strong correlation can be observed for LD (r=0.95, p<0.001) and ULD (r=0.93, p<0.001) (Figs. 1 (a) and (b)). Fig. 1 (c) shows a strong correlation between LD and ULD (r=0.98, p<0.001) and small ULD-LD differences can be observed in Fig. 1 (d) (mean difference 0.13±0.37 %). DenseNet and ground truth AT correlate strongly for LD (r=0.91, p<0.001) and ULD (r=0.75, p<0.01) (Fig. 2). Inputs, ground truth and the DenseNet output probability map are shown in Fig. 3 and 4 for LD and ULD, respectively. In both cases, the DenseNet achieves a good AT quantification.

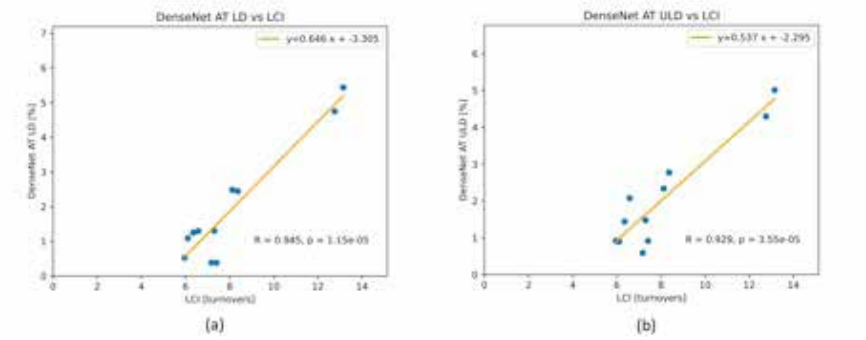

Fig. 1: DenseNet air trapping (AT) analysis comparing low dose (LD) and ultra-low dose (ULD). Normalized sum of the DenseNet output probabilities, computed over the entire lung, correlated with the LCI for (a) LD and (b) ULD. (c) Correlation between LD and ULD. (d) Bland-Altman analysis.

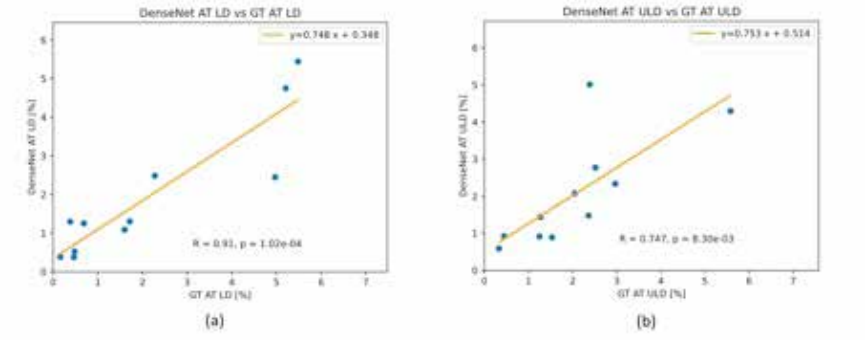

Fig. 2: Normalized sum of the DenseNet output probabilities, computed over the entire lung, correlated with the radiographic ground truth (GT) for (a) low dose (LD) and (b) ultra-low dose (ULD).

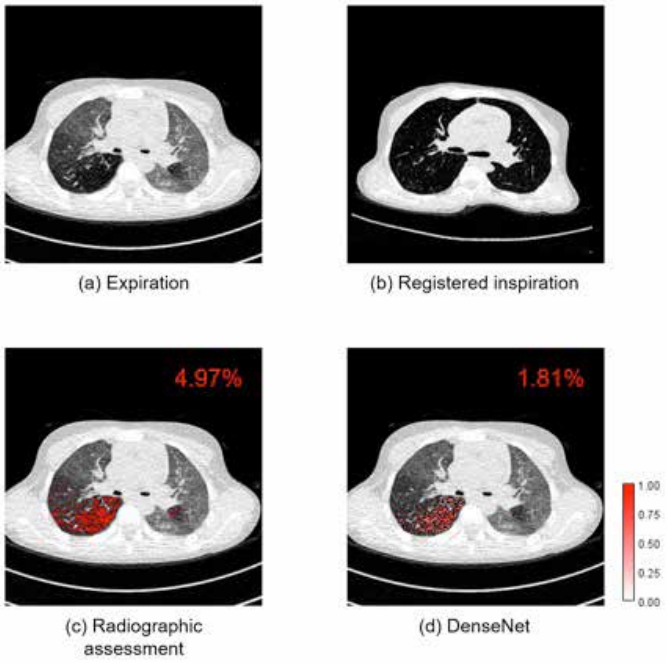

Fig. 3: Inputs (expiration, corresponding registered inspiration), radiographic assessment, and the resulting DenseNet probability map for a low dose CT scan. The percentage of air trapping computed over the entire lung is displayed in the upper right of image (c) and (d) (probability±0.5). WL: -400 HU, WW: 1100 HU.

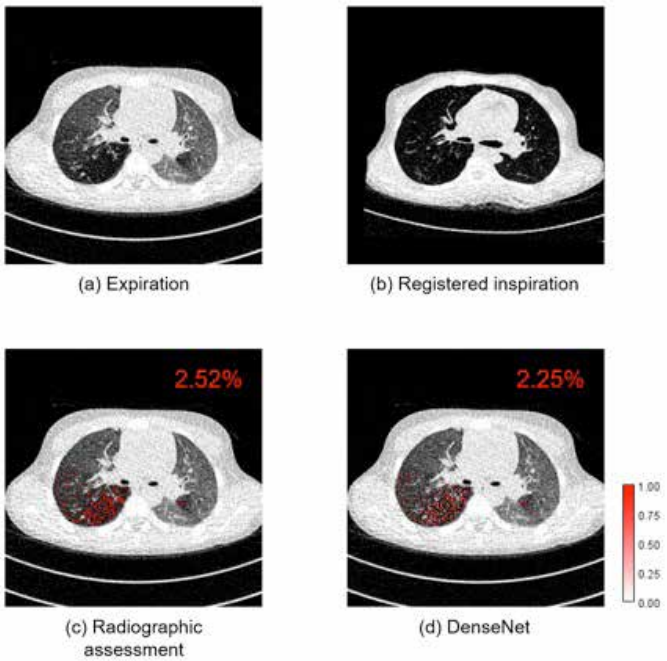

Fig. 4: Inputs (expiration, corresponding registered inspiration), radiographic assessment, and the resulting DenseNet probability map for the ultra-low dose CT scan corresponding to Fig. 3. The percentage of air trapping computed over the entire lung is displayed in the upper right of image (c) and (d) (probability±0.5). WL: -400 HU, WW: 1100 HU.

Conclusion: AT quantification results were comparable for ULD and LD while structure-function relationships were maintained. The results are limited to the available number of patients.

References:
[1] Hoesein, Firdaus A. Mohamed, and Pim A. de Jong, (2017), Air trapping on computed tomography: regional versus diffuse, European Respiratory Journal, 49.1
[2] Ram, Sundaresh, et al., (2021), Improved detection of air trapping on expiratory computed tomography using deep learning, Plos one, e0248902, 16.3, https://doi.org/10.1371/journal.pone.0248902
[3] Weinheimer, Oliver, et al., (2019), Influence of inspiratory/expiratory CT registration on quantitative air trapping, Academic radiology, 1202-1214, 26.9

Deep learning-based quantification of perfusion abnormalities in chest MRI for cystic fibrosis

F. Ringwald[1], L. Dulz[1], A. Martynova[1], U. Eisenmann[1], M.O. Wielpütz[2]; [1]Institute of Medical Informatics, University Hospital Heidelberg, Heidelberg, Germany; [2]Department of Diagnostic and Interventional Radiology, University Hospital Heidelberg, Heidelberg, Germany

Purpose/Objectives: In the assessment of cystic fibrosis (CF) lung disease, magnetic resonance imaging (MRI) has been introduced for routine imaging and interventional trials. A morpho-functional MRI scoring system was developed to monitor disease progression and therapy response, including scoring lung perfusion abnormalities [1]. Manual, visual scoring by a human operator is tedious, time-consuming and prone to inter- and intra-reader variability [2]. Hence, fully automated approaches such as deep learning are desirable for reader-independent, reproducible quantitative measurements of CF lung disease severity based on MRI. In this work we aimed for an automated classification of lung perfusion abnormalities in CF on subtracted perfusion MRI.

Methods and Materials: Standardised 1.5T MRI has been performed at our center for more than a decade, incl. 4D perfusion imaging with injection of 0.1mmol/kg bodyweight of gadolinium-based contrast material. From this data-pool, 669 individual MRI scans were retrieved for training of a custom pre-trained convolutional neural network. Patients' age ranged from three months to 51 years. A single reader scored all MRI exams for perfusion abnormalities on a scale of 0–12 as ground truth (low defects to high defects). The data was grouped in six different classes to account for the low frequency of low and high scores. A VGG-16 net was adapted to group the information of the individual slices of the perfusion series as seen in Figure 1. Pre-processing was conducted in form of normalization, lung segmentation and selection of regions of interests. Subsequently, data augmentation was applied and the image data were split into training, validation and test set and training was carried out.

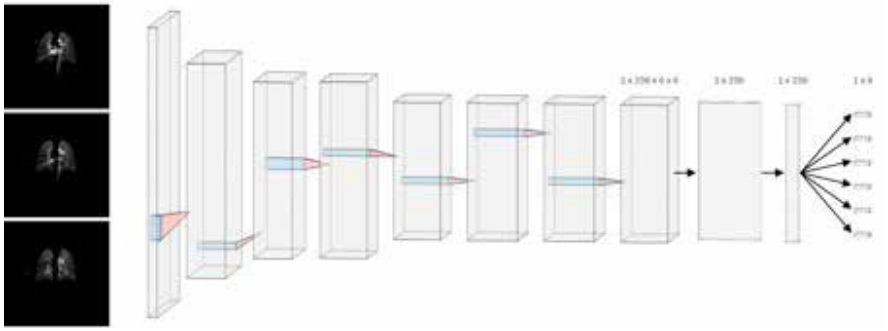

Figure 1: Network architecture of custom VGG-16 net. Scores from the global perfusion score were aggregated to create six subclasses as follows: Class [contained global perfusion score]: 0 [0,1]; 1 [2,3]; 2 [4,5]; 3 [6,7]; 4 [8,9]; 5 [10,11,12]. The final classification output ranges from 0 to 6.

Results: Preliminary classification results can be found in the confusion matrix in Table 1. The overall accuracy is 83.72 % with an average sensitivity of 47.32 % and specificity of 89.77 %. Although class 5 contains lungs from patients with the three highest perfusion scores, having five patients for classification is too few and incorrect classifications weigh heavy. As an overall trend, misclassification into the two adjacent classes is notable. This is in line with the general high inter- and intra-reader variability between observers [2]. If the adjacent classification were to be considered correctly, overall accuracy would increase to 90.43 %.

		Assigned class					
		0	*1*	*2*	*3*	*4*	*5*
Actual class	*0*	11	3	0	0	0	0
	1	10	18	3	4	1	1
	2	2	8	13	4	1	0
	3	0	0	9	18	10	2
	4	0	0	0	2	2	2
	5	0	0	0	0	1	4

Table 1: Confusion matrix showing summary of prediction results. The sum of each row is the true number of true labels of each class. The columns show the predictions for each class.

Conclusion: Further refinements are necessary. Having a lung-half specific score is expected to increase classification performance, as scores would no longer have to be grouped. As a final optimization step, the lobe specific classification should be the long-term goal after lung lobe segmentation on MRI.

References:
[1] Wielpütz, M. O., Puderbach, M., Kopp-Schneider, A., Stahl, M., Fritzsching, E., Sommerburg, O., Ley, S., Sumkauskaite, M., Biederer, J., Kauczor, H. U., Eichinger, M., & Mall, M. A., (2014), Magnetic resonance imaging detects changes in structure and perfusion, and response to therapy in early cystic fibrosis lung disease, American journal of respiratory and critical care medicine, 956-965, 189(8), https://doi.org/10.1164/rccm.201309-1659OC, 2022-01-19
[2] Eichinger, M., Optazaite, D. E., Kopp-Schneider, A., Hintze, C., Biederer, J., Niemann, A., Mall, M. A., Wielpütz, M. O., Kauczor, H. U., & Puderbach, M., (2012), Morphologic and functional scoring of cystic fibrosis lung disease using MRI, European journal of radiology, 1321-1329, 81(6), https://doi.org/10.1016/j.ejrad.2011.02.045, 2022-01-19

Performance of an AI Powered Algorithm to Detect Pulmonary Embolism on Virtual Monochromatic CTPA Images

E. Langius-Wiffen[1], R.A. van Dijk[1], E. de Boer[1], J. Nijboer-Oosterveld[1], I.M. Nijholt[1], P.A. de Jong[2], M.F. Boomsma1; [1]Isala, Radiology, Zwolle, Netherlands; [2]University Medical Center Utrecht, Radiology, Utrecht, Netherlands

Purpose/Objectives: Virtual monochromatic images (VMI) obtained with dual-energy CT are increasingly used in clinical practice as they provide the possibility to increase image quality through higher Contrast-to-Noise ratio. The goal of this study was to assess whether the diagnostic accuracy of an artificial intelligence (AI) powered tool (Aidoc Medical, Tel Aviv, Israel) to detect pulmonary embolism (PE) on CTPA was higher on VMI than on conventional images (CPI).

Methods and Materials: Paired 60 keV VMI and CPI, obtained with a detector-based spectral CT scanner (SDCT), of 114 consecutive patients suspected of PE were retrospectively analysed. As a reference standard a consensus between 3 radiologists who had access to CAD (Pulmonary Artery Analysis application within IntelliSpace Portal version 9; Philips Healthcare) was used. Cases were analysed by the AI algorithm and classified as PE positive or negative on a per-patient level. Sensitivity and specificity of the agorithm on VMI and CPI were calculated and compared using the McNemar test.

Results: PE was found in 39 of 114 patients (34.2 %). Diagnostic accuracy of the algorithm to detect PE on CTPA did not differ significantly on CPI and VMI. PE was correctly identified in 31/39 patients on CPI and in 33/39 patients on VMI, resulting in sensitivities of respectively 79.5 % (95 % confidence interval (CI) 63-90 %) and 84.6 % (95 % CI 69-94 %) (p = 0.16). On CPI 3 PE negative cases were falsely classified as PE positive, compared to 5 false positive cases on VMI, resulting in a specificity of respectively 96.0 % (95 % CI 88-99 %) and 93.3 % (95 % CI 85-98 %) (p = 0.32).

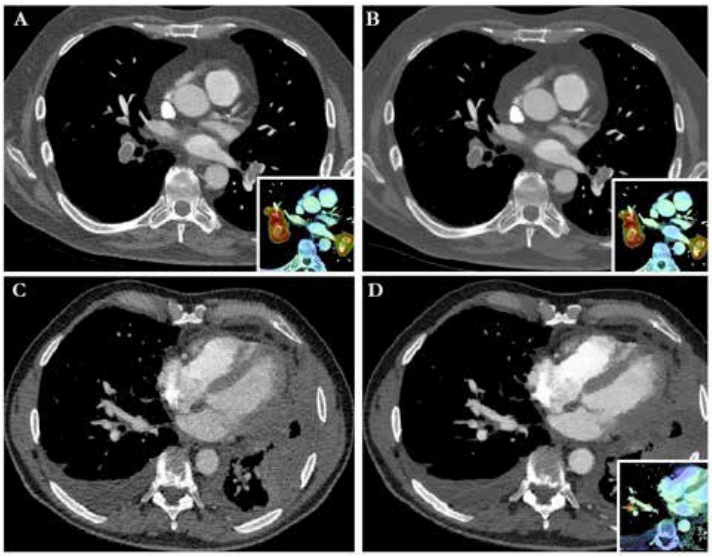

AI powered tool (Aidoc Medical, Tel Aviv, Israel) correctly identifying bilateral lobar pulmonary embolism on both conventional (A) and virtual monochromatic images (B). In a different patient a solitary segmental embolism was missed by the AI powered tool on conventional (C), but correctly marked on virtual monochromatic images (D).

Conclusion: Diagnostic accuracy of an FDA approved and CE marked AI powered algorithm detecting PE on CTPA did not differ significantly on virtual monochromatic images compared to conventional images. Future studies should point out whether the diagnostic accuracy of AI algorithms on VMI can be further improved by training of the AI on VMI or the use of lower keV VMI.

Clinical evaluation of a content-based image retrieval system for diagnosing diffuse parenchymal lung disease in pulmonary CTs

S. Roehrich[1], B. Heidinger[1], F. Prayer[1], R. Zhang[2], M. Krenn[2], H. Prosch[1], G. Langs[1, 2]; [1]Medical University of Vienna, Department for Biomedical Imaging and Image-Guided Therapy, Computational Imaging Research Lab, Vienna, Austria; [2]Contextflow GmbH, Vienna, Austria

Purpose/Objectives: Content-based image retrieval (CBIR) could be used to support radiologists while reading complex cases. However, clinical assessment of CBIR-systems is still scarce. Therefore we aimed at evaluating the clinical utility of a CBIR-system in patients with diffuse parenchymal lung diseases (DPLD).

Methods and Materials: 108 retrospectively included chest CT scans with 22 unique, clinically- and/or histopathologically-verified diagnoses were read by eight radiologists (four junior, four senior, median years reading chest CT scans 2.1±0.7 and 12±1.8, respectively). The radiologists read and provided the suspected diagnosis at a certified radiological workstation to simulate clinical routine. Half of the readings were done without CBIRS and half with the additional support of the CBIR-system. The CBIRS retrieved the most likely of 19 lung-specific patterns from a large database of 6542 thin-section CT scans and provided relevant information (e.g., a list of potential differential diagnoses).

Results: Radiologists searched for additional information more frequently when they had access to the CBIRS (154 [72 %] vs. 95 [43 %]). The average reading time decreased by 31.3 % (p<0.001) when CBIR was available. Additionally, there was a trend towards higher overall diagnostic accuracy (42.2 % vs 34.7 %, p=0.083) when they had access to the CBIR-system.

Conclusion: By using a CBIR-system during the reading of complex chest CT scans, a decrease in reading time could be shown. The use of supporting informational sources was also increased when there was access to the CBIR-system. Additionally, these effects were demonstrated both for junior and senior radiologists. Further research is necessary to validate the trend to higher diagnostic accuracy, when using the CBIR-system.

Reproducibility of Pulmonary Magnetic Resonance Angiography in Adults with Muco-Obstructive Pulmonary Disease

L. Wucherpfennig[1, 2, 3], S. Triphan[1, 2, 3], O. Weinheimer[1, 2, 3], M. Eichinger[1, 2, 3], S. Wege[4], R. Eberhardt[2, 5], M.U. Puderbach[1, 2, 3, 6], H.-U. Kauczor[1, 2, 3], C.P. Heussel[1, 2, 3], G. Heussel[3], M.O. Wielpütz[1, 2, 3]; [1]University Hospital Heidelberg, Department of Diagnostic and Interventional Radiology, Heidelberg, Germany; [2]German Lung Research Center (DZL), Translational Lung Research Center Heidelberg (TLRC), Heidelberg, Germany; [3]University Hospital Heidelberg, Thoraxklinik, Department of Diagnostic and Interventional Radiology with Nuclear Medicine, Heidelberg, Germany; [4]University Hospital Heidelberg, Thoraxklinik, Department of Pulmonology and Respiratory Medicine, Heidelberg, Germany; [5]Asklepios Clinic Barmbek, Department of Pulmonology and Internal intensive care, Hamburg, Germany; [6]Hufeland Hospital, Department of Diagnostic and Interventional Radiology, Bad Langensalza, Germany

Purpose/Objectives: Recent studies support magnetic resonance angiography (MRA) as a diagnostic tool for pulmonary arterial disease. To determine MRA image quality and reproducibility, and the dependence of MRA image quality and reproducibility on disease severity in patients with chronic-obstructive pulmonary disease (COPD) and cystic fibrosis (CF).

Methods and Materials: 20 patients with COPD (66.5±8.9y, FEV1%=42.0±13.3 %) and 15 with CF (29.3±9.3y, FEV1 %=66.6±15.8 %) underwent morpho-functional chest MRI including time-resolved MRA twice one month apart (MRI1, MRI2), and COPD patients underwent non-contrast CT. Image quality was assessed visually using standardised subjective 5-point scales. Contrast-to-noise-ratio (CNR) and signal-to-noise-ratio (SNR) were measured by regions-of-interest. Disease severity was determined by spirometry, a well-evaluated chest MRI score and by computational CT emphysema index (EI) for COPD.

Results: Subjective image quality was diagnostic for all MRA at MRI1 and MRI2 (mean score=4.7±0.6). CNR and SNR were 54.4±16.5 and 64.4±18.4, respectively. Neither image quality score nor CNR or SNR correlated with FEV1% or chest MRI score for COPD and CF (r=-0.159-0.280). CNR and SNR did not change from MRI1 to MRI2 (p=0.741 to 0.755). Further, insignificant differences in CNR and SNR between MRA at MRI1 and MRI2 did not correlate with FEV1% nor chest MRI score in COPD and CF (r=0.011-0.032), nor with EI in COPD (r=-0.013 to -0.061).

Conclusion: MRA achieved diagnostic quality in COPD and CF patients and was highly reproducible irrespective of disease severity. This supports MRA as a robust alternative to CT in patients with underlying muco-obstructive lung disease.

Look-locker based T1 relaxometry and high-resolution T2 in the evaluation of lung lesions: A unicentric prospective study

D. Wada[1], M.R. Lourenço[2], L. Siyuan Wada[3], C.V. Machado[2], R.H. Oliveira[1], G.C. Melges[1], C.E.G. Salmon[4], T.R. Nadai[5], F.E.G. Cipriano[3], A.A. Faccio[2], A.T. Fabro[6], M. Koenigkam-Santos[2]; [1]Clinics Hospital of Ribeirao Preto Medial School, Medical Imaging, Hematology, and Oncology, Ribeirao Preto, Brazil; [2]Ribeirao Preto Medical School – University of Sao Paulo, Medical Imaging, Hematology and Oncology department, Ribeirao Preto, Brazil; [3]Ribeirao Preto Medical School – University of Sao Paulo, Surgery and Anatomy, Ribeirao Preto, Brazil; [4]Faculty of Philosophy, Sciences and Letters at Ribeirão Preto, Ribeirao Preto, Brazil; [5]University of Sao Paulo, Bauru, Brazil; [6]Ribeirao Preto Medical School – University of Sao Paulo, Pathology and Forensic Medicine, Ribeirao Preto, Brazil

Purpose/Objectives: Many magnetic resonance imaging (MRI) sequences had never been tested in the evaluation of focal lung lesions (FLLs). The purpose of this study was to explore the feasibility of high-resolution T2 (T2HR) and T1 look-locker relaxometry (T1LL) images for FLLs. As a secondary goal, we analyzed the diagnostic accuracy of these sequences to differentiate benign from malignant.

Methods and Materials: In this prospective observational study, 39 subjects with FLLs were scanned in a 1.5T MRI system with T1LL and T2HR images focused on the FLLs region, in addition to a conventional protocol. Images were evaluated by two independent blinded radiologists. A Look-Locker sequence was performed (same as used at cardiac MRI), gated with a peripheral pulse transducer (finger PPT) at fixed intervals ranging from 160 to 691 ms (Figure 1).

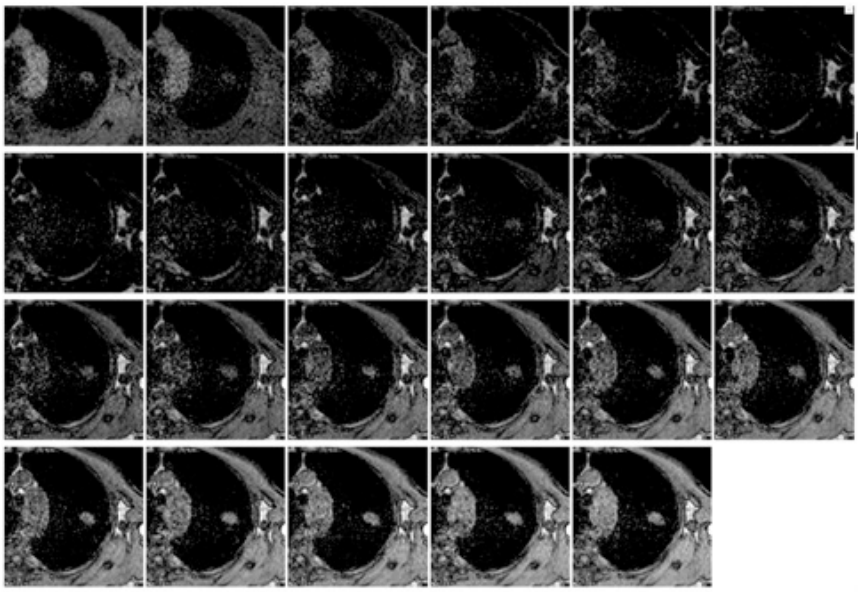

Fig. 1: T1 relaxometry sequence based on an inversion recovery sequence (Look-Locker) for evaluation of a pulmonary nodule (23 images of different inversion times ranging from 160 to 691 ms).

Images were obtained during a 10-20s single breath-hold (range varied due to patient's heart rate), in the axial plane, with a reduced coverage of the lungs focused on the lesion. A preliminary ROI-based analysis was performed comparing benign and malignant lesions, after calculation of the T1 times. Images from the T2HR sequence were evaluated qualitatively (regarding its capability of detect morphologic features such as spiculations, pleural tags, non-solid component and pseudocavitations) and quantitatively (signal intensity mean values and standard deviations).

Results: Most exams had adequate diagnostic quality in both sequences (T1LL in 31 exams and T2HR in 36). Exams considered non-diagnostic were mainly related to the limited coverage of the sequences (technical issues during images acquisition). Of the studied FLLs, 19 were malignant, 17 benign, and 3 cases were excluded from malignancy accuracy analysis by lacking a definitive diagnosis. Quantitative T1LL relaxometry couldn't distinguish between benign and malignant lesions (Figure 2), but the analysis of its first inversion time (160 ms) signal intensity differed between the groups (Figure 3).
The T2HR was considered the best sequence for assessing specific morphological characteristics, especially pseudocavitations and pleural tags (Figure 4).
MRI had best accuracy compared to CT (86 % and 74 %, respectively).

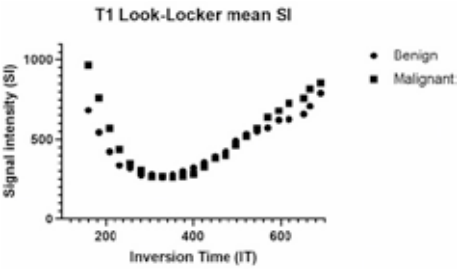

Fig. 2: Distribution of T1 Look-locker mean signal intensity of the benign and malignant groups at each inversion time.

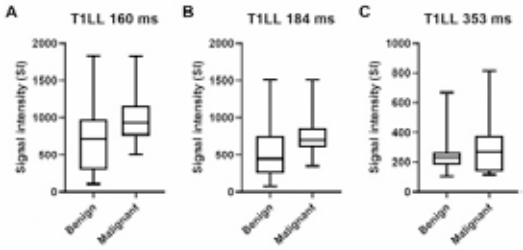

Fig. 3: Boxplot of each group mean signal intensity at T1 LL images at 160 ms (A), 184 ms (B) and 353 ms (C) inversion times.

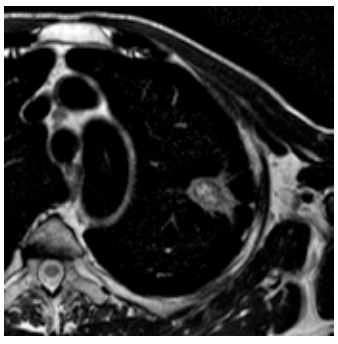

Fig. 4: T2 high resolution image depicting same nodule as in Fig. 1.

Conclusion: Both sequences were feasible in the evaluation of FLLs. T1 relaxometry based on an inversion recovery sequence was feasible and straightforward to perform, using tools already available in most of MRI machines that include a cardiac imaging pack. Images at 160 ms of the T1LL sequence may help distinguish benign from malignant lesions, and the T2HR was considered the best sequence in evaluating some specific morphological characteristics.

Impact of photon-counting CT (PCCT) in the evaluation of interstitial lung disease (ILD): Preliminary experience in 29 patients

Y. Gaillandre, A. Duhamel, S. Khung, A. Hutt, J. Remy, M. Remy-Jardin

Purpose: To compare lung parenchyma analysis based on the ultra-high resolution (UHR) mode of a PCCT scanner with that of the high-resolution (HR) mode of a 3rd-generation dual-source CT scanner.

Methods: 29 patients underwent a HRCT examination at T0 (collimation : 2 x 96 x 0.6 mm ; pitch : 2-3 ; Sn150 kV ; 150 mAs) and a UHR examination at T1 (collimation : 120 x 0.2 mm ; pitch : 1 ; Sn100 kV / Sn140 kV) with similar reconstructions (512 matrix; 1-mm thick sections. The rating ranged (a) from score 1 (« very sharp ») to score 4 ("marked blurring") for anatomical structures; and (b) from score 0 ("feature absent") to score 3 ("feature present and sharp") for ILD features.

Results: The anatomical structures were more precisely depicted at T1 with: (a) visualization of more distal bronchial divisions (median order; Q1-Q3) (T1: 9th division [9-10]; T0: 8th division [8-9]; $p<0.0001$); (b) greater scores of sharpness for bronchial walls ($p<0.0001$), right minor ($p<0.0001$) and major ($p=0.02$) fissures. The scores of visualization of micronodules ($p=0.25$), lines ($p=0.07$), bronchiectasis ($p=0.5$) and honeycombing ($p=0.06$) did not differ between T0 and T1. The scores of visualization (median ; Q1-Q3) of intralobular reticulation (T1 : score 3 [2-3]; T0: score 2 [2-2] ; $p<0.0001$) and bronchiolectasis (T1 : score 2 [0-3]; T0: score 2 [0-2] ; $p<0.0001$) were higher at T1. The DLP value was significantly lower at T1 (85.8 ± 21.3 mGy.cm) than at T0 (132.8 ± 41.7 mGy.cm) ($p<0.01$).

Conclusion: These preliminary results demonstrate the superiority of the UHR mode.

Chest CT angiography (CTA) in daily routine with a photon-counting CT equipment: Preliminary experience

I. Oufriche, L. Guiffault, S. Dujardin, A. Duhamel, P. Felloni, J.-B. Faivre, J. Remy, M. Remy-Jardin

Purpose: To validate basic scanning conditions for morphology and lung perfusion with photon-counting CT (PCCT)

Methods: Over a 7-month period, chest radiologists investigated (a) morphologic imaging of the PCCT technology; and (b) the overall quality of lung perfusion in comparison with that achievable on a 3rd-generation dual-source CT scanner (DSCT).

Results: The diagnostic image quality of chest CTAs was investigated on the basis of 1204 chest CTAs (a) acquired with a collimation of 144 x 0.4 mm, single source; pitch of 1.5; (b) injection of a 40 % contrast agent (80 mL; 4 mL/s); (c) reconstruction of mediastinal images at 55 keV; (d) ensuring attenuation values within pulmonary and systemic arteries >700 UH. A 42 % reduction in the amount of iodine administered to the patient (60 mL of a 35 % contrast agent; 3 mL/s) provided attenuation values ranging between 400-500 HU in both circulations.
Perfusion was compared in a subgroup of 50 patients (DSCT: n=28 patients; PCCT: n=22) with no difference in age ($p=0.5$), BMI categories ($p=0.15$) and attenuation within the pulmonary trunk on morphologic images ($p=0.10$), showing (a) no difference in the mean (± SD) level of attenuation on perfusion images obtained by subtraction of mono-energetic images (40-190 keV) (DSCT: 89.1 ± 19.9 UH; PCCT: 95.0 ± 15.4 UH ; $p=0.28$); and (b) a significant reduction in the mean (± SD) DLP (DSCT: 308.3 ± 63.4 mGy.cm; PCCT: 162.4 ± 51.5 mGy.cm ; $p<0.0001$).

Conclusion: High-quality morphologic and perfusion imaging was achieved with PCCT, enabling significant radiation dose reduction and reduced amount of iodine if needed.

Post-COVID-19 1-year follow-up: Radiologic and pathologic correlation

D. Cozzi[1], A. Bindi[1], E. Cavigli[1], C. Moroni[1], V. Luzzi[2], V. Pasini[3], C.E. Comin[3], S. Tomassetti[4], V. Miele[1]; [1]Careggi University Hospital, Emergency Radiology, Florence, Italy; [2]Careggi University Hospital, Department of Interventional Pneumology, Florence, Italy; [3]University of Florence, Division of Pathological Anatomy, Department of Experimental and Clinical Medicine, Florence, Italy; [4]Careggi University Hospital and University of Florence, Department of Experimental and Clinical Medicine, Florence, Italy

Purpose/Objectives: The aim is to evaluate the characteristics of post-COVID-19 interstitial lung changes, with the unique opportunity to evaluate radiologic-pathologic correlations using HRCT and transbronchial lung cryobiopsy specimens.

Methods and Materials: These are preliminary results of HRCT features of post-COVID-19 ILD. Authors collected data of hospitalized patients at baseline, then at 6 (+/-1) and 12 (+/-1) months after discharge. HRCT changes at 6 months involving more than 5 % of the total lung volume were considered significant. Patients with significant HRCT changes underwent BAL and/or cryobiopsy and a subsequent follow-up with HRCT and lung function evaluation at 18 (+/-1) months.

Results: At the time of the present interim analysis, 143 patients from our university hospital were enrolled (median age 67 years; 87 males – 60.8 %). After 1-year follow up, HRCT significant changes (both fibrotic-like and non-fibrotic) were detected in 55 subjects (38.4 %): of them, only 2/55 (3.6 %) patients have parenchymal progression of the disease, stability in 33/55 (60 %) and improvement in 20/55 (36.4 %). Cryobiopsies were performed in 10 patients, showing some discordance with radiological appearance. In particular, biopsy finds 2 cases of histological UIP/early-UIP where HRCT demonstrates an NSIP/OP pattern. Cryobiopsy confirms 2 cases of HRCT UIP-probable pattern and 4 cases of NSIP/OP/HP pattern. Moreover, we demonstrate a case of post-ventilation fibrosis. The last case is a cellular NSIP with persistent positivity for Sars-CoV-2 in BAL immunophenotype analysis after 12 months.

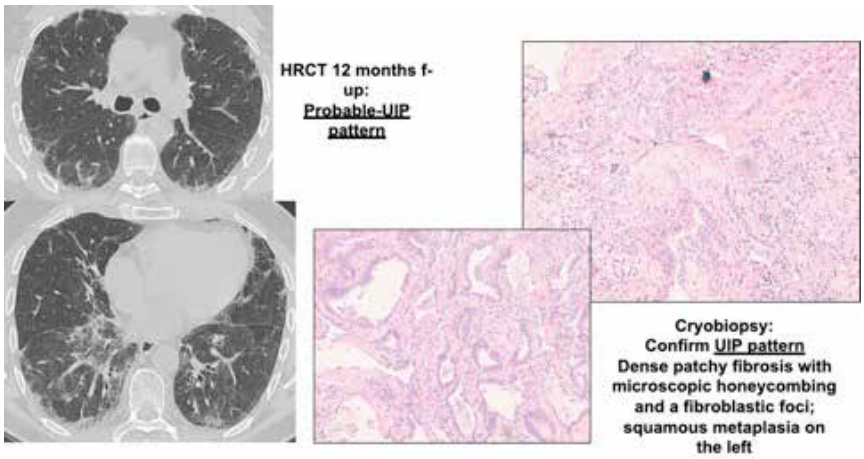

HRCT after 1-year follow up with a probable-UIP pattern; biopsy confirms the radiological pattern.

Conclusion: This preliminary analysis confirms that after COVID-19 infection a large minority of patients develop interstitial lung changes mostly with NSIP/OP or (early)UIP pattern. The hypothesis is that the infection could be a trigger for a possible underlying latent interstitial disease, in predisposed subjects.

Pulmonary arteries enlargement in pulmonary embolism related to COVID-19 pneumonia: A single-center experience

A. Grimaldi[1], A. Del Ciello[2], G. Savino[2], A. Infante[2, 3], G. D'Ambra[1], F. Lo Piccolo[1], G. Cicchetti[1, 2], A. Farchione[2], R. Marano[1, 2], L. Natale[1, 2], A.R. Larici[1, 2]; [1]Università Cattolica del Sacro Cuore, Rome, Italy; [2]Fondazione Policlinico Universitario Agostino Gemelli IRCCS, Rome, Italy; [3]Columbus Covid 2 Hospital, Rome, Italy

Purpose/Objectives: The enlargement of segmental/subsegmental pulmonary arteries on computed tomography (CT) has been previously reported in COVID-19 pneumonia. We aimed to assess differences in the diameter of pulmonary segmental arteries in lung zones with and without signs of pneumonia and/or pulmonary embolism (PE) on CT pulmonary angiography (CTPA) in a population of confirmed COVID-19 patients and suspected PE.

Methods and Materials: We retrospectively enrolled consecutive patients admitted to our emergency department from February to June 2020. Inclusion criteria were a positive nasopharyngeal swab for SARS-CoV-2 and a CTPA performed for suspicion of PE. Risk factors and laboratory tests were collected. Imaging evaluation was performed on a segmental basis (20 segments per-patient) by two thoracic radiologists, reporting the presence of pneumonia, PE, or both in each lung segment. A semi-quantitative evaluation of COVID-19 pneumonia abnormalities was performed within each segment (0-7 points), as well as a qualitative assessment of PE severity (0-2 points). The diameter of each segmental artery (measured 2 mm after its origin) was recorded; the mean diameter was reported for each of the following group of segments (group 0: no signs of pneumonia or PE) (group 1: with pneumonia only) (group 2: with PE only) (group 3: with both PE and pneumonia).

Results: 74 patients were enrolled; 29 required Intensive Care Unit (ICU) admission; 27/74 patients (36.4 %) demonstrated PE on CTPA, mostly in segmental and subsegmental branches. Half of the ICU patients developed PE (14/29). Patients with PE had significantly higher D-dimers (10.8 μg/ml vs 4.0 μg/ml; p = 0.003). A total of 1478 pulmonary segments were evaluated. Signs of pneumonia were reported in 1001/1478 segments (61 %); PE was found in 148/1478 (10 %) segmental arteries, among which 95/148 located in the same regions showing signs of pneumonia. Segmental arteries in segments with signs of PE demonstrated a significantly higher diameter than in those without PE (5.0 ± 1.3 vs 4.0 mm ± 1.0; p < 0.001). We found a significant difference in the mean segmental arterial diameter among all the groups of segments (p < 0.001), with a mean arterial diameter of 3.5 mm ± 0.8 in group 0, 4.2 mm ± 1.0 in group 1, 4.6 mm ± 1.1 in group 2 and 5.2 mm ± 1.3 in group 3, respectively. Larger segmental arterial diameters significantly correlated with higher pneumonia scores (p < 0.001).

Conclusion: Our results suggest that the enlargement of pulmonary segmental arteries on CT may be considered a marker of parenchymal and vascular abnormalities in COVID-19 pneumonia. Measurement of segmental arterial diameter could play a role in stratifying COVID-19 patients at higher risk of PE. Further larger prospective studies on unenhanced chest CT are needed.

References:
[1] Lei J, Li J, Li X, et al., (2020), CT Imaging of the 2019 Novel Coronavirus (2019-nCoV) Pneumonia, Radiology, 295(1):18, https://doi.org/10.1148/radiol.2020200236
[2] Danzi GB, Loffi M, Galeazzi G, et al., (2020), Acute pulmonary embolism and COVID-19 pneumonia: a random association?, Eur Heart J, 41(19):1858, https://doi.org/10.1093/eurheartj/ehaa254
[3] Revzin MV, Raza S, Warshawsky R, et al. , (2020), Multisystem Imaging Manifestations of COVID-19, Part 1: Viral Pathogenesis and Pulmonary and Vascular System Complications, Radiographics, 40(6):1574-1599, 10.1148/rg.2020200149
[4] Patel BV, Arachchillage DJ, Ridge CA, et al., (2020), Pulmonary angiopathy in severe COVID-19: physiologic, imaging, and hematologic observations, Am J Respir Crit Care Med, 202(5):690-699, https://doi.org/10.1164/rccm.202004-1412oc
[5] Qanadli SD, Sauter AW, Alkadhi H, et al. , (2021), Vascular Abnormalities Detected with Chest CT in COVID-19: Spectrum, Association with Parenchymal Lesions, Cardiac Changes, and Correlation with Clinical Severity (COVID-CAVA Study), Diagnostics (Basel), 11(4):606, https://doi.org/10.3390/diagnostics11040606
[6] Léonard-Lorant I., Delabranche X., Séverac F., et al, (2020), Acute Pulmonary Embolism in Patients with COVID-19 at CT Angiography and Relationship to d-Dimer Levels, Radiology, 296(3):E189-E191, https://doi.org/10.1148/radiol.2020201561
[7] Caruso D, Zerunian M, Polici M, et al, (2020), Chest CT features of COVID-19 in Rome, Italy, Radiology, 296(2):E79-E85, https://doi.org/10.1148/radiol.2020201237
[8] Huang G, Gong T, Wang G, et al, (2020), Timely Diagnosis and Treatment Shortens the Time to Resolution of Coronavirus Disease (COVID-19) Pneumonia and Lowers the Highest and Last CT Scores From Sequential Chest CT, AJR Am J Roentgenol, 215(2):367-373, https://doi.org/10.2214/AJR.20.23078
[9] Qanadli SD, El Hajjam M, Vieillard-Baron A, et al, (2001), New CT index to quantify arterial obstruction in pulmonary embolism: comparison with angiographic index and echocardiography, AJR Am J Roentgenol, 176(6):1415-20, https://doi.org/10.2214/ajr.176.6.1761415

Minimal Clinically Important Difference (MCID) for quantitative analysis of progressive pulmonary fibrosis on High Resolution Computed Tomography (HRCT)

G. Cicchetti[1, 2], G. Sgalla[3], A. Del Ciello[1], T. Magrì[4], L. Iaccarino[2], L. Calandriello[1], A. Farchione[1], L. Richeldi[3, 4], A.R. Larici[1, 2]; [1]Fondazione Policlinico Universitario Agostino Gemelli IRCCS, Dipartimento di Diagnostica per Immagini, Radioterapia Oncologica ed Ematologia, Rome, Italy; [2]Università Cattolica del Sacro Cuore, Dipartimento di Scienze Radiologiche ed Ematologiche, Rome, Italy; [3]Fondazione Policlinico Universitario Agostino Gemelli IRCCS, Dipartimento di Scienze Mediche e Chirurgiche, Pneumologia, Rome, Italy; [4]Università Cattolica del Sacro Cuore, Dipartimento di Scienze Cardiovascolari e Pneumologiche, Rome, Italy

Purpose/Objectives: Accurate monitoring of disease progression in interstitial lung disease (ILD) is crucial for predicting prognosis and optimizing management and the definition of specific thresholds for significant radiological progression could be critical in both research field and clinical practice. Aim of this study is to validate the visual semi-quantitative scoring of pulmonary fibrosis on High Resolution Computed Tomography (HRCT) scans against clinical parameters of ILD progression, in order to identify the minimal clinically important difference (MCID) of fibrotic extent over a 12-month period.

Methods and Materials: Patients with an ILD diagnosis were prospectively enrolled. Clinical data included demographics, Body Mass Index (BMI), tobacco use, family history, comorbidities and cancer history. Multiple composite clinical scores were collected. Patients underwent spirometry, carbon monoxide diffusion capacity (DLCO) tests, 6-minute walk tests (6MWTs) and HRCT scans at baseline and follow-up. A thoracic radiologist estimated the total extent of ILD changes (to the nearest 5 % of the lung parenchyma), both on a lobar basis and as an overall percentage of the entire lung volume. The ILD abnormalities were also scored as percentages of the following features: reticulation, ground glass opacities, consolidation, and honeycombing.

Results: 35 patients (median age 73 years) with an ILD diagnosis were included. The majority of patients had IPF (n=28, 80 %), while the remaining ones (20 %) had non-IPF ILDs. At 12-months follow-up, the median decline in FVC was 3 % (absolute decline 20 ml). At 12-months follow-up the median increase in ILD extent was 5 % (IQR 0-10). 12-months changes in ILD extent significantly correlates with FVC (r=-0.412; p=0.046) and Shortness of Breath (SOB) scores (r=0.504; p=0.012).
Patients with progressive disease (n=21) had a mean ILD extent of 33.8 %, as compared to 22.9 % of non-progressive patients (n=14) (mean difference 10.9 %; p=0.042). A MCID for total ILD extent of 10 % was estimated, after approximating to the nearest 5 %, consistently with the visual scoring method.
Time to meaningful disease progression was significantly lower in patients with more than 10 % increase in ILD extent at 12 months (log-rank p=0.007). On Cox proportional hazard regression, such difference corresponded to a 3.5-fold increased risk of disease progression or death (HR: 3.5, 95 %CI:1.33-9.22; p=0.011).

Conclusion: The visual evaluation of fibrotic extent on HRCT is a valid and responsive measure of disease progression in ILD patients, and a 12-month increase of ILD extent greater than 10 % on HRCT represents a clinically meaningful difference that could help in the discrimination of progressive fibrosing ILDs (PF-ILDs).

References:
[1] Kolb M, Vašáková M. , (2019), The natural history of progressive fibrosing interstitial lung diseases, Respir Res, 20(1):57
[2] Cicchetti G, del Ciello A, Calandriello L, Larosa E, Franchi P, Farchione A, et al. , (2021), Focus on progressive fibrosing interstitial lung diseases (PF-ILDs), J Radiol Rev, 8:121-131
[3] George PM, Spagnolo P, Kreuter M, Altinisik G, Bonifazi M, Martinez FJ, et al. , (2020), Erice ILD working group. Progressive fibrosing interstitial lung disease: clinical uncertainties, consensus recommendations, and research priorities, Lancet Respir Med, 8:925-934
[4] Flaherty KR, Wells AU, Cottin V, Devaraj A, Walsh SL, Inoue Y, et al., (2019), INBUILD Trial Investigators. Nintedanib in progressive fibrosing interstitial lung diseases, N Engl J Med, 381:1718–1727
[5] Jacob J, Bartholmai BJ, Rajagopalan S, Kokosi M, Nair A, Karwoski R, et al. , (2016), Automated Quantitative Computed Tomography Versus Visual Computed Tomography Scoring in Idiopathic Pulmonary Fibrosis: Validation Against Pulmonary Function, J Thorac Imaging, 31(5):304-311
[6] Humphries SM, Yagihashi K, Huckleberry J, Rho BH, Schroeder JD, Strand M, et al. , (2017), Idiopathic Pulmonary Fibrosis: Data-driven Textural Analysis of Extent of Fibrosis at Baseline and 15-Month Follow-up, Radiology, 285:270–278

Assessing The Proportion of PA vs AP Chest X-rays Performed Amongst Emegency Department and Inpatients at a District General Hospital

Z. Nisar[1], A. Sinha[1], L. Zhi Wong[2], B. Annan[3]; [1]East and North Hertfordshire NHS Trust, Stevenage, United Kingdom; [2]University College London, London, United Kingdom; [3]East and North Hertfordshire NHS Trust, Radiology, Stevenage, United Kingdom

Purpose/Objectives: Chest x-rays (CXR) are the most common diagnostic x-ray examination performed.[1] Erect posterio-anterior (PA) projections are considered the gold standard, while Antero-posterior (AP) CXRs are indicated when patients cannot stand or leave their beds.[2] The Royal College of Radiology (RCR) recommends a target ratio of 75 % PA to 25 % AP CXRs for Emergency Department (ED) and inpatient radiographs.[3] An audit was conducted at Lister Hospital to identify the number of adult ED and inpatient CXR's performed over one month. The percentage of PA and AP films were assessed, and variables affecting this percentage were analysed.

Methods and Materials: Data on all CXRs performed over August 2021 were obtained from the coding department. Data extracted included: Hospital number, examination date, request location (ED vs inpatient), x-ray time and patient mobility, while paediatric patients, fracture clinic, and mobile x-rays were all excluded. Radiographs were reviewed manually by all three authors using PACS to identify if PA or AP films were performed. Patient Mobility and time of day were assessed for statistical significance in relation to CXR type. Data collection was completed in Microsoft Excel and Chi-squared testing was used for analysis.

Results: 2107 CXRs were performed between 00:00 1st and 23:59 31st August 2021, with 483 (22.9 %) inpatient, and 1624 (77.1%) ED x-rays. 1045 (49.6 %) were AP and 1062 (50.4 %) were PA radiographs in total. Figure 1 illustrates all mobility options and percentages. PA CXR was performed for most 'Chair' and 'Walking' patients, whereas 'Trolley', 'Bed', and 'Mobile' formed majority of the AP CXR done. Figure 2 illustrates proprtion of AP and PA CXR for each mobility type. Association between mobility of patient and film type was statistically significant ($p<0.05$).
Figure 3 shows the timing options and percentages. The majority of CXRs done between 09:00-17:00 were AP, whereas between 17:00-20:00 and 20:00-09:00 the majority of CXRs were PA. Figure 4 shows percentages of AP and PA CXR's for each timing increment. Association between time of x-ray and type of film was statistically significant result ($p<0.05$).

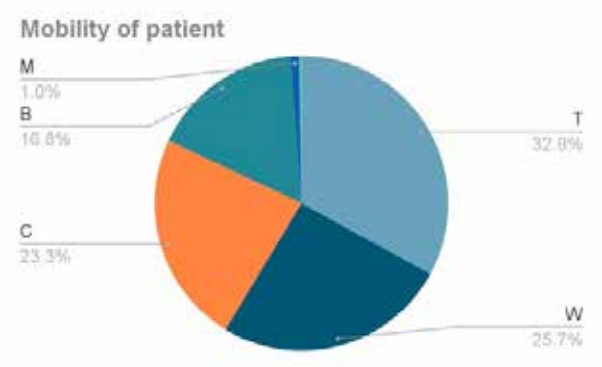

Fig. 1: Distribution of the mobility of all patients assessed

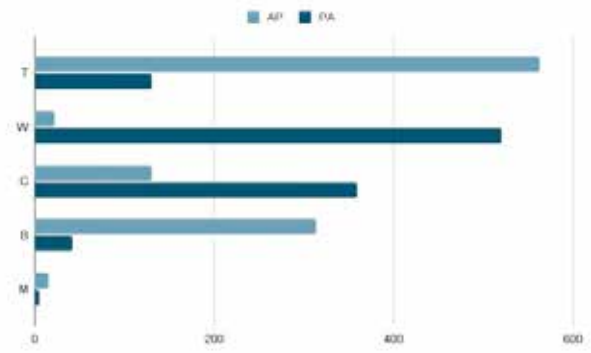

Fig. 2: Proportion of AP and PA CXR for each mobility type

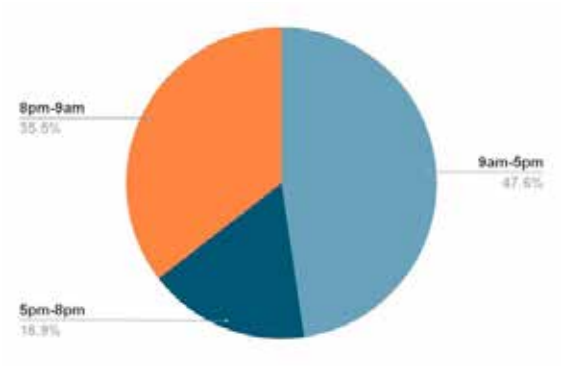

Fig. 3: Distribution of timing of x-ray for all patients assessed

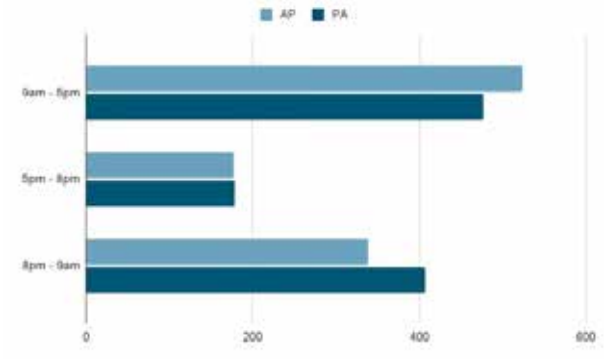

Fig. 4: Proportion of AP and PA CXR for each timing increment

Conclusion: Standards set by RCR of 75% PA CXR's are currently not being met. Both patient mobility status and time at which the x-ray was taken significantly affected CXR type. Our interventions include faculty education on diagnostic utility of PA over AP films, encouragement of radiographers to mobilise patients when safe, and regular 24-hour audits to assess practice intermittently. A re-audit will be conducted in 6 months to assess success of these interventions.

References:
[1] RadiologyInfo, (2020), X-ray (Radiography) - Chest, Radiologyinfo, https://www.radiologyinfo.org/en/info/chestrad#:~:text=The%20chest%20x%2Dray%20is., 2021-12-23
[2] (2021), The difference between Chest Posterior Anterior (PA) and Anterior Posterior (AP) radiographs, SRRT e-Learning, https://www.elearning.isrrt.org/mod/book/tool/print/index.php?id=321., 2021-12-24
[3] Catriona Stoddart, (2016), Quality of chest x-rays, Royal College of Radiology, https://www.rcr.ac.uk/audit/quality-chest-x-rays, 2021-12-24

Radiology-Pathology Correlation in Coatomer Subunit Alpha (COPA) Syndrome with Novel Finding of Pulmonary Lymphangiectasia

S. Ghosh; The Cleveland Clinic, Thoracic Imaging, Imaging Institute, Cleveland, United States

Purpose/Objectives: To describe the imaging and pathology findings of a 25-year-old patient with Coatomer Subunit Alpha (COPA) Syndrome who underwent bilateral lung transplantation for end stage fibrosis and cystic changes.

Methods and Materials: A 25-year-old, non-smoking male was referred to our institution for lung transplantation. The patient suffered from severe and disabling respiratory complications since birth. A mutation of the COPA gene was detected few years before his referral and he was diagnosed with COPA syndrome.
A complete physical examination, spirometry and High-Resolution Computed Tomography (HRCT) of the chest were performed prior to bilateral lung transplantation. The HRCT results were correlated with macroscopic and histopathologic features of the explanted lungs.

Results: High-Resolution Computed Tomography (HRCT) lung images revealed diffuse, small (<10 mm), cystic lucencies with thin or imperceptible walls throughout both lungs, with mid and lower zone predominant coarse reticular opacities associated with minimal ground-glass changes, mild bronchiectasis, interlobular septal thickening as well as thickening of the subpleural and peribronchovascular interstitium.
Macroscopically, the explanted lungs were markedly distorted, with marked pleural adhesions, and cystic/emphysematous changes. On histopathology, the lungs showed interstitial pneumonitis and fibrosis, panlobular bronchiectasis and emphysema, pulmonary vasculopathy, and focal hemosiderin-laden macrophages. Notably, extensive lymphangiectasia and abnormally increased lymphatic vessels were present. In contrast to normal lungs, in which the lymphatic vessels are distributed along the pleura, interlobular septae, and bronchovascular bundles, and range in diameter from 10 to 20 μm, both the density and diameter of the lymphatics in the explanted lungs of our patient were significantly increased. In addition to normal lymphatic routes, lymphatic vessels were also present within the lobular interstitium, and dilatation was evident, with average diameter of 500 μm.

Conclusion: COPA syndrome is an autosomal dominant disorder with variable expressivity and histopathologic abnormalities. COPA syndrome manifests with non-erosive arthritis, occasionally immune complex-mediated renal disease, and invariably, lung disease. This is the first report of the radiologic and histopathologic features of the explant pneumonectomies in a patient with COPA syndrome with the unique finding of lymphatic alterations. It is important that physicians are aware of COPA syndrome, in particular those caring for young patients with pulmonary disease of unknown etiology, in order to increase its detection and contribute to new insights for the understanding of the disease and the histopathologic findings.

How often pleural appendages resemble pleural tumours on chest radiographs?

A. Villanueva, S. Beardsmore-Rust, A. Peternac; East Surrey Hospital. SASH NHS Trust, Radiology, Redhill, United Kingdom

Purpose/Objectives: Pleural appendages (PA) are portions of extra pleural fat that hang from the chest wall and mediastinum (1). When present, PA are easily visible in CT images of patients with pneumothorax (PNTX) (image1)

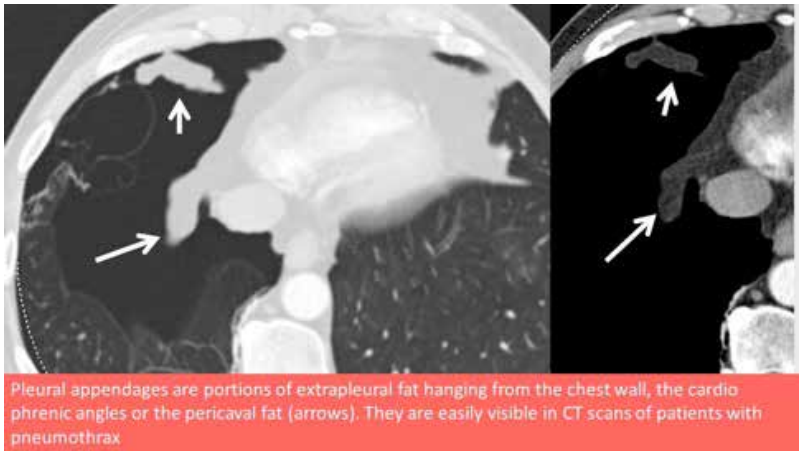

Pleural appendages are portions of extrapleural fat hanging from the chest wall, the cardio phrenic angles or the pericaval fat (arrows). They are easily visible in CT scans of patients with pneumothrax

However, the detectability of PA on a chest X-Ray (CXR) in patients with PNTX is **unknown** (image2)

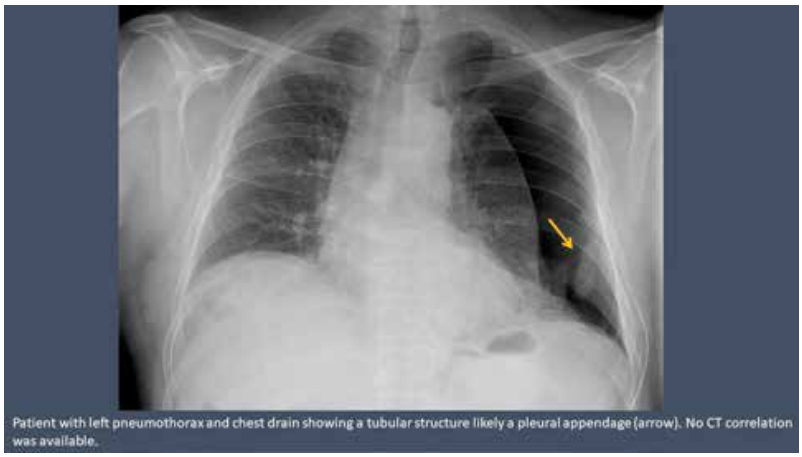

Patient with left pneumothorax and chest drain showing a tubular structure likely a pleural appendage (arrow). No CT correlation was available.

This is relevant as they can **mimic pleural tumours** (2) which may impact patient's management. (image3)

Patient with left sided pneumothorax and a pleural appendage (arrows). Appearances in the chest X radiograph simulated a pleural mass but CT chest easily demonstrated the fat nature of the pleural appendage.

Our aim is to determine how frequently PA can be detected on CXR and how often they resemble pleural tumours on CXR.

Methods and Materials: 1007 patients with the word pneumothorax (PNTX) in the report of a CT chest were collected. **65 out of 1007 patients** fullfilled inclusion criteria and did not present exclusion criteria. **Criteria of inclusion** were: 1. PNTX present on CT. 2. Moderate or severe PNTX. 2 CXR showing PNTX available within 24 hours before or after the date of the CT chest. **Exclusion criteria** included patients with known pleural disease, previous thoracic surgery, minimal pneumothorax and an elapsed time between CT scan and CXR of more than 24h.
Axial CT images and CXR of the 65 valid patients were retrospectively reviewed. The presence and number of PA in the CT chest of each patient along with their position and size were recorded. Findings in CXR were correlated with the subsequent CT scan, (considered the gold standard investigation). It was documented whether the PA were detected or non detected on the CXR. The appearance of PA in the CXR was clasified in 1. Tubular dense appearance consistent with PA.2. Consistent with a pleural tumor. (image4)

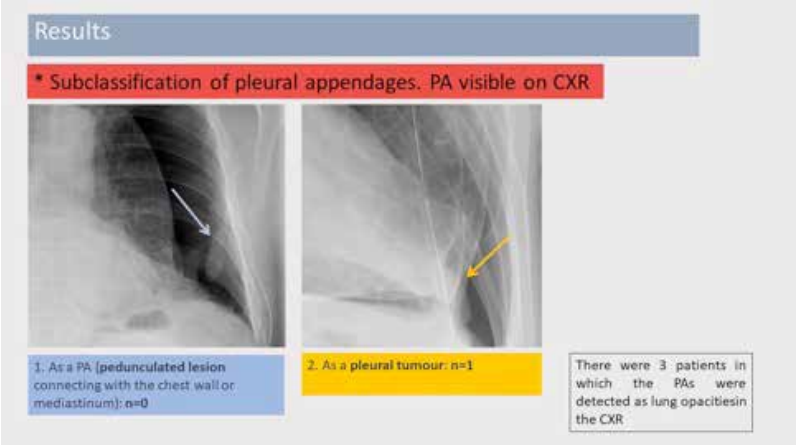

Results: PA were found in 44 of the 64 CT scans in our patients with pneumothorax (68%). One of these patients (1.5%), showed a visible PA in the CXR and this presented plaim film criteria consistent with a pleural tumour. None of the PA detected on CT chest examinations showed an appearance consistent with PA in the CXR. 3 of the 43 non detected PA likely produced opacities superimposed on the lung.

Conclusion:
- PA were rarely visible on the CXR: 1 out of 64 (1.5%) patients showed PA on the CXR in this series.
- When visible PA resemble pleural tumours on CXR in 1.5 % of patients of this study.
- When reporting medium or large size PNTX with CRX, it is important to be aware that PA can mimic pleural tumours, as this may have impact on patient's further management.
- PA are easily detected on CT chest of patients with PNTX as pedunculated fatty structures within the pleural cavity hanging from the chest wall or mediastinum

References:
[1] Villanueva Campos AM, Etxano Cantera J, Patel N, Villanueva Marcos AJ., (2021), Extrapleural fat: description, incidence, and relation with body mass index. , Elsevier, Radiologia, S0033-8338(21)00087-4. , doi: 10.1016/j.rx.2021.03.008.
[2] Fernandez de Paula MC et al. , (2015), Focal pleural tumorlike conditions: Nodules and masses beyond mesotheliomas and metastasis. , Respiratory Medicine, 1235e1243, 109

Pre-operative cardiothoracic ratio's prognostic value in adult cardiac surgery under cardiopulmonary bypass

H. Ramdani[1], H. En-Nouali[1], E.A. Bouaiti[2], M. Ait Houssa[3], M. Drissi[4]; [1]Mohammed V military hospital, Radiology, Rabat, Morocco; [2]Mohammed V Military Hospital, Laboratory of Biostatistics, Clinical Research and Epidemiology, Rabat, Morocco; [3]Mohammed V Military Hospital, Cardiac surgery department, Rabat, Morocco; [4]Mohammed V military hospital, Cardiac surgery's anesthesiology and intensive care department, Rabat, Morocco

Purpose/Objectives: To investigate the impact of pre-operative cardiomegaly -defined by a cardiothoracic ratio (CTR) >0,5 on a postero-anterior chest x-ray- on outcomes of cardiac surgery under cardiopulmonary bypass (CPB) in adult patients.

Methods and Materials: Data from patients undergoing cardiac surgery aged 17 years or older, with a pre-operative CTR >0.5, were reviewed and analyzed. Patients were divided into 4 subgroups according to their cardiothoracic ratios : [0,5-0,54], [0,55-0,59], [0,6-0,64] and >0,65. Pre, per and post-operative variables were extracted from medical records, analyzed and compared between the 4 intervals groups. To identify variables associated with 30 day-mortality, univariable and multivariable Cox proportional hazards regression was performed and hazard ratios for 30 day-mortality were calculated with their 95% confidence intervals.

Results: A total of 2502 patients underwent cardiac surgery during the study period. Out of these, 1788 patients (71,4%) had a pre-operative CTR >0,5 and were included in the analysis. The most frequently performed surgical procedure was double valve surgery (23,8%), followed by CABG (23,4%), mitral valve replacement (19,2%), and aortic valve replacement (17,1%). Overall peri-operative mortality was 7%. Low cardiac output syndrome occurred in 275 (15,4%) patients, post-operative myocardial infarction in 67 (3,8%) patients, and acute kidney injury in 148 (8,3%) patients

Post-operative complications-Outcome	[0,5-0,54] (n=694)	[0,55-0,59](n=483)	[0,6-0,64](n=398)	>0,65(n=213)	P
Complicated post-operative course	95(13,7%)	100(20,7%)	99(24,9%)	66(31%)	<0.0001
Cardiovascular complications					
Myocardial infarction	35(5,1%)	20(4,2%)	11(2,8%)	1(0,5%)	0.014
Arrhythmias	18(2,6%)	18(3,7%)	23(5,8%)	13(6,2%)	0.094
LCO syndrome	39(5,6%)	50(10,4%)	69(17,3%)	46(21,6%)	<0.0001
Inotropes use	54(7,8%)	59(12,2%)	91(22,9%)	71(33,3%)	<0.0001
IABP use	32 (4.6 %)	27 (5.6 %)	34 (8.5 %)	12 (5.6 %)	0.065
Renal complications					
AKI	32(4,6%)	39(8,1%)	45(11,3%)	32(15,1%)	<0.0001
RRT	7(1%)	12(2,5%)	12(3%)	3(1,4%)	0.079
Neurologic complications					
Stroke	6 (0,9%)	6(1,3%)	8(2,1%)	5(2,4%)	0.245
MV > 48 hours	27(3,9%)	38(7,9%)	42(10,6%)	34(16,3%)	<0.0001
Infections	47 (6,8%)	34(7,1%)	32(8,1%)	27(12,7%)	0.036
Surgical complications					
Bleeding	56(8,1%)	37(7,7%)	34(8,5%)	21(9,9%)	0.796
Transfusion	242(35,1%)	139(29,3%)	135(34,4%)	87(41,8%)	0.014
Re-intervention	18(2,6%)	19(3,9%)	18(4,5%)	10(4,7%)	0.278
Digestive complications	15(2,2%)	7(1,4%)	12(3%)	2(0,9%)	0.248
Multi-organ failure	6(0,9%)	18(3,8%)	36(9,2%)	24(11,4%)	<0.0001
Outcome					
30 day mortality	19(2,7%)	30(6,2%)	45(11,3%)	31(14,6%)	<0.0001
ICU length of stay , h	47 (24-48)	48 (24-48)	48 (24-64)	48(30-72)	0.001
Hospital length of stay , d	11 (9-13)	11 (9-14)	11 (9-15)	12 (10-15)	0.049

Table 1: Post-operative complications

The incidence of complications and 30 day-mortality significantly increased with increasing CTRs and reached a high of 31% and 14,6% in patients with a CTR >0,65 compared to 13,7% and 2,7% in patients with a CTR ranging from 0,5 to 0,54, respectively (p<0.0001)

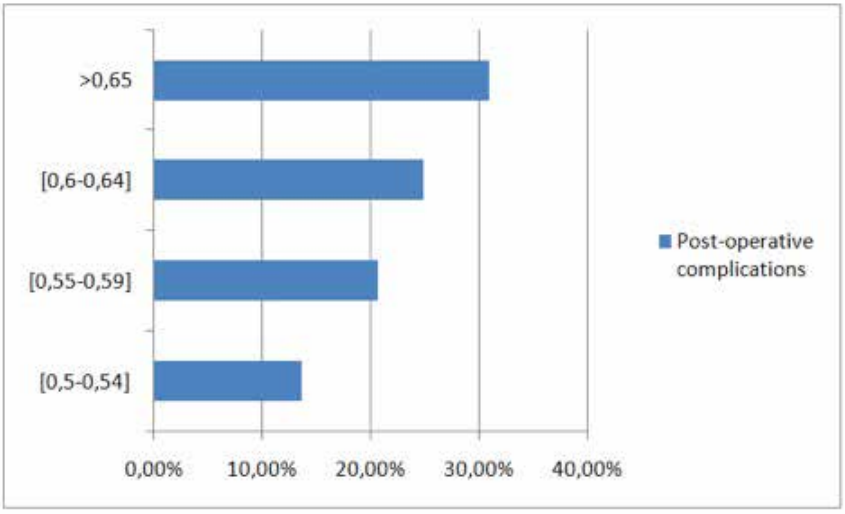

Figure 1: Post-operative complications in the different cardiothoracic ratio (CTR) intervals

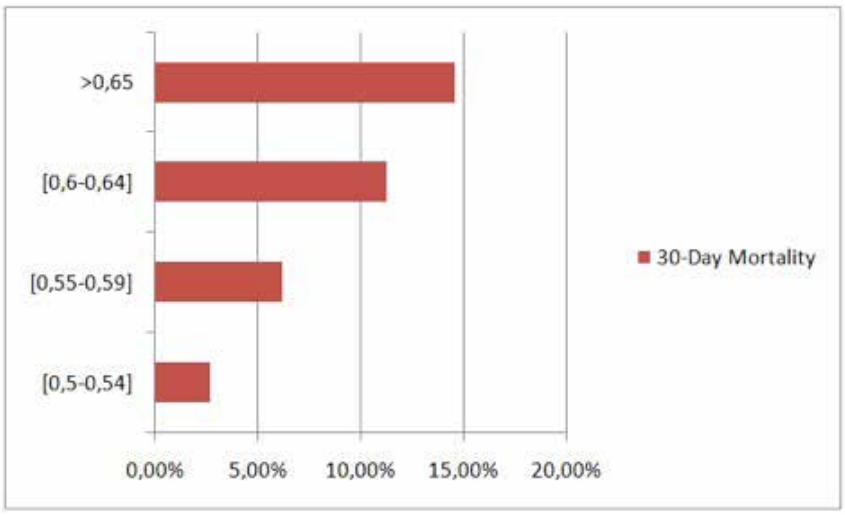

Figure 2: 30-day mortality in the different cardiothoracic ratio (CTR) classes

Stepwise multivariate analysis identified a pre-operative CTR ranging from 0,6 to 0,64 (HR 2.43, 95% CI (1.02-5.82); p<0.045), prolonged mechanical ventilation (HR 9.42, 95% CI (4.72-18.77); p<0.0001) and LCOS (HR 11.61, 95% CI (5.72-23.57); p<0.0001) as independent predictors of 30-day mortality

Variables	Univariable		Multivariable	
	HR (95 % CI)	P value	HR (95 % CI)	P value
Pre-operative factors				
Age	1,02(1,01-1,03)	<0.0001	1,01(0.99-1,03)	0.224
Dyspnea (NYHA III-IV)	3,33(2,33-4,75)	<0.0001	1,44(0,68-3,03)	0.333
Anemia	2,46(1,68-3,59)	<0.0001	1,06(0,86-3,00)	0.134
Low LVEF	2,81(1,94-4,09)	<0.0001	0.48(0.23-1,02)	0.059
Redo surgery	2,42(1,57-3,71)	<0.0001	1,61(0,70-3,71)	0.261
CTR				
0,55-0,59	2,35(1,30-4,23)	0.004	1,58(0,66-3,80)	0.304
0,6-0,64	**4,52(2,60-7,86)**	**<0.0001**	**2,43(1,02-5,82)**	**0.045**
>0,65	6,08(3,35-11,02)	<0.0001	1,796(0,66-4,83)	0.246
Per-operative factors				
Prolonged CPB time	3,13(2,23-4,39)	<0.0001	1,49(0,81-2,74)	0.196
Post-operative factors				
LCOS	**53,16(35,51-79,59)**	**<0.0001**	**11,61(5,72-23,57)**	**<0.0001**
AKI	9,16(6,07-13,83)	<0.0001	2,19(0,85-5,69)	0.104
Prolonged MV	**46,459(31,15-69,283)**	**<0.0001**	**9,42(4,72-18,77)**	**<0.0001**
Infections	5,04(3,38-7,51)	<0.0001	1,68(0,76-3,68)	0.194

Table 2: Logistic regression analysis for significative variables predictive of 30-day mortality

Conclusion: Cardiac surgical patients with a high pre-operative CTR are at an increased risk of post-operative morbidity and 30 day-mortality. Meticulous patients' selection, risk/benefit assessment, and organization of surgical and anesthesiological management are indispensable to better outcome.

Long-term follow-up of pulmonary arterial circulation after hospitalization for SARS-CoV-2 pneumonia: Dual-energy CT angiographic study in 79 patients

I. Mohamed, A. Duhamel, J. Giordano, A. Ego, N. Fonne, J. Remy, M. Remy-Jardin

Purpose: To evaluate pulmonary vascular abnormalities more than 6 months after hospitalization for SARS-CoV-2 pneumonia.

Methods and Materials: In a cohort of 739 patients having been hospitalized for SARS-CoV-2 pneumonia between March 2020 and April 2021 (T0 period), 222 patients remaining symptomatic more than 6 months after the initial infection underwent a delayed specialized follow-up. The eligibility criteria for the long-term assessment of pulmonary circulation (T1 period) included: (a) a dual-energy CT angiographic (CTA) examination obtained with the same equipment; and (b) interpretable lung perfusion images. 143 patients were excluded because (a) chest CTA had been obtained <6months after pneumonia (n=126); (b) a non-interpretable lung perfusion (n=17). The final study group included 79 patients with morphologic and lung perfusion imaging at T1(mean ± SD between T0 and T1: 7.9 ± 1.7 months).

Results: At T1, morphologic images showed (a) complete resolution of acute PE (12/79; 15.2 %) and newly developed features of chronic PE (3/79; 3.8 %); (b) newly diagnosed acute PE (2/79; 2.5 %). Lung perfusion was abnormal in 69 patients (87.4 %), depicting (a) perfusion defects of 3 types: patchy defects (n=60; 76 %); areas of non-systematized hypoperfusion (n=27; 34.2 %) and/or PE-type defects (n=14; 17.7 %) with (2/14) and without (12/14) endoluminal filling defects; and (b) areas of increased perfusion in 59 patients (74.9 %), superimposed on ground-glass opacities (58/59) and/or areas of vascular tree-in-bud (5/59).

Conclusion: Delayed follow-up showed newly developed CT features of acute and chronic PE but also two types of perfusion abnormalities, suggestive of persistent hypercoagulability as well as unresolved/sequelae of the widespread microangiopathy described in the acute phase of the disease.

Improving Image Resolution in 3-D Lung MRI Images by Combining Two Orthogonal Scans Using Super Resolution Reconstruction

J. Grolig[1, 2, 3], S. Triphan[1, 2], A. Koeppe[3], B. Nestler[3], M.O. Wielpütz[1, 2]; [1]University Hospital of Heidelberg, Department of Diagnostic and Interventional Radiology, Heidelberg, Germany; [2]German Lung Research Center (DZL), Translational Lung Research Center Heidelberg (TLRC), Heidelberg, Germany; [3]Karlsruhe Institute of Technology, Institute for Applied Materials – Computational Materials Science, Karlsruhe, Germany

Purpose/Objectives: Due to time constraints induced by breath holds during 3-D lung MRI imaging, multiple images of different orientations with anisotropic resolution are commonly acquired. Having images with isotropic resolution may help with tasks like automatic segmentation. The idea is to combine two orthogonal scans with high in-plane resolution into one 3-D image with high isotropic resolution using a super-resolution reconstruction (SRR) algorithm.

Methods and Materials: Coronal and axial 3-D T1-weighted gradient echo sequence scans (VIBE) of the same patient and timepoint were interpolated to the target size. The original coronal and axial images had a size of 240 x 320 x 451 mm and 241 x 320 x 45 0mm with resolutions of 4 x 0.9766 x 0.9766 mm and 0.8789 x 4 x 0.8789 mm respectively. To compensate for different breathing positions between the two images, both images were registered onto each other using nonrigid registration. A first high resolution (HR) image estimate was created by averaging the two images. In an iterative process, simulated low resolution (LR) image versions were constructed from the HR image by simulating the imaging process, which were then compared to the original LR images. The error between the original and simulated LR images was calculated and was used together with additional a-priori knowledge based on image gradients to update the SRR image estimate in each iteration.

Results: The resulting SRR images had a size of 240 x 320 x 450 mm with isotropic resolution of 0.8789 mm. In comparison to upsampled images, generated by zero filling in the frequency domain, artefacts due to partial volume effects or interpolation were reduced (see figure 1). Furthermore, anatomic structures such as the trachea could be better depicted in the SRR image (see figure 2). The process of SRR is fully automatic and the final SRR image is generated within fifteen minutes.

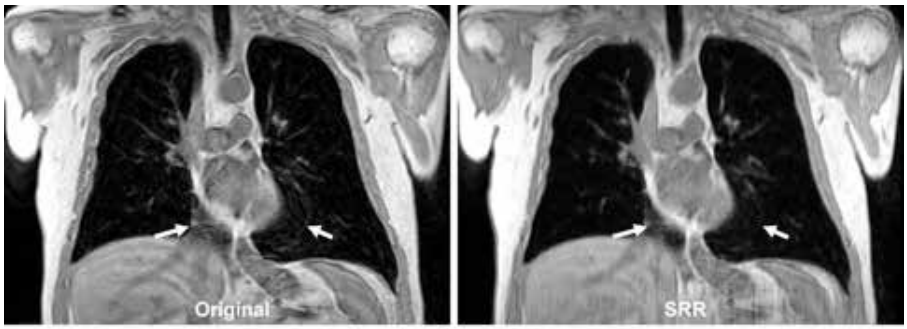

Figure 1: Comparison between interpolated version of original image and the generated SRR image. Less artefacts (marked by arrows) are visible in the SRR image on the right.

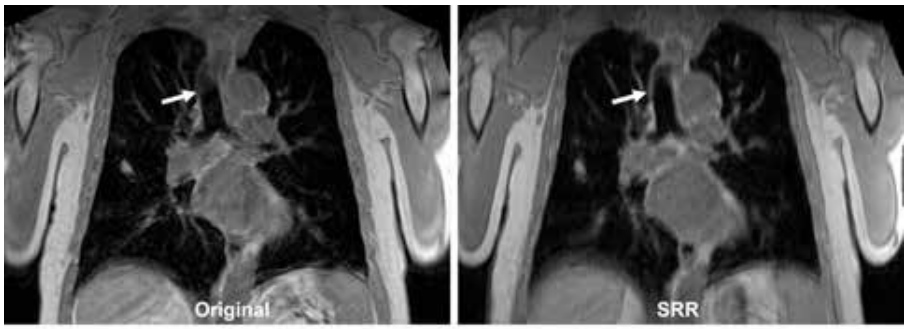

Figure 2: Comparison between interpolated version of original image and the generated SRR image. Anatomic structures like the trachea (arrow) can be better depicted in the SRR image on the right.

Conclusion: Adapting the SRR method, which has been used for other organs, modalities or MRI sequences before, to lung MRI, we were able to generate 3-D images with an isotropic resolution. The SRR images do not show any artefacts, which are apparent in the interpolated versions of the original images. This might help to improve segmentation accuracy, which will be evaluated in further studies. Being able to create isotropic 3-D images from two scans measured at two different breath holds by using conventional, widely available sequences is an important step in MRI imaging of the lung. Since the utilized sequence is widely used and is available on most scanners this technique can be applied to a variety of applications.

AI detection of normal chest radiographs in clinical practice

S. Schalekamp[1], B. van Ginneken[2], K. van Leeuwen[2], K. Murphy[2], M. Prokop[2]; [1]Radboudumc, Imaging, Nijmegen, Netherlands; [2]Radboudumc, Nijmegen, Netherlands

Purpose/Objectives: To assess the clinical performance of a commercial artificial intelligence (AI) product for identification of normal chest radiographs as prerequisite for automated report generation.

Methods and Materials: All consecutive chest radiographs from 1st Oct 2016 to 14th Oct 2016 in a single tertiary medical center were retrospectively analyzed. Bedside radiographs, children, incomplete imaged chest radiographs, and radiographs imported from other hospitals were excluded. If more than one radiograph was available per patient, only the first radiograph was included. The reference standard was set by a chest radiologist who reviewed posteroanterior and lateral radiographs together with the original report and classified the radiographs into the following categories: normal, clinically irrelevant findings (e.g. medical devices), clinically relevant findings (e.g. cardiomegaly), urgent findings (e.g. air space consolidation), and critical findings (e.g. pneumothorax). All posteroanterior radiographs were processed by Lunit INSIGHT CXR3 (Seoul, Korea), which detects 10 different chest abnormalities on a 0-100 confidence scale. The highest score of any abnormality was used to calculate the image normality score, which is 100 - abnormality score. Area under the ROC curve (AUC) was used to assess performance of the AI algorithm for the detection of normal radiographs. Sensitivity at a threshold of a 95% specificity was calculated. Errors at this threshold were analyzed.

Results: A total of 1398 radiographs were acquired in 1008 unique patients. After exclusion of follow-up exams (n=390), bedside images (n=181), external images (n=60), incomplete images (n=9), and children (n=77), 681 radiographs were included. Among these, 223 were normal, 131 had clinically irrelevant findings, 114 clinically relevant findings, 202 urgent findings, and 11 contained critical findings. AUC of the algorithm was 0.916 for the detection of normal cases. At a specificity of 95 % the algorithm reaches a sensitivity of 57 % for detecting normals and identified 126 of the 681 radiographs as normal (19%). At this threshold, AI misclassified 15 radiographs with clinically irrelevant findings, 7 radiographs with clinically relevant findings, and one radiograph with an urgent finding, which was a hilar mass. None of the critical cases were classified as normal.

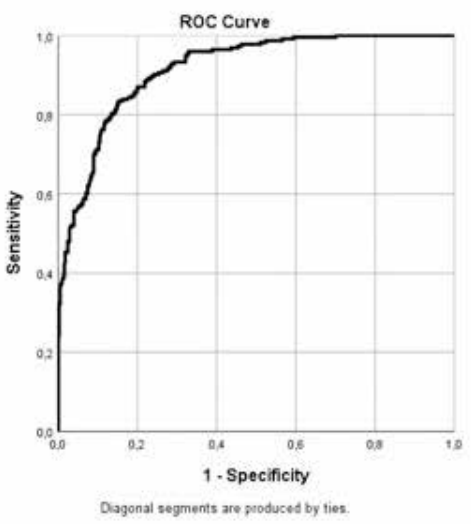

ROC curve of Lunit INSIGHT CXR3 for the identification of normal chest radiographs in a consecutive dataset (n=681).

Conclusion: More than half of the normal radiographs could be identified by AI at a specificity of 95%. A proportion of the radiographs could therefore be removed from the normal routine workflow.

Radiomics in pulmonary neuroendocrine tumours (NETs)

D. Cozzi, E. Bicci, E. Cavigli, A. Bindi, S. Luvarà, C. Moroni, V. Miele; Careggi University Hospital, Emergency Radiology, Florence, Italy

Purpose/Objectives: The aim of this study is to find a correlation using Radiomics between the analysis of CT texture features of primary lesion of neuroendocrine (NET) lung cancer subtypes (typical and atypical carcinoids, large and small cell neuroendocrine carcinoma), Ki-67 index and the presence of lymph nodal mediastinal metastases.

Methods and Materials: This is a single-centre, observational, retrospective study. Between September 2008 and January 2020, all patients with a histological diagnosis of pulmonary NET were retrospectively analysed. Forty-seven patients with histological diagnosis of pulmonary NET with known Ki-67 status and metastases who have performed pre-treatment CT in our department were included. After segmentation of primary lesions, quantitative texture parameters of first and higher orders were extracted. Statistics non-parametric tests and linear correlation tests were conducted to evaluate the relationship between different textural characteristics and tumour subtypes.
Textural features extraction was carried out by means of SlicerRadiomics tool. A total of 107 features of the PyRadiomics lists were selected, belonging to First Order, Shape Based 3D, Gray Level Co-occurrence Matrix (GLCM), Gray Level Size Zone Matrix (GLSZM), Gray Level Run Length Matrix (GLRLM), Neighbouring Gray Tone Difference Matrix (NGTDM) and Gray Level Dependence Matrix (GLDM) classes

Results: Statistically significant ($p < 0.05$) differences were seen in post-contrast enhanced CT in multiple first and higher-order extracted parameters regarding the correlation with classes of Ki-67 index values. Statistical analysis for direct acquisitions was not significant. Concerning the correlation with the presence of metastases, one histogram feature (Skewness) and one feature included in the Gray-Level Co-occurrence Matrix (ClusterShade) were significant on contrast-enhanced CT only. These results suggest that the values of these two features may be associated with the severity of the disease. Skeweness and ClusterShade boxplots with the values that these features showed in the different groups are reported below.

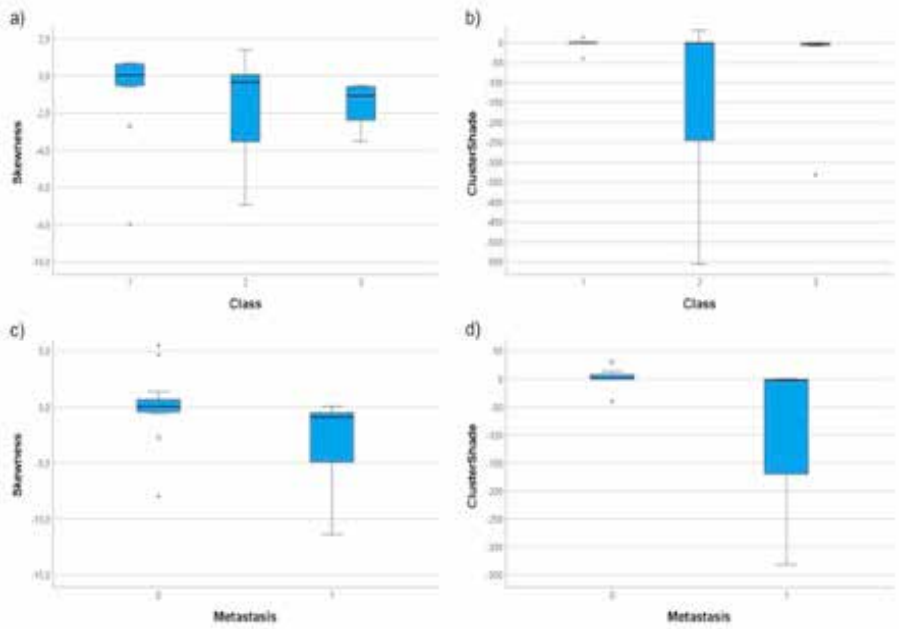

a) Boxplot of Skewness feature vs Ki-67 classes;
b) boxplot of ClusterShade feature vs Ki-67 classes;
c) boxplot of Skewness feature vs absence (0) or presence (1) of metastases;
d) boxplot of ClusterShade feature vs absence (0) or presence (1) of metastasis.

Conclusion: To the best of our knowledge, no correlation has been reported in the literature between radiomics analysis of NETs of the lung and their stratification according to Ki-67 value and the presence or absence of metastases. Despite radiomics has not yet been translated into clinical practice, radiomics feature-based evaluation of primary pulmonary NETs has potential for predicting occult metastases. CT texture analysis may be used as a valid tool for predicting the subtype of lung NET and its aggressiveness, thus aiding in accurate multidisciplinary decision making.

Anterior mediastinal masses – can CT morphologic and radiomic features predict pathologic classification?

M. Mayoral[1, 2], A.M. Pagano[1], J.A.B. Araujo-Filho[1, 3], R. Perez-Johnston[1], J. Zheng[4], K.S. Tan[4], P. Gibbs[1], A.F. Shepherd[5], A. Rimner[5], C.B. Simone[5], G. Riely[6], J. Huang[7], M.S. Ginsberg[1]; [1]Memorial Sloan-Kettering Cancer Center, Radiology, New York, United States; [2]Hospital Clinic, Radiology, Barcelona, Spain; [3]Hospital Sirio-Libanes, Radiology, São Paulo, Brazil; [4]Memorial Sloan-Kettering Cancer Center, Epidemiology and Biostatistics, New York, United States; [5]Memorial Sloan-Kettering Cancer Center, Radiation Oncology, New York, United States; [6]Memorial Sloan-Kettering Cancer Center, Medicine, New York, United States; [7]Memorial Sloan-Kettering Cancer Center, Surgery, New York, United States

Purpose/Objectives: Thymoma and thymic carcinoma are rare thymic epithelial tumors (TET). Surgery is the mainstay of localized TET treatment, with radiologic findings, predominantly by computed tomography (CT), guiding resectability [21070982] [21266921] [21623235] [23667206] [24722150] [26295375] [33447449]. When risk of an incomplete resection is high, neoadjuvant therapy may improve the likelihood for a complete resection [14667602]. More accurate diagnosis of TET through radiomic analysis of CT images has the potential for clinical benefit in the preoperative assessment of these patients [32323834] [28624025]. The aim of this study was to differentiate benign from malignant tumors in the anterior mediastinum, which could be useful in preoperative planning. Additionally, our secondary aim was to differentiate thymoma from thymic carcinoma based on imaging characteristics, which could guide the use of neoadjuvant therapy.

Methods and Materials: From February 2008 to June 2019, 318 consecutive patients referred for thymectomy were selected from our database. We excluded 79 patients who had no pretreatment CT available. Twenty-five morphological characteristics were evaluated by visual analysis, and 101 radiomic features were extracted from each CT. Highly correlated radiomic features were removed using dimension reduction techniques in order to reduce collinearity and noise. Data were split into 70% training set and 30% testing set. In the step of model training, we applied support vector machines to train classification models, performing 5-fold cross validations that were repeated 10 times. Model performance was assessed using the empirical receiver operating curves.

Results: Our final cohort included 239 patients, 59 of whom had benign mediastinal lesions and 180 had malignant thymic tumors. For the benign versus malignant differentiation, the model that integrated both morphologic and radiomic features achieved the highest diagnostic performance (AUC = 0.715), in comparison to the morphological (AUC = 0.605) and radiomic (AUC = 0.678) models alone. Similarly, regarding thymoma versus thymic carcinoma differentiation, the model that integrated both morphologic and radiomic features also achieved the highest diagnostic performance (AUC = 0.810), in comparison to the morphological (AUC = 0.558) and radiomic (AUC = 0.774) models alone.

Conclusion: Benign mediastinal lesions and TET have some distinctive qualitative and quantitative radiological features by machine learning analysis. The diagnostic performance of these models was moderate for differentiating benign from malignant lesions and good for differentiating thymomas from thymic carcinomas. The best diagnostic performance was achieved when both morphological and radiomic features were integrated in the machine learning algorithms

References:
[14667602] Venuta F, Rendina EA, Longo F, et al, (2003), Long-term outcome after multimodality treatment for stage III thymic tumors, Ann Thorac Surg, 1866-1872
[21070982] Yanagawa M, Tomiyama N, (2011), Prediction of thymoma histology and stage by radiographic criteria, Thorac Surg Clin, 1274-1281
[21266921] Ruffini E, Van Raemdonck D, Detterbeck F, et al., (2011), Management of thymic tumors: a survey of current practice among members of the European Society of Thoracic Surgeons, J Thorac Oncol, 614-623
[21623235] Marom EM, Milito MA, Moran CA, et al, (2011), Computed tomography findings predicting invasiveness of thymoma, J Thorac Oncol, 1274-1281
[23667206] Ettinger DS, Riely GJ, Akerley W, et al., (2013), Thymomas and thymic carcinomas: Clinical Practice Guidelines in Oncology, J Natl Compr Canc Netw, 562-76
[24722150] Marx A, Strobel P, Badve SS, et al., (2014), ITMIG consensus statement on the use of the WHO histological classification of thymoma and thymic carcinoma: refined definitions, histological criteria, and reporting, J Thorac Oncol, 596-611
[26295375] Marx A, Chan JK, Coindre JM, et al., (2015), The 2015 World Health Organization Classification of Tumors of the Thymus: Continuity and Changes, J Thorac Oncol, 1383-1395.
[28624025] Yasaka K, Akai H, Nojima M, et al, (2017), Quantitative computed tomography texture analysis for estimating histological subtypes of thymic epithelial tumors, Eur J Radiol, 92:84-92
[32323834] Chen X, Feng B, Li C, et al, (2020), A radiomics model to predict the invasiveness of thymic epithelial tumors based on contrastenhanced computed tomography, Oncol Rep, 1256-1266.
[33447449] Prosch H, Rohrich S, Tekin ZN, Ebner L, (2020), The role of radiological imaging for masses in the prevascular mediastinum in clinical practice, J Thorac Dis, 7591-7597

Prediction of disease severity in COVID-19 patients identifies predictive disease

J. Pan[1], J. Hofmanninger[2], I. Selby[3], J. Aston[4], J. Rudd[5], C.-B. Schönlieb[4], M. Roberts[3], E. Sala[3], M. Pieler[2], A. Markopoulos[2], H. Prosch[1], G. Langs[1]; [1]Medical University of Vienna, Department of Biomedical Imaging and Image-guided Therapy, Vienna, Austria; [2]Contextflow GmbH, Vienna, Austria; [3]University of Cambridge School of Clinical Medicine, Department of Radiology, Cambridge, United Kingdom; [4]University of Cambridge, Department of Pure Mathematics and Mathematical Statistics, Cambridge, United Kingdom; [5]University of Cambridge, Department of Medicine, Cambridge, United Kingdom

Purpose/Objectives: Studies have shown that prediction of coronavirus disease 2019 (COVID-19) severity is difficult, but feasible and important to guide patient management and treatment. However, our understanding of the exact image patterns contributing to accurate prediction is poor. The aim of this study was to predict severe illness in COVID-19 patients based on CT scans early in the disease course, and to identify specific disease patterns holding predictive value.

Methods & Materials: A total of 329 patients from 19 different centers with positive confirmation of COVID-19 by RT-PCR and an initial CT chest scan after the test were used in this study. We used an automated image analysis software to process the first CT scan after positive RT-PCR. It segmented the lung, and then segmented 8 disease patterns based on their CT appearance (ground-glass opacity (GGO), reticular pattern, emphysema, nodular pattern, coarse reticulation or honeycombing, effusion, pneumothorax, consolidation). We calculated the relative volume of each pattern as a percentage of the overall lung volume forming a pattern profile. A random forest classifier was trained to predict severe (ICU and/or deceased) versus non severe (no ICU and survived) disease course based on these pattern profiles in a 10-fold-cross validation experiment.

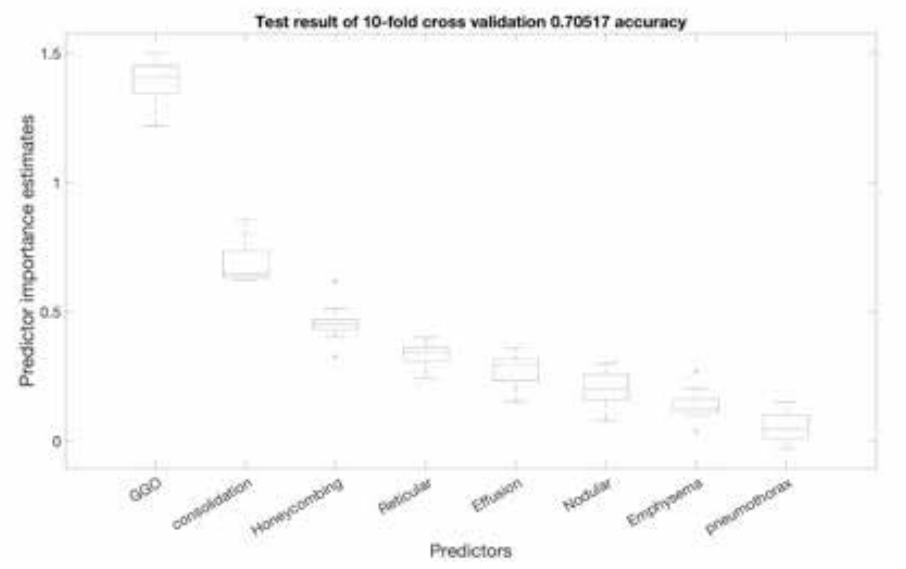

Prediction of severe illness versus non severe illness based on the CT pattern profiles.

Results: Overall 262 patients survived, and overall 106 patients were treated in an ICU. 149 patients developed severe illness. Of the patients being treated in the ICU, 82 survived. Prediction of severe illness versus non severe illness based on the CT pattern profiles yielded 70.52 % accuracy (specificity: 72.19 % , sensitivity: 68.31 %). The top three predictors ranked based on Gini importance were GGO, consolidation and coarse reticulation or honeycombing. Summarizing all 8 patterns into one "diseased" class led to a reduction of accuracy to 57.45% (specificity: 60.99 % , sensitivity: 53.06 %). For the sub-cohort of 223 patients who did not go to ICU, survival prediction with the CT pattern profiles yielded accuracy of 81.61 %. Top ranked predictors for this sub-cohort were GGO, effusion, and reticular pattern.

Conclusion: Quantitative profiles of 8 different disease patterns in lung CT data enable prediction of disease severity in COVID-19 patients. Using the profile of individual disease patterns yields higher accuracy compared to only considering if lung tissue is normal or diseased. The multivariate Gini importance score quantifies how much information a pattern contributes to the prediction. It identified key predictors in the studied COVID-19 cohort, and the sub-cohort not being treated in the ICU.

Automatic quantification of COVID-19 viral pneumonia in chest computed tomography images using an artificial intelligence algorithm developed at a Brazilian university

J.C. Nather-Junior[1], D.T Wada[2], R.V Barros[2], Y.B Frota[2], V.F Muglia[2], M. Koenigkam-Santos[3]; [1]Ribeirao Preto Medical School – University of Sao Paulo, Internal Medicine, Ribeirao Preto, Brazil; [2]Ribeirao Preto Medical School – University of Sao Paulo, Anatomy and Surgery, Ribeirao Preto, Brazil; [3]Ribeirao Preto Medical School - University of Sao Paulo, Medical Imaging, Hematology and Clinical Oncology, Ribeirao Preto, Brazil

Purpose/Objectives: The extent of pulmonary involvement on computed tomography (CT) has been associated with unfavorable clinical outcomes in COVID-19, with prognostic value. In this work, an automatic tool for quantification of COVID-19 viral pneumonia based on artificial intelligence (AI) processing was developed.

Methods and Materials: A local database of chest CT images of patients with COVID-19 viral pneumonia was created (diagnosis confirmed by real-time polymerase chain reaction). Manual segmentation of lungs and pneumonia opacities was first performed by radiologists in training and reviewed by experienced radiologists. Two neural networks with UNET-based architectures were developed, one for lung and the other for pneumonia segmentation. The data augmentation feature was used to increase the sample size before training the networks. In all, 18128 thousand images of 63 different patients were used for training, 15 % of which were separated for the test, using images that were not used in the training data set. The Jaccard index (IoU) was used to assess the similarity between the segmentation performed by the networks and the gold standard performed by radiologists.

Results: After the training and testing stages, the locally created neural networks reached IoU values of 0.89 for lung segmentation and 0.81 for segmentation of opacities compatible with viral pneumonia. After its development, the tool was made available in a secure web environment for open use by users outside the institution. Patients confidentiality was guaranteed. Radiologists from 10 Brazilian states freely registered and used the tool in their clinical routine.

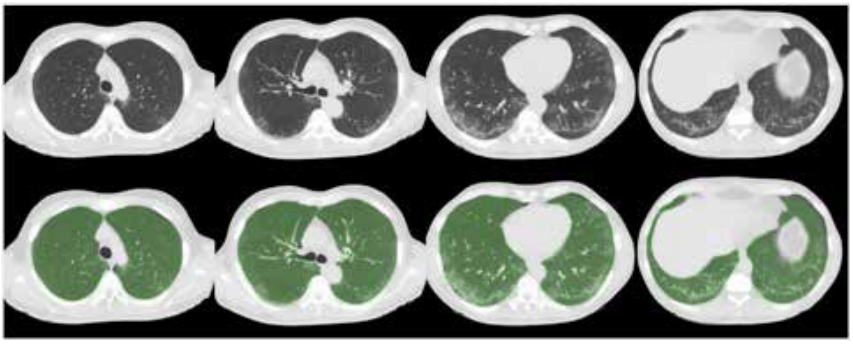

Example of a lung volume segmentation network performance.

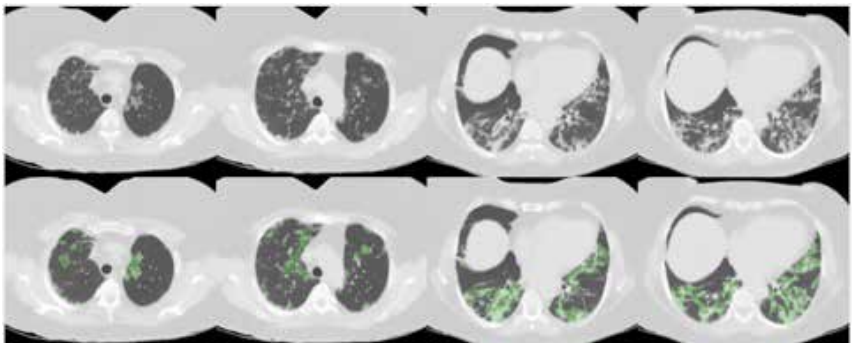

Example of a pneumonia opacities segmentation network performance.

Id do Exame	x
Status	**completo**
Data/Hora inserido	2021- 21:09:21
Data/Hora concluído	2021- 21:12:01
Porcentagem de acometimento	**21.38 %**
Volume pulmões	5843.86 cm³
Volume lesões	1297.25 cm³

Example of the final report generated by the tool (in Portuguese). Processing was carried out completely automatically in about 3 minutes. The last 3 columns show pneumonia extent in percentage, pulmonary volume and opacities (lesions) volume in cm³.

Conclusion: The AI tool created to quantify COVID-19 viral pneumonia showed good performance, using a local database of chest CT images, with segmentation supervised by experienced radiologists as the gold standard. Such a tool can help to make the assessment of COVID-19 viral pneumonia more objective, also facilitating the comparison between studies and longitudinal analysis of the disease.

Evaluation of radiologists' performance compared to a deep learning algorithm for the detection of thoracic abnormalities on chest X-ray

S. Bennani[1], N.-E. Regnard[2], L. Lassalle[2], T. Nguyen[3], C. Malandrin[2], H. Koulakian[4], P. Khafagy[5], G. Chassagnon[1], M.-P. Revel[1]; [1]Hôpital Cochin, Department of Radiology, Paris, France; [2]Réseau Imagerie Sud Francilien, Lieusaint, France; [3]Hôpital Armand Trousseau, AP-HP, Paris, France; [4]Centre interprofessionnel étude et examens médicaux, Paris, France; [5]Groupe Hospitalier Intercommunal Le Raincy-Montfermeil, Montfermeil, France

Purpose/Objectives: To compare the performance of radiologists to that of an artificial intelligence (AI) algorithm for the detection of thoracic abnormalities on chest- X-ray (CXR).

Methods and Materials: Thoracic images of patients who underwent CXR and had a thoracic CT scan within 72 hours at Cochin university hospital were collected over a 10-year period (2010-2020). A senior radiologist specialized in thoracic imaging annotated CXR images for 5 main anomalies (pneumothorax, pleural effusion, mediastino-hilar mass, nodule, and alveolar pattern), with the corresponding CT scan as the standard of reference. Each abnormality was classified by the same chest radiologist into two different categories: detectable on the CXR or only detectable on CT. Twelve readers (4 chest radiologists, 4 general radiologists, 4 radiology residents) read half of the dataset, blinded to the chest radiologist's annotations, CT findings, and AI algorithm (ChestView, Gleamer) results. Their readings were compared to that of the AI algorithm which was previously trained on 89,229 X-ray images, validated on 3687, and tested on 3722.

Results: The study included 500 exams of which 267 presented at least one abnormality seen on CT whereas 233 CXR showed no abnormality. The AI had a sensitivity of 71.43 % to detect visible pneumothoraces whereas chest radiologists, general radiologist and radiology residents had a sensitivity of 70.68 %, 38.86 %, 37.73 % respectively. For visible pleural effusions, the sensitivity was as follows: 86.75 %, 71.12 %, 65.87 %, and 64.02 % for the AI, chest radiologists, general radiologists, and radiology residents respectively. The sensitivity for visible mediastino-hilar masses was 50 %, 48.02 %, 40.44 %, and 32.75 % for the AI, chest radiologists, general radiologists, and radiology residents respectively. Alveolar syndromes were detected with a sensitivity of 73.13 % by the AI, 59.23 % by the chest radiologists, 54.97 % by the general radiologists, and 38.35 % by the radiology residents. For the detection of lung nodules, the sensitivity was 41.91 %, 39.33 %, 29.73 %, and 26.44 % for the AI, chest radiologists, general radiologists, and radiology residents respectively. The specificity of the AI algorithm was equivalent to that of the chest radiologists for all 5 abnormalities.

Conclusion: These preliminary results show that the AI algorithm has higher sensitivity than all readers and equivalent specificity to experts for detecting CXR abnormalities and thus has the potential to decrease diagnostic errors.

The HUNCHEST project – Lung cancer screening pilot studies in Hungary

A. Kerpel-Fronius[1], D. Solymosi[1], Z. Monostori[1], Z. Markóczy[2], L. Rojkó[3], Z. Megyesfalvi[4], K. Bogos[3]; [1]National Korányi Institute of Pulmonology, Radiology, Budapest, Hungary; [2]National Korányi Institute of Pulmonology, Bronchology, Budapest, Hungary; [3]National Korányi Institute of Pulmonology, Pulmonology, Budapest, Hungary; [4]National Korányi Institute of Pulmonology, Tumor Biology, Budapest, Hungary

Purpose/Objectives: In 2013, based on the results of the major international LDCT programs, the HUNCHEST program was initiated in the National Korányi Institute for pulmonology. The main objective of the first trial, which ceased new enrollment in 2019, was to demonstrate the feasibility of a LDCT lung cancer screening project in Hungary. In 2020, a multicenter project was launched to clarify patient pathways in different institutional settings, in the anticipation of a potential nationwide screening program.

Methods and Materials: In HUNCHEST-1, a total of 1890 participants between 50-79 years of age were assigned to undergo lo LDCT. Depending on the volume of solitary pulmonary nodules, participants were classified into negative (no solid nodules, ≤5 mm), indeterminate (nodules between 5-10 mms) and positive screens (solid nodules ≥10 mm). The tumor growth and volume doubling time of negative and indeterminate subjects were reassessed at 1 year and 3 months, respectively. Participants with positive screening results were referred to an expert pulmonologist. In HUNCHEST-2, over 4000 participants were screened in 17 Hungarian centers by using the same methodology. One of the major endpoints constituted the elapsed time between the first positive scan and definitive diagnosis by a multidisciplinary team.

Results: In HUNCHEST-1, results comparable to the NELSON trial were achieved. Based on these results, the implementation of HUNCHEST-2 was approved. Unfortunately, the COVID pandemic was unforeseen, and although the evaluation of the data is still ongoing the patient pathways following a positive screen have been affected. Preliminary results will be however presented at the conference.

Conclusion: HUNCHEST-1 has proven the feasibility of LDCT screening in Hungary, while HUNCHEST-2 will provide data on patient pathways to further assess the equitableness of patient care across the country. Nevertheless, further studies must be initiated to appraise the patient enrollment side, as accurately identifying the at-risk population is one of the major obstacles in the roll-out of a nationwide screening program.

[^{68}Ga]Ga-DOTA-(RGD)$_2$ PET/CT imaging of endothelial activation in COVID-19 patients

E. van Genugten[1], J. van Steenis[1, 2], R. ten Heggeler[1, 2], D. Lobeek[1], M. Brink[1], W. Hoefsloot[3], F. van de Veerdonk[4], M. Netea[4], E. Aarntzen[1], M. Prokop[1]; [1]Radboudumc, Medical Imaging, Nijmegen, Netherlands; [2]University of Twente, MIRA institute for Biomedical Technology and Technical Medicine, Enschede, Netherlands; [3]Radboudumc, Respiratory Diseases, Nijmegen, Netherlands; [4]Radboudumc, Infectious Diseases, Nijmegen, Netherlands

Purpose/Objectives: Endothelial cells are regulators of inflammatory processes[1] and interact with immune cells and tissue components via integrin signaling[2]. During SARS-CoV2 infection, endothelial cells play a central role[3][4]. As endothelial cells express ACE2, they might primarily be infected and subsequent loss of ACE2 function might result in pulmonary angioedema[5] and angiopathy[4]. Inadequate endothelial responses associate with vascular complications[6] and are a major risk factor for multi-organ failure[7].
Positron emission tomography (PET) with [^{68}Ga]Ga-DOTA-(RGD)$_2$ targets $\alpha_v\beta_3$ integrin expression on endothelium. We hypothesized that this could provide insight in localization and magnitude of endothelial activation in lung parenchyma of COVID-19 patients, complementary to anatomical imaging, and in relation to changes in lung perfusion.

Methods and Materials: We performed a prospective observational study in 10 patients with proven SARS-CoV2 infection admitted with respiratory insufficiency (NCT04596943). Patients underwent a [^{68}Ga]Ga-DOTA-(RGD)$_2$ PET/CT scan followed by a CT-subtraction scan of the lungs after intravenous contrast to assess parenchymal enhancement. Segmentation of lung lobes as well as affected lung parenchyma, defined as presence of groundglass opacity or consolidations, were used to quantify tracer uptake using Standardized Uptake Values (SUV)[8]. CT-severity score and local perfusion differences in the lung parenchyma on subtraction CT were correlated to this uptake with Pearson's r. [^{68}Ga]Ga-DOTA-(RGD)$_2$ PET data from a previous study of patients without pulmonary inflammation[9] served as reference and RGD uptake was compared to our study data with an independent T-test.

Results: Patients included in the study had a mean age of 65 years, 7/10 were males and PET/CT scans were obtained a mean of 15 days (range 10-24) after onset of symptoms. RGD uptake in total lung parenchyma (SUVmean 0,99) was significantly increased as compared to controls (SUVmean 0,45) (p=0.0045), and correlated with CT-severity score (R2 = 0.64). Uptake in affected lung parenchyma (SUVmean 1,4) was significantly increased in all patients (p<0.0001).
In non-affected lung parenchyma, RGD uptake (SUVmean 0,83) was increased, although not statistical significantly (p=0.0054).
CT-subtraction showed local variations in lung enhancement, which partly correlated with RGD uptake.

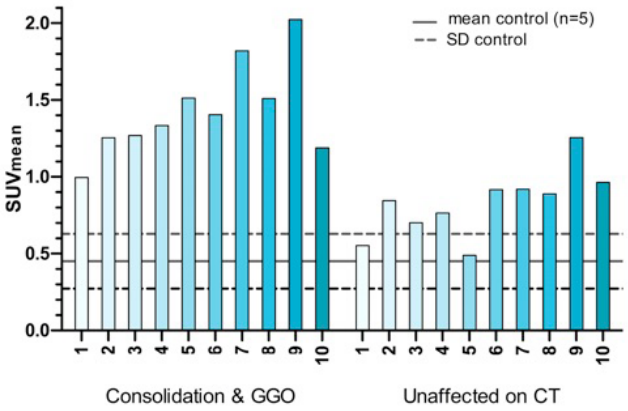

Quantified SUV mean within affected and unaffected parts of the lungs

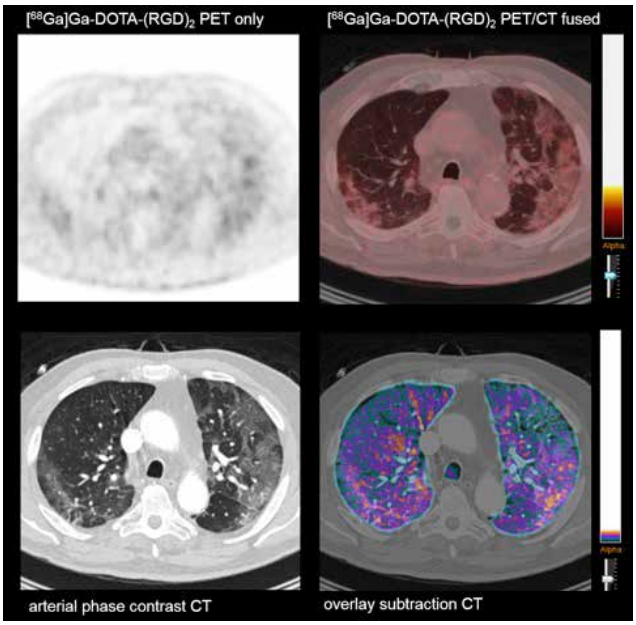

An example of uptake of [^{68}Ga]Ga-DOTA-(RGD)$_2$ witchin the lungs, compared with arterial phase contrast CT and CT subtraction

Conclusion: [^{68}Ga]Ga-DOTA-(RGD)$_2$ PET imaging for in vivo quantification of endothelial cell activation in lung parenchyma in COVID-19 patients with respiratory insufficiency is feasible. Our results suggest involvement of endothelial cells in affected lung parenchyma on CT, as well as at distant sites which supports the notion that endothelium is involved in systemic inflammatory responses.

References:
[1] Pober, J.S., Sessa, W.C., (2007), Evolving functions of endothelial cells in inflammation, Nat Rev Immunol, 803-15, 7(10), https://www.nature.com/articles/nri2171
[2] Cooper, J., Giancotti, F.G., (2019), Integrin Signaling in Cancer: Mechanotransduction, Stemness, Epithelial Plasticity, and Therapeutic Resistance, Cancer Cell, 347-67, 35(3), https://www.sciencedirect.com/science/article/pii/S1535610819300418?via%3Dihub
[3] Ackermann, M. et al., (2020), Pulmonary Vascular Endothelialitis, Thrombosis, and Angiogenesis in Covid-19, N Engl J Med, 120-8, 383, https://www.nejm.org/doi/10.1056/NEJMoa2015432?url_ver=Z39.88-2003&rfr_id=ori%3Arid%3Acrossref.org&rfr_dat=cr_pub++0pubmed
[4] Jin, M.Z., Jin, W.L., (2020), The updated landscape of tumor microenvironment and drug repurposing, Sig Transduct Target Ther, 5(166), https://www.nature.com/articles/s41392-020-00280-x
[5] van de Veerdonk, F. L., et al. , (2020), Outcomes associated with use of a kinin B2 receptor antagonist among patients with COVID-19, JAMA network open, e2017708-e2017708, 3(8), https://jamanetwork.com/journals/jamanetworkopen/fullarticle/2769237
[6] Klok, F.A., et al. , (2020), Incidence of thrombotic complications in critically ill ICU patients with COVID-19, Thromb Res, 145-7, 191, https://www.thrombosisresearch.com/article/S0049-3848(20)30120-1/fulltext
[7] Bikdeli, B. et al. , (2020), COVID-19 and Thrombotic or Thromboembolic Disease: Implications for Prevention, Antithrombotic Therapy, and Follow-Up: JACC State-of-the-Art Review, J Am Coll Cardiol, 2950-73, 75(23), https://www.sciencedirect.com/science/article/pii/S0735109720350087?via%3Dihub
[8] Lessmann N., et al. , (2021), Automated Assessment of COVID-19 Reporting and Data System and Chest CT Severity Scores in Patients Suspected of Having COVID-19 Using Artificial Intelligence, Radiology, E18-E28, 298(1), https://pubs.rsna.org/doi/full/10.1148/radiol.2020202439
[9] Lobeek, D. et al., (2020), Imaging angiogenesis in patients with head and neck squamous cell carcinomas by [68Ga]Ga-DOTA-E-[c(RGDfK)]2 PET/CT, Eur J Nucl Med Mol Imaging, 2647-55, 47, https://link.springer.com/article/10.1007%2Fs00259-020-04766-2

Pre-treatment metastatic site-specific 18F-FDG PET markers are associated with clinical outcomes in patients with NSCLC receiving immunotherapy

D. Kifjak[1, 2], L. Beer[1], A.R. Haug[1], M.E. Mayerhoefer[1, 3], R. Ambros[1], M. Hochmair[4], H. Prosch[1]; [1]Medical University of Vienna, Department of Biomedical Imaging and Image-guided Therapy, Vienna, Austria; [2]UMass Chan Medical School, Department of Radiology, Worcester, United States; [3]Memorial Sloan Kettering Cancer Center, Department of Radiology, New York, United States; [4]Karl Landsteiner Institute of Lung Research and Pulmonary Oncology, Krankenhaus Nord, Department of Respiratory and Critical Care Medicine, Vienna, Austria

Purpose/Objectives: To analyse the prognostic value of metastatic site-specific pre-treatment metabolic tumour burden in patients with advanced non-small-cell lung cancer (NSCLC) treated with PD-1/PD-L1 inhibitors using 18F-FDG-PET-CT.

Methods and Materials: This prospective, single-centre study included 87 patients who underwent 18F-FDG PET-CT before PD-1/PD-L1 inhibitor treatment initiation. We semi-automatically extracted the following parameters: MTV (metabolic tumour volume) and TLG (total lesion glycolysis) for all malignant lesions. TLG and MTV were then separately extracted for each anatomic site (e.g., intrapulmonary lesions, lymph nodes, bone lesions). Each metabolic parameter was dichotomised using the median as a threshold. We compared progression-free survival (PFS) and overall survival (OS) using the Kaplan-Meier test and Cox regression analysis.

Results: Patients were followed-up for a median of 11 months (range 1-63 months). High total baseline MTV and high total baseline TLG were associated with decreased PFS and OS. Particularly, an MTV>112ml and a TLG >690 SUV*ml were significantly associated with decreased median PFS (5 months vs. 9 months, p=0.024; 3 months vs. 9 months, p<0.001) as well as OS (9 months vs 20 months, p=0.002; 11 months vs. median not met, p<0.001). In the univariate analysis, total baseline MTV, TLG as well as bone metastasis TLG were associated with a decreased PFS (p=0.006; p<0.001; p<0.001) and OS (all p<0.001).

Conclusion: In patients with advanced NSCLC treated with PD-1/PD-L1 inhibitors pre-treatment total and bone metastasis metabolically active tumour burden correlate with progression-free survival and overall survival.

CT characteristics of solid lung adenocarcinomas with low FDG uptake

S. Schalekamp[1], H. Prokop[2], G. Lammers[3], I. Kovacs[3], C. Schaefer-Prokop[1, 3]; [1]Radboudumc, Imaging, Nijmegen, Netherlands; [2]Stradins University, Riga, Latvia; [3]Meander Medical Center, Amersfoort, Netherlands

Purpose/Objectives: There is a general understanding that solid adenocarcinomas and the solid part in subsolid adenocarcinomas show an increased FDG uptake on PET corresponding to malignancy. Literature reports a correlation between FDG avid tumor load and prognosis [1]. However, a proportion of solid adenocarcinomas, especially (micro)papillary predominant and mucinous adenocarcinoma of the lung do not show high FDG uptake [2], potentially leading to misinterpretation. Little is known about CT morphology in this subgroup of tumors.

Methods and Materials: From our hospital pathology database, all biopsied and resected adenocarcinoma of the lung between 01-01-2017 and 12-31-2019 were retrieved. Patient age, sex, tumor location and size, as well as CT imaging characteristics and SUVmax on FDG PET/CT with EARL reconstruction were documented. Only lesions with a completely solid appearance on chest CT were analyzed. Adenocarcinomas were classified based on histology subtype according to the IASLC/ATS/ERS lung adenocarcinoma classification [3]. CT characteristics, such as size, location, shape, presence of necrosis or air bronchograms, of adenocarcinomas with a SUVmax <2.5 were compared with adenocarcinomas with a higher FDG uptake (SUVmax ≥2.5).

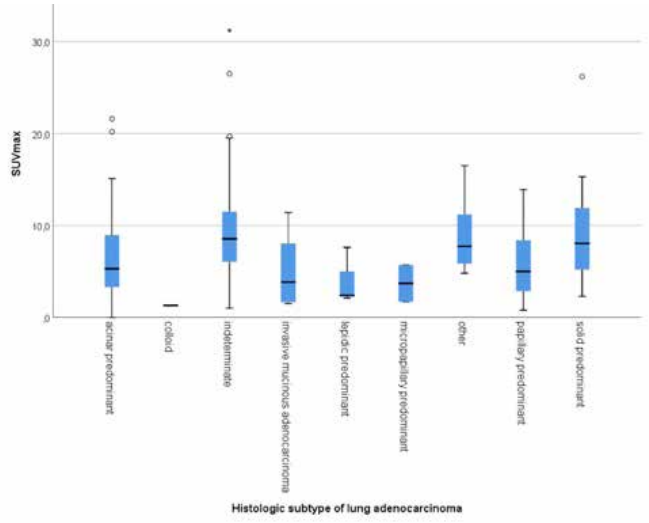

Boxplot of SUVmax on FDG PET/CT by histologic subtype of lung adenocarcinoma.

Results: The study group included 174 solid adenocarcinomas, of which 64 were resected. 19/174 (11%) adenocarcinomas had a SUV max < 2.5. Three of 19 (16%) adenocarcinomas with low FDG uptake were larger than 3 cm, with the biggest lesion a mucinous adenocarcinoma of 77 mm. Size was the only significant discriminator between adenocarcinomas of low and high SUV (mean size of 22 mm (± 19) versus 38 mm (± 22; p < 0.004)). No differences between adenocarcinomas with low or higher FDG uptake were found regarding lesion location, shape, or presence of necrosis or air bronchograms. Only 2 of 10 (micro)papillary predominant adenocarcinomas had a SUVmax < 2.5, both of them < 3 cm. Four of 8 invasive mucinous adenocarcinomas had a SUVmax < 2.5, with two exceeding 5 cm.

Conclusion: Low FDG uptake of small solid lesions in de lung should not be misinterpreted as non-malignant. Adenocarcinomas with low FDG uptake were significantly smaller than adenocarcinomas with higher FDG uptake, but had similar CT morphology and range of histology. Only the relatively rare invasive mucinous adenocarcinomas present with significant size, solid character and low FDG uptake.

References:
[1] Kwon W, Howard BA, Herndon JE, Patz EF, Jr., (2015), FDG Uptake on Positron Emission Tomography Correlates with Survival and Time to Recurrence in Patients with Stage I Non-Small-Cell Lung Cancer., J Thorac Oncol., 897-902, 10(6)
[2] Suarez-Pinera M, Belda-Sanchis J, Taus A, Sanchez-Font A, Mestre-Fusco A, Jimenez M, et al., (2018), FDG PET-CT SUVmax and IASLC/ATS/ERS histologic classification: a new profile of lung adenocarcinoma with prognostic value., Am J Nucl Med Mol Imaging., 100-9, 8(2)
[3] Travis WD, Brambilla E, Nicholson AG, Yatabe Y, Austin JHM, Beasley MB, et al., (2015), World Health Organization Classification of Lung Tumors: Impact of Genetic, Clinical and Radiologic Advances Since the 2004 Classification., J Thorac Oncol., 1243-60, 10(9)

Diagnostic impact of quantitative dual-energy computed tomography perfusion imaging for the assessment of subsegmental chronic pulmonary thromboembolism

K. Hekimoglu[1], P. Celtikci[1], S. Bozbas[2], B. Gultekin[3], T. Akay[3]; [1]Baskent University, Radiology, Ankara, Turkey; [2]Baskent University, Pulmonary Diseases, Ankara, Turkey; [3]Baskent University, Cardiovascular Surgery, Ankara, Turkey

Purpose/Objectives: Chronic thromboembolic pulmonary hypertension (CTEPH) is the only potentially curable form of pulmonary hypertension via surgery. Therefore, it is of great importance to precisely locate all thrombus, including subsegmental pulmonary thromboemboli (SSPE), before embolectomy surgery.
Here we aim to demonstrate the impact of dual-energy computed tomography perfusion imaging (DE-CTPI) in SSPE diagnosis and investigate the quantitative differences between normal lung parenchyma and hypoperfused areas with and without corresponding dual-energy CT angiography (DE-CTA) findings in CTEPH patients.

Methods and Materials: Fourty-three consecutive CTEPH patients detected chronic SSPE with a DE-CTA examination and DE-CTPI were enrolled this study. All DE-CTA and DE-CTPI examinations were acquired with a 3rd generation dual-source multidetector computed tomography scanner.
Two radiologists reviewed DE-CTA and DE-CTPI images retrospectively and in consensus, blinded to radiology report, within two seperate study groups. Iodine maps were evaluated for perfusion defects (which are represented as black areas of pulmonary parenchyma on the color-coded images) and location of hypoperfused segments were noted. Any perfusion defect with a corresponding lesion on lung images such as; pleural effusion, fibrotic sequelae changes, or emphysema were not included.
On each hypoperfused segment, three measurement regions of interest were placed for measuring mean lung parenchyma attenuation (HU), iodine density (mg/mL) and normalized uptake (HU) values.
A one-way repeated measures ANOVA statistical test was performed to determine any significant difference in normally distributed groups and Kruskal-Wallis analysis was performed for groups which are not normally distributed. Post-hoc comparisons for normally distributed groups were conducted by using Tukey's test.

Results: In 45 segments (55.6%) there was PE of the feeding segmental/subsegmental artery whereas for the remaining segments (n=36; 44.4%) there was a perfusion defect without any visible thrombus. Tamhane's T2 post-hoc analysis demonstrated mean lung attenuation values (HU) of hypoperfused areas with PE on CTA, were significantly different from normally perfused areas (P<0.001).
One-way ANOVA test and Tukey's post-hoc analysis demonstrated Iodine density and normalized uptake values of hypoperfused areas with PE were significantly lower than hypoperfused areas without PE on CTA. (P<0.001, F=94.4; P<0.01, F=225 respectively).

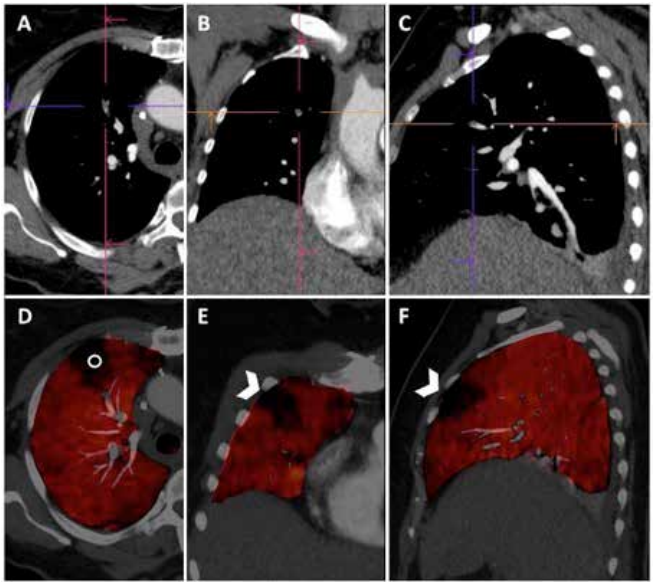

Filling defect in CTA and corresponding perfusion defect in iodine map are seen in the anterior segmentary artery of the right lung upper lobe.

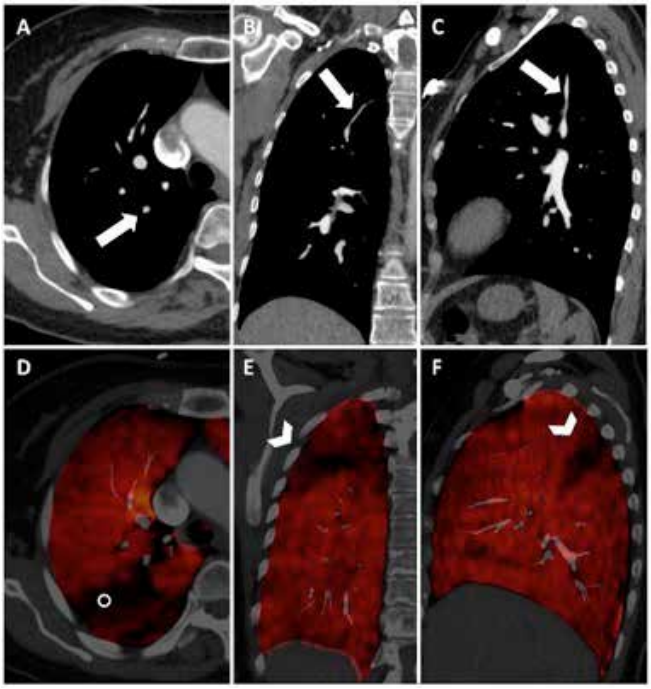

Perfusion defect in the posterior segment of the right lung upper lobe (white circle and white arrowheads) in the patient without filling defect in CTA

Hypoperfused Segment	Thrombus on CTA	No thrombus on CTA	Total
Right Upper Lobe	9	10	19
Right Middle Lobe	5	2	7
Right Lower Lobe	21	6	27
Left Upper Lobe	3	5	8
Left Lower Lobe	7	13	20
Total	45	36	81

Location of hypoperfused segments and presence of thrombus on CTA.

	Lung Attenuation (HU)	Iodine Density (mg/mL)	Normalized Uptake (HU)
Normal	38.7±10.8	1.815±0.529	219.5±58.3
Hypoperfusion without thrombus	1.30±5.59	0.391±0.848	25.74±59.5
Hypoperfusion with thrombus	-2.01±6.54	0.004±0.564	-3.68±41

Mean ± SD values of dual-energy perfusion measurements.

Conclusion: Chronic SSPEs that cannot be seen on routine CTA, could be detected as hypoperfused segments on DE-CTPI due to different iodine density. DE-CTPI iodine maps should be created in addition to CTA in order to accurately diagnose SSPE in CTEPH patients.[1][2][3][4][5][6]

References:
[1] Thieme SF, Hoegl S, Nikolaou K, (2010), Pulmonary ventilation and perfusion imaging with dual-energy CT., Eur Radiol., 2882-2889
[2] Thieme SF, Graute V, Nikolaou K, (2012), Dual Energy CT lung perfusion imaging--correlation with SPECT/CT., Eur Radiol., 360-365
[3] Weidman EK, Plodkowski AJ, Halpenny DF, (2018), Dual-Energy CT Angiography for Detection of Pulmonary Emboli: Incremental Benefit of Iodine Maps., Radiology, 546-553
[4] Pontana F, Faivre J-B, Remy-Jardin M, (2008), Lung perfusion with dual-energy multidetector-row CT (MDCT): feasibility for the evaluation of acute pulmonary embolism in 117 consecutive patients., Acad Radiol, 1494-1504
[5] Grob D, Smit E, Prince J, (2019), Iodine Maps from Subtraction CT or Dual-Energy CT to Detect Pulmonary Emboli with CT Angiography: A Multiple-Observer Study, Radiology, 197-205
[6] Hoey ETD, Mirsadraee S, Pepke-Zaba J, Jenkins DP, Gopalan D, Screaton NJ, (2011), Dual-energy CT angiography for assessment of regional pulmonary perfusion in patients with chronic thromboembolic pulmonary hypertension: initial experience., AJR, 524-532

Maximising radiologist adherence to nodule management protocols in lung screening – A comparison of three radiologist support tools

E. Bartlett[1], S. Zebari[1], S. Desai[2], C. Ridge[2], S. Padley[2], S. Mirsadraee[2], A. Devaraj[2]; 1King's College Hospital NHS Foundation Trust, London, United Kingdom; [2]Royal Brompton Hospital, London, United Kingdom

Purpose/Objectives: Radiologist adherence to nodule management protocols in lung screening is important to ensure optimal and consistent participant management, and to facilitate data collection. The aim of the study was to assess radiologist compliance with a lung screening nodule management protocol, using three different radiologist visual support tools.

Methods and Materials: CT lung screening reports from a UK lung screening programme of 225 consecutive scans containing 328 nodules, from 6 experienced thoracic radiologists were retrospectively reviewed by an independent reader. The cohort was divided into 3 groups of 75 consecutive cases with lung nodules for which radiologists were provided with three different visual support tools to report: i) a nodule management flow-chart similar to that published in the BTS guidelines (Fig.1)

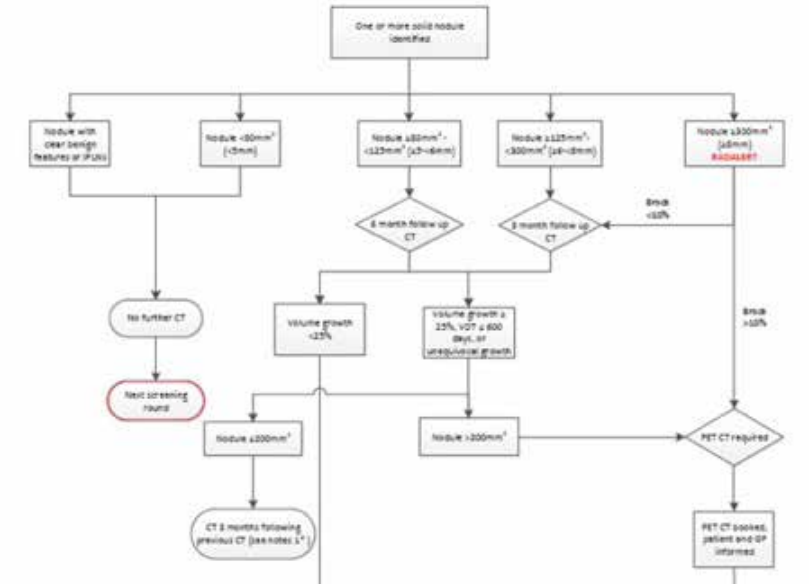

Fig. 1: Excerpt from BTS-style flow chart

ii) a tabulated format with nodule categories, based on LUNG-RADS, modified to BTS guidelines (Fig. 2); and iii) a bespoke mobile phone app (Fig. 3) based on LUNG-RADS modified to BTS guidelines.

Category Descriptor	Score	Descriptor	Management: Imaging time from current scan
Incomplete	**0**	Part or all of lungs cannot be evaluated	6-week LDCT
Negative	**1**	At any scan: No lung nodules *AND/OR* Benign lung nodules: specific calcifications – complete, central, popcorn, concentric rings and fat containing nodules *AND/OR* Intrapulmonary lymph nodes *AND/OR* Non nodular opacities (e.g. atelectasis, scars, vessel confluence, definitely inflammatory nodules) *OR* At baseline: Micronodules <50mm³ (<3mm) (do not require documentation) OR At ≥12-month scan New nodule <30mm³ (<2mm) (do not require documentation) *OR* At any follow-up scan: Resolved nodules (solid, part-solid or ground-glass or nodular consolidation)	Continue with/return to next LDCT screening round
Indeterminate nodule: Very likely benign or indolent	**2**	**Solid nodule(s)** At baseline: ≥50mm³ to <80mm³ (≥3mm to <5mm) *OR* At 6-week, 3-month or 6-month scan: Resolving/shrinking nodules *OR* At ≥12-month scan: Nodule stable or shrinking by volumetric measurements[5] *AND/OR* Growing nodule with VDT >600 days. *OR* At 24-month scan: Old nodule stable by visual assessment when volumetry not possible **PSN(s):** At any follow-up scan: Resolving/shrinking nodule *OR* At 24-month scan: Stable and solid component <8mm *OR* Nodule with solid component growing <2mm since earliest scan and <8mm **pGGN(s):** At any time: <5mm *OR* At any follow-up scan: Resolving/shrinking nodule **Nodular consolidation** At 6-week follow-up scan: Resolving nodular consolidation	Continue with/return to next LDCT screening round

Fig. 2: Excerpt from tabulated nodule management guidelines similar to LUNG-RADS

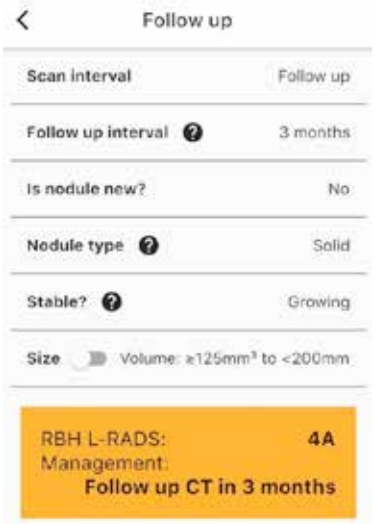

Fig. 3: Example of output from mobile phone app.

The proportion of correct nodule categorizations and management recommendations, as per the protocol, were calculated for each group.

Results: Radiologist compliance with the nodule management protocol in the format of a flow chart, tabulated algorithm, and with use of an app is demonstrated in Table 1.
Radiologist compliance with the nodule management protocol when reporting using a flow chart algorithm, tabulated algorithm and mobile phone app.
The final outcome recommendation was most accurate when using the tabulated algorithm, and least accurate using a flow chart algorithm. On a per nodule basis, the correct classification of a nodule was most accurate when using the mobile phone app.

Table 1	Radiologist nodule management support tool		
	Flow chart algorithm	Tabulated algorithm	Mobile phone app
Number of nodules reported on 75 consecutive scans	94	131	102
Number of individual nodules correctly categorized (%) according to modified Lung-RADS	Not applicable in BTS	121/131 (92.4%)	97/102 (95.1%)
Number of scans with correct overall management recommendation (%)	65/75 (86.7%)	71/75 (94.7%)	69/75 (92.0%)

Conclusion: Radiologists did not adhere to the screening protocol nodule management recommendations in up to 13% of cases with nodules. The study has demonstrated that a modified BTS protocol based on LUNG-RADS can be used either in a tabulated format or with a bespoke mobile phone application, as a safe and reliable adjunct to reporting in lung cancer screening and can improve radiologist accuracy and performance.

Association between Large Arteries Diameter and Heart Function in Subjects free of Cardiovascular Diseases

R. von Krüchten[1], R. Lorbeer[2], A. Peters[3, 4, 5], F. Bamberg[1], C. Schlett[1], B. Mujaj[1]; [1]University Medical Center Freiburg, Department of Diagnostic and Interventional Radiology, Freiburg, Germany; [2]Ludwig-Maximilians-University Hospital, Department of Radiology, Munich, Germany; [3]Biometry and Epidemiology, Medical Faculty, Ludwig-Maximilians-Universität München, Chair of Epidemiology, Institute for Medical Information Processing, Munich, Germany; [4]4. Institute of Epidemiology, Helmholtz Zentrum München, Germany Research Center for Environmental Health, Neuherberg, Germany; [5]German Center for Diabetes Research, Neuherberg, Germany

Purpose/Objectives: Despite a close positional relationship, the relationship between the diameter of the aorta (Ao) and pulmonary artery (PA), and the volumetric properties of the right (RV) and left ventricle (LV) remains unclear. We aimed to investigate the association between Ao segments and PA diameters with RV and LV volumetric properties, as well as the PA/Ao ratio with RV, and LV volumetric properties.

Methods and Materials: In the KORA-MRI study, 339 subjects (mean age 56.3±9.1 years; 43.7 % female) underwent whole-body 3T-MRI. Measurements of the Ao and PA were performed with Syngo.via using DIXON sequences (opposite phase). Cvi42 was used to quantify cardiac functional parameters from a cine-steady-state free precession sequence. The relationship between ascending aorta (AAo), and descending aorta (DAo), as well as PA diameters, and RV and LV function were assessed using linear regression models adjusted for age, sex, and cardiovascular risk factors.

Results: AAo and DAo diameter were positively associated with LV end-diastolic volume (β=5.13, p=0.005; β=7.52, p=<0.001), LV end-systolic volume (β=2.55, p=0.016; β=3.82, p=0.001), while DAo associated with RV end-diastolic volume (β=6.62, p=0.004), and RV end-systolic volume (β=3.75, p=0.012). PA diameter was positively associated with LV end-diastolic volume (β=2.55, p=0.016). Interestingly, the PA/Ao ratio was only positively associated with RV end-diastolic volume and end-systolic volume (β=5.82, p=0.004; β=3.30, p=0.012). When gender differences were assessed, we observed different relationships between males and females.

Conclusion: Aorta and pulmonary artery diameter were associated with LV and RV volumetric parameters in subjects free of cardiovascular diseases suggesting that ventricular volumetric performance directly relates to vascular diameter properties.

Dual-energy CT lung perfusion in systemic sclerosis: Preliminary experience in 101 patients

A. Dupont, V. Koether, A. Duhamel, P. Felloni, T Perez, D. Launay, J. Remy, M. Remy-Jardin

Purpose/Objectives: To investigate lung perfusion in systemic sclerosis (SSc).

Methods and Materials: 101 patients underwent dual-energy CT (DECT) in the follow-up of SSc with pulmonary function tests obtained within two months. Fifteen patients had right heart catheterization-proven PH.

Results: 37 patients had no SSc-related lung involvement (Group A), 56 patients had SSc-related interstitial lung disease (Group B) of variable extent (Group B mild: ≤10 % of lung parenchyma involved: n=17; Group B moderate: between 11-50 %: n=31; Group B severe: >50 %: n=8) and 8 patients had PVOD/PCH (Group C). Lung perfusion was abnormal in 8 patients in Group A (21.6 %), 14 patients in Group B (25 %) and 7 patients in Group C (87.5 %). In Group A and Group B mild (n=54): (a) patients with abnormal lung perfusion (n=14; 26 %) had a higher proportion of NYHA III/IV scores of dyspnea (7 [50 %] vs 7 [17.5 %]; p=0.031), a shorter mean walking distance at the 6MWT (397.0 [291.0;466.0] vs 495.0 [381.0;549.0]; p=0.042) but no evidence of difference in the DLCO % predicted (61.0 [53.0;67.0] vs 68.0 [61.0; 78.0]; p=0.055) when compared to patients with normal lung perfusion (n=40; 74 %); (b) a negative correlation was found between the iodine concentration in both lungs and the DLCO % predicted but it did not reach statistical significance (r=-0.27; p=0.059) and no correlation was found with the PAPs (r=0.16; p=0.29) and walking distance during the 6MWT (r=-0.029; p=0.84).

Conclusion: DECT lung perfusion provides complementary information to standard HRCT scans, depicting perfusion changes in SSc patients with normal or minimally infiltrated lung parenchyma.

Deep learning-based survival prediction model for COPD patients using chest radiographs: Development and validation

C.M. Park[1], J.G. Nam[1], H. Kim[1], S.M. Lee[2], J.M. Goo[1]; [1]Seoul National University Hospital, Radiology, Seoul, South Korea; [2]Asan Medical Center, Radiology, Seoul, South Korea

Purpose/Objectives: Pre-existing indices predicting the prognosis of COPD do not contain radiologic information and are impractical because they involve complex history-taking or exercise tests. We aimed to develop and validate a deep learning-based survival predictor for COPD utilizing chest radiographs ($DLSP_{CXR}$) and integrate it with other clinical factors ($DLSP_{integ}$).

Methods and Materials: Patients with COPD who underwent post-bronchodilator spirometry and CXR in 2011-2015 were retrospectively collected and split into training (n=3,475), validation (n=435), and internal test (n=315) datasets. A deep-learning algorithm predicting survival from CXR was trained ($DLSP_{CXR}$), and was integrated with clinical factors, including age, body mass index, and forced expiratory volume in 1 second (FEV1) ($DLSP_{integ}$). For the external tests, three cohorts were collected from different institutions (n=337-416). The discrimination performance of DLSP was evaluated using time-dependent area-under-the receiver-operating characteristic curves (TD-AUROCs) for 5-year survival. Using one external test cohort, $DLSP_{integ}$ was compared with four COPD-specific clinical indices: BODE, ADO, CAT, and SGRQ. Goodness-of-fit was assessed using the Hosmer-Lemeshow test.

Results: $DLSP_{CXR}$ showed TD-AUROC of 0.670-0.761 for 5-year survival, significantly higher than that of FEV1 in two of three external validation cohorts. $DLSP_{CXR}$ exhibited good calibration for all cohorts ($p>0.05$) and worked as an independent survival predictor from FEV1 in all cohorts ($p<0.01$). Integrated with age, BMI, and FEV1, $DLSP_{integ}$ exhibited TD-AUROC of 0.724-0.825, high than FEV1 in all three cohorts ($p<0.05$). $DLSP_{integ}$ also showed a comparable-to-higher TD-AUROC than BODE (0.866 vs. 0.801; p=0.34), ADO (0.860 vs. 0.889; p=0.51), CAT (0.930 vs. 0.549; $p<0.001$), and SGRQ (0.858 vs. 0.702; p=0.09).

Conclusion: $DLSP_{CXR}$ utilizing CXR worked as a significant survival predictor for COPD, surpassing and independent from FEV1. When integrated with age, BMI, and FEV1, $DLSP_{integ}$ successfully predicted the survival of COPD, comparable to other complex COPD-specific clinical indices.

Quantitative CT Image Matching Analysis of Multiscale Airway and Lung Structure-Function Responses to Bronchodilator in Asthma

C. Lee[1], C. Jiwoong[2], I.K. Lee[2], H.-R. Kang[1]; [1]Seoul National University Hospital, Seoul National University College of Medicine, Allergy and Clinical Immunology, Seoul, South Korea; [2]The University of Kansas School of Medicine, Pulmonary Critical Care and Sleep Medicine, Kansas City, United States

Objectives: Despite the common use of bronchodilator (BD) to improve lung functions in obstructive lung diseases, the physiological mechanism of regional lung structure-function relationship in response to BD is not fully understood. The purpose of this study is to further investigate multiscale lung and airway responses to BD inhalation, using QCT analysis with cross-volume and cross-time image matching.

Methods and Materials: From 67 never-smoking asthmatic patients (M:F=23:44, age=64.6±10.7), we collected full inspiratory (TLC) and full expiratory (RV) CT images and PFT results acquired before and after BD inhalation. We used VIDA Apollo software (Coralville, IA) for individual CT segmentation and measurement, and used in-house QCT software for multiscale lung structure and function assessment that includes non-rigid image registration for cross-volume and cross-time CT image matching and entire conducting airway modeling for linking airways and the lung parenchymal regions. 87 regional airways and parenchymal structure-function features were analyzed. Paired t-test and Pearson's correlation were used to evaluate pre- and post-BD changes and inter-variable association.

Results: After BD inhalation, inspiratory low attenuation area percent (LAA_{IN}%) increased in the whole lung (m±SD=0.8%±2.6%, p=0.013) and all five lobes, while no significant change was found in expiratory low attenuation area percent (LAA_{EX}%), relative regional air volume change (RRAVC), local volume expansion ratio (*J*), or local lung motion (s*). End-tracheal angle was decreased (-2.7±4.4°, p<0.0001) and airway cross-sectional circularity (Cr) was improved in the trachea, the right main bronchus (RMB), and the left main bronchus (LMB) (0.009±0.034,0.011±0.025,0.006±0.022; p=0.0367,0.001,0.020). Normalized airway hydraulic diameter (D_h*) was increased in the trachea, RMB, LMB, bronchus intermedius (BI), left lower lobe bronchus (LLB) (p=0.0001,<0.0001,<0.0001,0.018,<0.0001), and segmental branch subsets of the lobes (p<0.05)

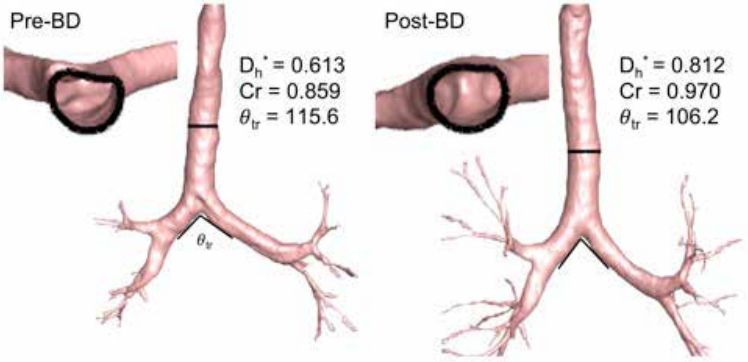

Figure. Demonstration of BD-induced changes in a severe asthma patient (F, 56): airway dilation in the trachea denoted by D_h^*, and associated improvements in Cr (increased, becoming more circular), and end-tracheal angle (θ_{tr}) (reduced). LAA_{IN} increased from 0.15% to 1.61%.

An increase in D_h* at was correlated with the increase in circularity in the trachea, RMB, and LMB (r=0.86,0.48,0.68). Pre-BD D_h* at LLB had a mild correlation with changes in FEV1%pred and FEV1/FVC (r=0.22, 0.29), which may imply the impact of LLB constriction in BD inhalation in the distal airways.

Conclusion: QCT analysis of pre-and post-BD TLC and RV CT image matching provided multiscale structural and functional variables in responses to BD inhalation in asthma. Results showed quantitative evidence of airway dilation and association with other airway and lung function features.

Quantitation of HRCT Findings Using a Texture-Based Automated System for Relation With Clinical Manifestations of IPF-Patients

J.S. Park, J.W. Lee, K.E. Shin; Soonchunhyang University Hospital, Bucheon, Radiology, Bucheon, South Korea

Objectives: To evaluate the usefulness of an automated system for quantification and discrimination of idiopathic pulmonary fibrosis (IPF) and analyze correlation with clinical parameters

Methods and Materials: We retrospectively reviewed the HRCT images of 187 patients with IPF who underwent HRCT between January 2000 and December 2020. An automated system to quantify six regional high-resolution CT (HRCT) patterns: normal, ground-glass opacity, reticular opacity, honeycombing, emphysema; and consolidation was developed using texture and shape features. The volume of the 6 patterns were calculated over the total lung volume and presented as the percent.
The clinical course of IPF patients was evaluated using survival rate and serial measurement of FVC and DLCO. Spirometry was performed as recommended by the American Thoracic Society. The percentages of inflammatory cells in BAL fluids were analyzed with the parameters of HRCT in supine and prone position.

Results: FVC was correlated with reticulation followed by honeycomb and emphysema scores in supine position (beta: -0.393, -0.177 and 0.186, p=0.000, 0.027 and 0.019, respectively) and prone position (beta: -0.403, -0.169 and 0.185, p=0.000, 0.037, and 0.023, respectively). DLCO was correlated with reticulation followed by honeycomb and emphysema scores in supine position (beta: -0.336, -0.227 and -0.158, p=0.000, 0.007, and 0.056, respectively) and in prone position (beta: -0.376, -0.219 and -0.196, p=0.000, 0.011 and 0.021, respectively).
On analysis of BAL fluids, consolidation scores were correlated with macrophage percentages in prone position (r=0.325, p=0.0008) and in supine position (r=0.204, p=0.0296) and neutrophil percentages in prone position (r=0.310, p=0.0014) and in supine position (r=0.1835, p=0.051).

Conclusion: The texture-based automated quantification for various regional patterns of IPF can be used for objective and reproducible assessment of disease severity and were found to correlate with results of lung function and BAL fluid in patients with IPF.

Predictive CT Features of Visceral Pleural Invasion by Lung Cancer That Abut the Pleura

S.R. Kang, J.Y. Rho; Wonkwang university hospital, Radiology, Iksan, South Korea

Objectives: To evaluate the association between pleural signs and visceral pleural invasion (VPI) of lung cancer that abut the pleura.

Methods and Materials: From January 2010 to November 2021, primary lung cancer that abuts the pleura in 100 patients (30 patients [30%] with pathologically proven visceral pleural invasion and 70 patients [70%] without pleural invasion) were enrolled. Pleural signs, including pleural shift, pleural thickening, the contour of the fissure, increased density of extrapleural fat, tumor border, and angle between the margin of the mass and the pleural surface were retrospectively assessed on preoperative CT. Pleural signs were categorized into four types of interlobar fissure pleura (group A) and non-interlobar fissure pleura (group B), respectively: type I, tumor abuts the pleura with no pleural retraction or bulging appearance; type II, tumor with pleural retraction; type III, tumor with bulging pleural appearance; type IV, tumor with both pleural retraction and bulging appearance. We evaluated the association between pleural signs and pathologically confirmed visceral pleural invasion (VPI).

Results: Clinicopathologic features of enrolled 100 patients are in Table 1. In group A, type I accounted for 7.0%, type II for 48.8%, type III for 9.3%, type IV for 34.9%. In group B, type I accounted for 50.9%, type II for 36.8%, type III for 8.8%, type IV for 3.5%. The relationship between pleural signs and VPI is in Tables 2 and 3. Type IV in group A showed the highest rate of VPI (66.7%). Among them, the convex tumor border and obtuse angle presented the highest rate of VPI (66.7%, 66.7%, respectively).

Parameter	Result
Age (years)	67.9 ± 8.4
Sex	
Men	66
Women	34
Tumor size (mm)	29.8 ± 14.7
Tumor histologic analysis	
Adenocarcinoma	72
Squamous cell ca	18
Others	10
Tumor location	
RUL	23
RML	13
RLL	16
LUL	27
LLL	21
T stage	
T1	42
T2	50
T3	6
T4	2
Pleural invasion grade	
PL0	70
PL1+PL2	28
PL3	2
Lung resection	
Wedge resection	12
Segmental resection	3
Lobectomy	85
CT~op interval (days)	25.0 ± 15.3
Nodule density	
Solid	76
Subsolid	24
Interlobar fissure pleura (group A)	43
Non-interlobar fissure pleura (group B)	57
Costal pleura	48
Mediastinal pleura	7
Diaphragmatic pleura	2

Table 1. Clinicopathologic features of 100 patients with primary lung cancer that abut the pleura

Type Total = 43(16)	Pleural thickening (-) = 24(9) Contour smooth = 23(8)	irregular = 1(1)	(+) = 10(7) Contour Smooth = 9(6)	irregular = 1(1)
I = 3(0)	3(0)	0(0)	0(0)	0(0)
II = 21(5)	18(3)	0(0)	3(2)	0(0)
III = 4(1)	2(0)	0(0)	1(0)	1(1)
IV = 15(10)	9(5)	1(1)	5(4)	0(0)

Note. Data are number of tumors. Data in parentheses are number of tumors with visceral pleural invasion

Table 2. Association between pleural signs and visceral pleural invasion, in group A

Type Total = 57(14)	Pleural thickening (-) = 25(3) Increased extrapleural fat density (-) = 35(5)	(+) = 6(2)	(+) = 4(1) Increased extrapleural fat density (-) = 10(4)	(+) = 6(3)
I = 29(4)	23(2)	2(1)	4(1)	0(0)
II = 21(7)	7(1)	3(0)	5(3)	6(3)
III = 5(2)	3(1)	1(1)	1(0)	0(0)
IV = 2(1)	2(1)	0(0)	0(0)	0(0)

Table 3. Association between pleural signs and visceral pleural invasion, in group B

Conclusion: When the tumor shows both pleural retraction and bulging appearance (Type IV of group A) with convex border and obtuse angle, it can be helpful finding for prediction of VPI by primary lung cancer that abut the fissure.

References:
[1] Shuyi Yang, Liang Yang, Lin Teng, et al., (2018), Visceral pleural invasion by pulmonary adenocarcinoma ≤3 cm: the pathological correlation with pleural signs on computed tomography, Journal of Thoracic Disease, 3992-3999, 10(7)
[2] Jui-Sheng Hsu, Twei-Shiun Jaw, Chih-Jen Yang, et al., (2017), Convex border of peripheral non-small cell lung cancer on CT images as a potential indicator of pleural invasion, Medicine, (e7323), 96:42

Association of 10-year Mortality and Incidental Abnormalities on Screening Thoracic Computed Tomography: A Single-center Study

J.E. Lee[1], W.G. Jeong[2], J.H. Kim[1], H.M. Park[1], Y.-H. Kim[1]; [1]Chonnam National University Hospital, Radiology, Gwangju, South Korea; [2]Chonnam National University Hwasun Hospital, Radiology, Gwangju, South Korea

Objectives: To investigate whether there is association between long-term all-cause mortality and incidental abnormalities on thoracic computed tomography (CT) among general screening population.

Methods and Materials: In this retrospective cohort study, we analyzed at data from subjects visited within a single health promotion center between 2007 and 2010. Screening thoracic CT scans of study subjects were visually assessed by two thoracic radiologists for three CT abnormalities status including interstitial lung abnormality (ILA) (non-fibrotic or fibrotic), coronary artery calcification (CAC) (moderate or heavy), and emphysema (≥ 5% of the lung). All-cause mortality over a 10-year follow-up time was compared according to three CT abnormalities status using Kaplan-Meier analysis with log-rank test. Cox proportional hazards models were used to analyze associations of three CT abnormalities with all-cause mortality.

Results: A total of 859 health screening subjects with thoracic CT were evaluated, the mean age was 59 years and 582 (68%) were men. Of the entire study subjects, 21 (2%) had findings of fibrotic ILA, 35 (4%) had findings of non-fibrotic ILA, 36 (4%) had findings of heavy CAC, 64 (7%) had findings of moderate CAC, and 32 (3%) had findings of emphysema (≥ 5% of the lung). Study subjects with CT abnormalities including fibrotic ILA, moderate/heavy CAC, and emphysema (≥ 5% of the lung) had higher cumulative incidence of death than others (P <. 05). After adjustment for covariates, fibrotic ILAs were independently associated with a higher risk of death (hazard ratio, 2.95, [95% confidence interval, 1.25 – 6.93], P = .013) among the CT abnormalities and clinical relevant factors.

Conclusion: Incidental abnormalities on screening thoracic CT were associated were associated with a higher risk of all-cause mortality. Among the CT abnormalities, fibrotic ILAs were independently associated with a higher risk of all-cause mortality.

Lateral Chest Radiograph: "Spine sign" and More

E.S. Lee; Hangang Sacred Heart Hosp. Medical College Hallym Univ, Dept. of Diagnostic Radiology, Seoul, South Korea

Objectives: On lateral chest view obtained in normal subjects, the overall posterior opacity tends to decrease from the level of the upper thoracic spine to that of diaphragm. The "spine sign" is any alternating in this typical pattern and is suggestive of pathology in the lower part of the chest.

Methods and Materials: In these days, the lateral chest radiograph has received decreasing attenuation and routine chest radiographs are often confined to frontal views probably due to chest CT becoming the imaging gold standard for mediastinum and lung. But lateral chest radiograph allows better visualization of certain structures including lower lobes.

Results: The "spine sign" shows useful diagnostic performance for detecting lower lobe abnormalities. I will illustrates various abnormalities by this sign.

Conclusion: On lateral chest radiographs, the spine sign is useful to detect lower chest abnormalities and is related to various underlying abnormalities and is, per se, non-specific.

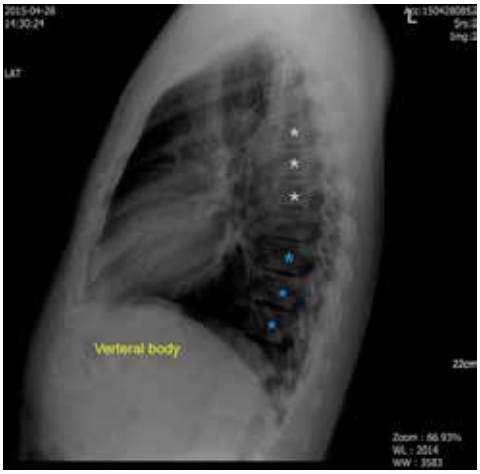

Spine sign on vertebral body

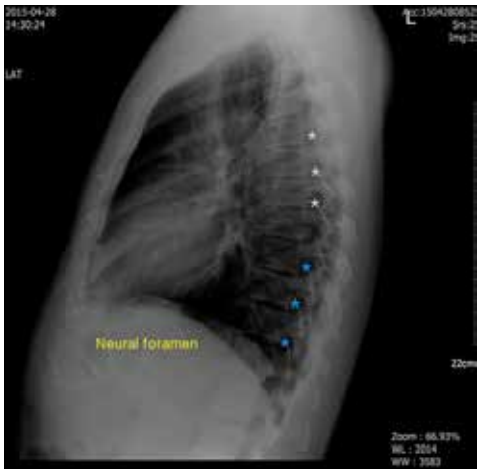

Spine sign on neural foramen

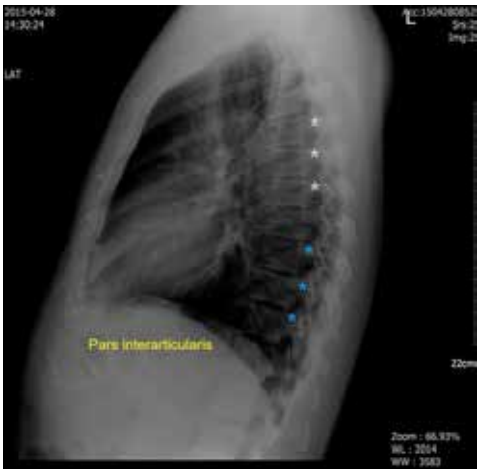

Spine sign on pars interarticularis

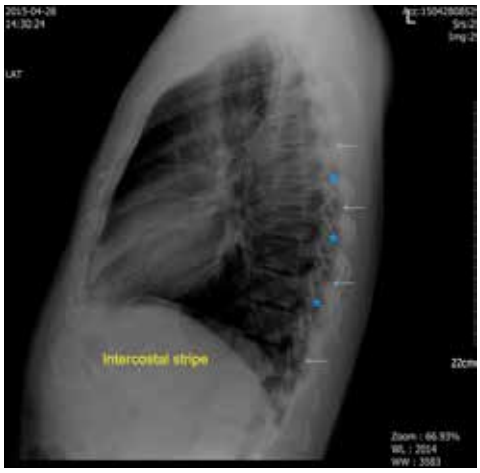

Spine sign beneath intercostal stripe

Prediction of Total Lung Capacity Using Chest Radiographs: Validation of Technical Performance and Clinical Utility

H. Kim[1], K.N. Jin[2], S.-J. Yoo[3], C.H. Lee[4], H. Hong[5], J. Witanto[6], S.H. Yoon[1]; [1]Seoul National University Hospital, Radiology, Seoul, South Korea; [2]SMG-SNU Boramae Medical Center, Radiology, Seoul, South Korea; [3]Hanyang University Medical Center, Radiology, Seoul, South Korea; [4]Seoul National University Hospital, Internal medicine, Seoul, South Korea; [5]Seoul National University Hospital, Medical Research Collaborating Center, Seoul, South Korea; [6]MEDICALIP Co. Ltd., Seoul, South Korea

Purpose/Objectives: Estimation of the total lung capacity (TLC) using chest radiographs has been based on time-consuming methods such as planimetric techniques and manual measurements. We aimed to develop and validate a deep learning-based, end-to-end, multidimensional model which can estimate TLC from chest radiographs and demographic variables (age and sex) with high accuracy and reproducibility using multicenter retrospective cohorts.

Methods and Materials: Our model was pretrained using 50,000 chest CT scans and fine-tuned on 3,523 pairs of posteroanterior chest radiograph and plethysmographic TLC, which was validated in three separate, retrospective cohorts: 1) external validation set 1 (EVAL1; n = 207) and external validation set 2 (EVAL2; n = 216) for technical performance; 2) idiopathic pulmonary fibrosis (IPF) cohort (n= 217) for clinical utility. Technical performance was evaluated using various agreement measures, and the clinical utility was assessed in terms of the prognostic value for overall survival using multivariable Cox regression adjusting for the clinical risk factors and pulmonary function test results. Feasibility of substituting predicted TLC for forced vital capacity in a well-validated risk score for IPF was also evaluated.

Results: Between the observed and predicted TLC, the mean difference and within-subject standard deviation were 0.04 L and 0.24 L, respectively, in EVAL1 and 0.02 L and 0.23 L, respectively, in EVAL2. The repeatability coefficient was 2.03 L (95% confidence interval [CI]: 1.86, 2.25 L) for EVAL1 and 1.45 L (95% CI: 1.33, 1.61 L) for EVAL2.
In patients with IPF, greater predicted TLC at baseline was associated with lower risk of mortality (adjusted hazard ratio for 2-year overall survival, 0.56 [95% CI: 0.34, 0.91; P=.02]; adjusted hazard ratio for 3-year overall survival, 0.55 [95% CI: 0.38, 0.80; P=.002]). Prognostic discrimination of the risk scoring system was well maintained after substituting predicted TLC for forced vital capacity (C-index for 2-year overall survival before substitution, 0.79 [95% CI: 0.73, 0.86]; C-index after substitution, 0.77 [95% CI: 0.70, 0.82]; P=.29).

Conclusion: TLC can be estimated using age, sex, and chest radiograph. The predicted TLC is associated with overall survival in patients with IPF after adjusting for the clinical risk factors and pulmonary function test results.

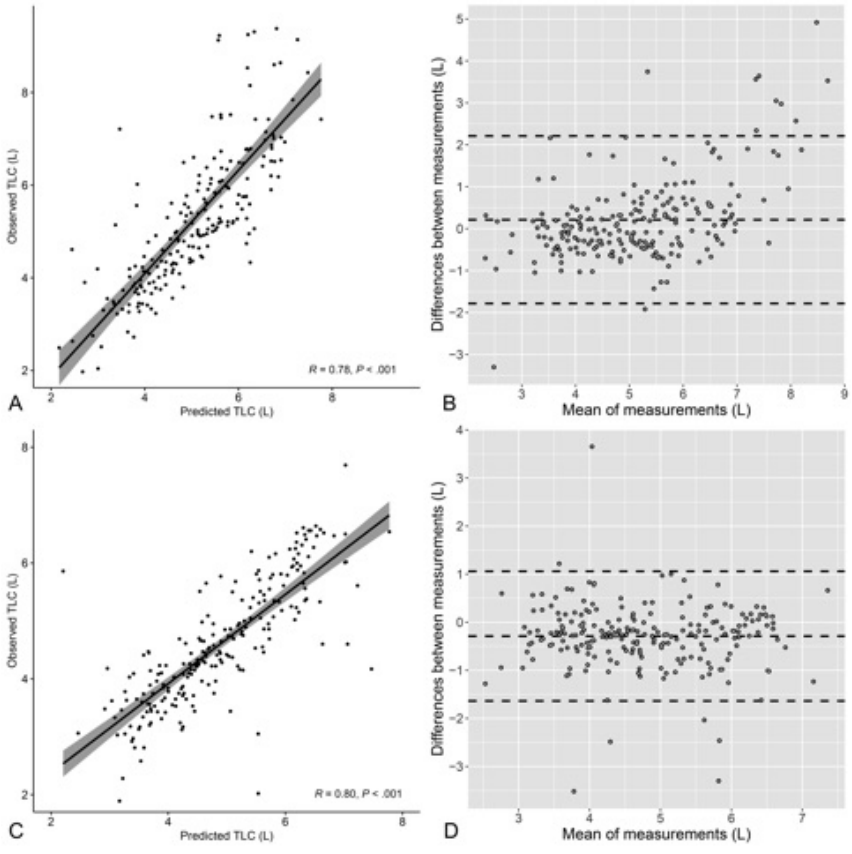

(A) Scatter plot and (B) Bland-Altman plot in the external validation set 1.
(C) Scatter plot and (D) Bland-Altman plot in the external validation set 2.

EDUCATIONAL POSTERS

Abstracts appear as submitted to the system and have not been checked for correctness and completeness.
Please visit the ePoster gallery to view the final posters.

A-129 **A case series over a 5-year period of incidental myocardial uptake on nuclear medicine bone studies in an Irish oncology centre**
R. Hayden, I. Irvine, P. Cooper, G. Allen, L. Greene, L. McCarthy, A. Francis, I. Crosbie; University Hospital Waterford, Radiology, Waterford, Ireland

A-146 **MitraClip-related infective endocarditis**
M. Pudis, I. Sánchez-Rodríguez, P.C. Notta, A. Palomar-Muñoz, S. Bondia-Bescós, B. Hervás-Sanz, L.M. Gràcia-Sánchez; Hospital Universitario de Bellvitge, Nuclear Medicine – PET, Barcelona, Spain

A-187 **Bronchial artery embolization-an endovascular approach to manage massive haemoptysis**
L. Shiu; PYNEH, Radiology, Hong Kong, Hong Kong SAR, China

A-155 **Complications of imaging guided thoracic intervention. What every radiologist should know beyond pneumothorax**
L.B. Cabanzo Campos[1], M. Perez Toran[2], A.L. Sánchez Martínez[1], O. Persiva Morente[1], D. Varona Porres[1], L.A. Del Carpio Bellido[1], J. Andreu Soriano[2]; [1]Hospital Universitari Vall d'Hebron IDI, Radiología torácica, Barcelona, Spain; [2]Hospital Universitari Vall d'Hebron, Radiología torácica, Barcelona, Spain

A-118 **Approach to multinodular pattern on HRCT**
O.W. Hamer[1], S. Meiler[1], B. Pregler[2]; [1]University Medical Center Regensburg, Radiology, Regensburg, Germany; [2]Ernst von Bergmann Klinikum, Radiology, Potsdam, Germany

A-153 **Benign thoracic asbestos related disorders: An ongoing matter**
P. Olmedilla[1], S. Hernandez Muñiz[2], V. Quintana Checa[1], P. Caballero[2], F. Fernandez Alarza[1], M.J. Olivera[2]; [1]Hospital Universitario Fundación Alcorcón, Radiology, Alcorcón, Spain; [2]Hospital Universitario de La Princesa, Radiology, Madrid, Spain

A-180 **Beyond the solid lung cancer: Raising awareness of less common lung cancer types**
L. Tamkeviciute[1, 2, 3], A. Gupta[1], D. Penha[4, 5], E. Pinto[4], K. Irion[1]; [1]Manchester University NHS Foundation Trust, Radiology, Manchester, United Kingdom; [2]Lithuanian University of Health Sciences hospital Kaunas Clinics, Radiology, Kaunas, Lithuania; [3]National Cancer Institute, Radiology, Vilnius, Lithuania; [4]Universidade da Beira Interior, Covilha, Portugal; [5]Liverpool Heart and Chest Hospital NHS Foundation Trust, Liverpool, United Kingdom

A-136 **Chronic pulmonary thromboembolism: Imaging findings and differential diagnoses**
T.R. Yamanari, M. Valente Yamada Sawamura, R.V. Almeida Torres, G. Guido Cerri; Hospital Sirio Libanes, Sao Paulo, Brazil

A-111 **CT aspects of pulmonary tuberculosis in children**
H. Ramdani[1], S. El Haddad[2], N. Allali[2], L. Chat[2]; [1]Mohammed V military hospital, Radiology, Rabat, Morocco; [2]Children's hospital – Ibn Sina University Hospital, Radiology, Rabat, Morocco

A-160 **Drug-induced lung disease: What to expect in an oncologic scenario?**
S. Rodrigues, R. Martins, H. Rodrigues, D. Fonseca; Instituto Português de Oncologia Francisco Gentil, Porto, Porto, Portugal

A-137 **Histoplasma infection: Imaging spectrum of thoracic histoplasmosis**
T.R. Yamanari, M. Valente Yamada Sawamura, R.V. Almeida Torres, G. Guido Cerri; Hospital Sirio Libanes, Sao Paulo, Brazil

A-141 **Imagin findings in Silicosis: A pictorial review**
A. Antolin Redondo[1], L.B. Cabanzo Campos[2], A.L. Sánchez Martínez[2], D. Varona Porres[2], O. Persiva Morente[2], L.A. Del Carpio Bellido[2], J. Andreu Soriano[1]; [1]Hospital Universitari Vall d'Hebron, Radiología torácica, Barcelona, Spain; [2]Hospital Universitari Vall d'Hebron IDI, Radiología torácica, Barcelona, Spain

A-152 **Interstitial lung disease in collagen vascular disease: A pattern approach**
J. Arenas-Jiménez[1], E. García-Garrigós[1], S. Ruiz-Alcaraz[2], I. Gayá García-Manso[3], M. Sirera[1], R. García-Sevila[3]; [1]Hospital General Universitario de Alicante, Radiology, Alicante, Spain; [2]Hospital General Universitario de Elche, Pneumology, Elche, Spain; [3]Hospital General Universitario de Alicante, Pneumology, Alicante, Spain

A-103 **Large airway diseases: A pictorial review of non-neoplastic pathology**
E. Cavigli[1], D. Cozzi[1], C. Moroni[1], A. Bindi[1], S. Luvarà[1], V. Miele[1], M. Bartolucci[2]; [1]Careggi University Hospital, Emergency Radiology, Florence, Italy; [2]Santo Stefano Hospital, Radiology, Prato, Italy

A-154 **Left isomerism: Review of CT imaging findings**
R. Silva Martins, S. Rodrigues, D. Fonseca; IPO Porto, Imaging Department, Porto, Portugal

A-170 **Pulmonary function tests – What the radiologist needs to know**
S. Saujani[1], J. Briggs[2]; [1]Oxford University Hospitals, Oxford, United Kingdom; [2]Royal Berkshire Hospital, Reading, United Kingdom

A-192 **Pulmonary metastases or not: That is the question!**
C. Strappa[1], G. Cicchetti[1, 2], L. Iaccarino[1], S. Amodeo[1], A. Grimaldi[1], A. del Ciello[2], L. Calandriello[2], A. Farchione[2], A.R. Larici[1, 2]; [1]Università Cattolica del Sacro Cuore, Rome, Italy; [2]Fondazione Policlinico Universitario Agostino Gemelli IRCCS, Rome, Italy

A-179 **Radiological assessment of donor and recipient before lung transplantation**
W. Bernard[1], M. Jelitto[2], W. Karolak[3], J. Wojarski[3], S. Żegleń[4], K. Dziadziuszko[2], E. Szurowska[2]; [1]University Clinical Centre in Gdansk, Department of Radiology, Gdansk, Poland; [2]Medical Univerisity of Gdansk, 2nd Division of Radiology, Gdansk, Poland; [3]Medical Univerisity of Gdansk, Department of Cardiac & Vascular Surgery, Gdansk, Poland; [4]Medical Univerisity of Gdansk, Division of Pulmonology, Gdansk, Poland

A-181 **Revisiting the 4T´s: A pictorial review of anterior mediastinal masses on CT**
R. Silva Martins, S. Rodrigues, D. Fonseca; IPO Porto, Imaging Department, Porto, Portugal

A-104 **Role of Chest Imaging in Viral Lung Diseases**
D. Cozzi, A. Bindi, E. Cavigli, C. Moroni, S. Luvarà, V. Miele; Careggi University Hospital, Emergency Radiology, Florence, Italy

A-114 **Searching in the mediastinum: Atypical and unusual mediastinal masses**
D. Varona Porres[1], I. Sansano[2], L.B. Cabanzo[1], A.L. Sánchez Martínez[1], A. Chaachou Charradi[2], Ó. Persiva[1], L. Del Carpio[1], J. Andreu[1]; [1]Hospital Vall de Hebrón, Radiology, Barcelona, Spain; [2]Hospital Vall de Hebrón, Pathology, Barcelona, Spain

A-182 **Silicosis: Radiological findings on chest radiograph and CT**
J.P. Meneses[1], T.P. Fonseca Torres[1], M.J.N. Bento e Silva[1], C. Oliveira[1], R. Ramos[1], J. Abrantes[1], C. Parra[2]; [1]Centro Hospitalar de Trás-os-Montes e Alto Douro, Imagiology Department, Vila Real, Portugal; [2]Centro Hospitalar de Trás-os-Montes e Alto Douro, Pulmonology Department, Vila Real, Portugal

A-166 **The dark spectrum of tobacco lung damage**
J. Veiga, C. Ruano, O. Fernandes; Centro Hospitalar Lisboa Central, Radiology, Lisbon, Portugal

A-124 **The Trials and Triumphs of a DGH Pulmonary Nodule MDT**
S. Malekout[1, 2], R. Findlay[3], C. Stephenson[3], A. Rhodes[1]; [1]Kingston Hospital NHS Foundation Trust, Radiology, London, United Kingdom; [2]Chelsea & Westminster Hospital NHS Foundation Trust, Radiology, London, United Kingdom; [3]Kingston Hospital NHS Foundation Trust, Respiratory Medicine, London, United Kingdom

A-127 **Treatment-related pulmonary manifestations of immunotherapy**
S. Patel, A. Nair, A. Ahmed, A. Procter, M. Duncan, M. Taylor; University College London Hospital, Imaging, London, United Kingdom

A-163 **Tree key features for diagnosing Heterotaxy Syndrome. A relevant and perhaps not so uncommon anomaly**
C. Vilá[1], A. Villanueva Campos[2], O. Persiva[3], R. Vidal[1], L. Jiménez Juan[4], S. Isarria[5], A. Villanueva[6]; [1]Centro Médico Teknon – Grupo Quirónsalud, Radiology, Barcelona, Spain; [2]Hospital Ramon y Cajal, Radiology, Madrid, Spain; [3]Hospital Vall de Hebron, Radiology, Barcelona, Spain; [4]St. Michael's Hospital, Radiology, Toronto Ontario, Canada; [5]Hospital Peset, Radiology, Valencia, Spain; [6]East Surrey Hospital. SASH NHS Trust, Radiology, Redhill, United Kingdom

SCIENTIFIC POSTERS

Abstracts appear as submitted to the system and have not been checked for correctness and completeness.
Please visit the ePoster gallery to view the final posters.

A-134 **Diagnosis of Transthyretin Cardiac Amyloidosis by 99mTc-diphosphonate Scintigraphy**
M. Pudis, P.C. Notta, A. Palomar-Muñoz, I. Sánchez-Rodríguez, S. Bondia-Bescós, B. Hervás-Sanz, L.M. Gràcia-Sánchez; Hospital Universitario de Bellvitge, Nuclear Medicine – PET, Barcelona, Spain

A-175 **Incidental findings regarding the coronaries in noncardiac chest computed tomography: What the radiologist need to report**
E. Detorakis[1], C. Skiadas[2]; [1]University Hospital of Heraklion, Radiology, Department of Computed Tomography, Heraklion Crete, Greece; [2]University Hospital of Heraklion Crete, Radiology, Department of Computed tomography, Heraklion, Greece

A-133 **Right-sided aortic arch: Clinical associations and radiological findings in a case series**
D.T. Wada[1], L. Siyuan[1], R.A.O. Haddad[2], C.G.S. Souza[2], G.C. Melges[3], M.F.B. Santos[2], M. Koenigkam-Santos[3]; [1]Ribeirao Preto Medical School – University of Sao Paulo, Anatomy and Surgery, Ribeirao Preto, Brazil; [2]Ribeirao Preto Medical School – University of Sao Paulo, Internal Medicine, Ribeirao Preto, Brazil; [3]Ribeirao Preto Medical School – University of Sao Paulo, Medical Imaging, Hematology and Clinical Oncology, Ribeirao Preto, Brazil

A-169 **Fully Automated Deep Learning Powered Calcium Scoring in Patients undergoing Myocardial Perfusion Imaging**
T. Sartoretti, A.G. Gennari, E. Sartoretti, S. Skawran, A. Maurer, R.R. Buechel, M. Messerli; University Hospital Zurich, Nuclear Medicine, Zurich, Switzerland

A-110 **The role of deep learning-based artificial intelligence diagnostic system in detecting pulmonary nodules**
I. Matos, F. Antunes, C. Mota, C. Senra, F. Santos, I. Marques, P. Sousa; Centro Hospitalar Vila Nova de Gaia/Espinho, Imagiology, Vila Nova de Gaia, Portugal

A-186 **Automated quantitative analysis of high-resolution chest tomography can assist in differentiating the patterns of interstitial lung disease**
F.A.C. Sarmento Neto[1, 2], C.V.B. Machado[1], D.T. Wada[1], J.A. Baddini Martinez[1], A.T. Fabro[1], M. Koeningkam Santos[1]; [1]Ribeirao Preto Medical School – University of São Paulo, Radiologia, São Paulo, Brazil; [2]Real Hospital Portugues de Beneficência em Pernambuco, Radiologia, Recife, Brazil

A-149 **Comparison of radiation dose, vascular and parenchymal enhancement and image quality in contrast-enhanced thoracoabdominal CT between two models of scanners, with and without integrated detector and tin filter**
J. Arenas-Jiménez, S. Checa, E. García-Garrigós, M. Sirera; Hospital General Universitario de Alicante, Radiology, Alicante, Spain

A-117 **COVID-19 associated thrombotic complication: Is it pulmonary embolism or in-situ thrombosis?**
R. AL Umairi, K. AL Adawai, M. AL Khoori, A. AL Lawati; The Royal Hospital, Radiology, Muscat, Oman

A-201 **CT imaging manifestations of pulmonary nocardiosis**
G. Zantonelli[1], C. Moroni[2], O. Smorchkova[2], A. Botta[2], D. Cozzi[2], E. Cavigli[2], A. Bindi[2], S. Luvarà[2], V. Miele[2]; [1]Careggi Hospital, Florence, Florence, Italy; [2]Careggi Hospital, Florence, Italy

A-188 **Influence of pulmonary comorbidities on the outcome of COVID-19 positive patients and the severity of pneumonic infiltrates: A CT-based study**
B.Z. Botos[1], D. Mangold[1, 2], D. More[1, 2], H.-U. Kauczor[1, 2], H.P. Heußel[2, 3], R.F. Sowade[1, 2], O. Weinheimer[1, 2], K. Hellbach[1, 2]; [1]Univerity Hospital Heidelberg, Department of Diagnostic and Interventional Radiology, Heidelberg, Germany; [2]Translational Lung Research Center (TLRC), Member of the German Center for Lung Research (DZL), Heidelberg, Germany; [3]Thoraxklinik at University Hospital Heidelberg, Diagnostic and Interventional Radiology with Nuclear Medicine, Heidelberg, Germany

A-171 **Inter- and intra-observer agreement in MRI evaluation of inflammatory- and fibrotic-predominant interstitial lung disease**
C.A. Ruano[1], J. Veiga[1], N. Antunes[1], V. Carvalho[1], O. Fernandes[1], M.F. Moraes-Fontes[2], T. Bilhim[3], K. Irion[4]; [1]Hospital de Santa Marta, Centro Hospitalar Lisboa Central, Lisbon, Portugal; [2]Fundação Champalimaud, Lisbon, Portugal; [3]Hospital Curry Cabral, Centro Hospitalar Lisboa Central, Lisbon, Portugal; [4]Manchester University NHS Foundation Trust, Manchester, United Kingdom

A-195 **Pulmonary findings in COVID-19: Radiological-pathological correlation made from the counterpart location**
A.M. Svensson[1], A. Kistner[2], L. Szekely[3], H. Brunnström[4], T. Hansen[5], S. Nyrén[1], C. Ortiz-Villalón[3]; [1]Karolinska University Hospital, Department of Radiology, Stockholm, Sweden; [2]Karolinska University Hospital, Medical Radiation Physics and Nuclear Medicine, Stockholm, Sweden; [3]Karolinska University Hospital, Department of Pathology/Cytology, Karolinska University Laboratory, Stockholm, Sweden; [4]Lund University, Skåne University Hospital, Division of Pathology, Lund, Sweden; [5]Uppsala University Hospital, Department of Radiology, Uppsala, Sweden

A-159 **Restrictive Allograft Syndrome after lung transplantation: Correlation between radiological subtypes and histopathology**
A. Dubbeldam[1], R. Vos[2], W. De Wever[1], J. Coolen[1], S. Verleden[3], J. Verschakelen[1]; [1]UZ Leuven, Department of Radiology, Leuven, Belgium; [2]UZ Leuven, Department of Respiratory Diseases, Leuven, Belgium; [3]University Hospital Antwerpen, Department of Thoracic and Vascular Surgery & Pneumology, Antwerp, Belgium

A-196 **The ''CT target sign'': May be pathognomonic in COVID-19 patients?**
E. Detorakis[1], C. Skiadas[2]; [1]University Hospital of Heraklion, Radiology, Department of Computed Tomography, Heraklion Crete, Greece; [2]University Hospital of Heraklion Crete, Department of Computed tomography, Heraklion Crete, Greece

A-174 **The ''negative relapsing sign'': A new computed tomography sign associated to the organizing pneumonia pattern**
J. Arenas-Jiménez[1], E. García-Garrigós[1], I. Gayá García-Manso[2], R. García-Sevila[2], M. Sirera[1], A. Ureña[1], E. Feliu[1]; [1]Hospital General Universitario de Alicante, Radiology, Alicante, Spain; [2]Hospital General Universitario de Alicante, Pneumology, Alicante, Spain